https://ntrs.nasa.gov/search.jsp?R=20190001543 2020-05-10T04:07:26+00:00Z

WindBots

September 2016

Phase I Final Report

by Adrian Stoica

Virgil Adumitroaie

Marco Quadrelli

Georgios Matheou

Marcin Witek

Marco Cipolato

Marco Dolci

James Roggeveen

Kyle Petersen

Kristina Andreyeva

Pre-decisional: for information and discussion purposes only

FINAL REPORT

Early Stage Innovation
NASA Innovative Advanced Concepts (NIAC)

WindBots:
A Concept for Persistent In-Situ Science Explorers for Gas Giants

Adrian Stoica, Principal Investigator
Co-Investigators: Virgil Adumitroaie, Marco Quadrelli, Georgios Matheou, and Marcin Witek
Interns: Marco Cipolato, Marco Dolci, James Roggeveen, Kyle Petersen, Kristina Andreyeva

Jet Propulsion Laboratory

September 2016

ACKNOWLEDGEMENT

This research was carried out at the Jet Propulsion Laboratory (JPL), California Institute of Technology (Caltech), under a contract with the National Aeronautics and Space Administration (NASA).

The principal investigator (PI) wishes to acknowledge the contributions of several 2015–2016 JPL interns. James Roggeveen (Massachusetts Institute of Technology), Kyle Peterson (University of Idaho), and Kristina Andreyeva (University of Columbia) were supported by the Caltech Summer Undergraduate Research Fellowship (SURF) with funding provided by the Innovation to Flight pilot study at JPL, managed by Dr. Leon Alkalai. Marco Cipolato and Marco Dolci were supported by grants from the Politecnico di Torino, Italy. We thank Professor William Engblom, from Embry-Riddle University, for providing the analysis of a glider in the Jovian atmosphere. We acknowledge the continuous support received during the proposal preparation and performance of the study from Dr. Andrew Shapiro, Manager, Early Stage Innovation, Space Technology Program Office; Dr. Leon Alkalai, Assistant Division Manager, Systems Engineering and Formulation Division, Lead for Formulation, Engineering and Science Directorate; and Dr. Richard Volpe, Manager, the Mobility and Robotic Systems Section. We thank the NIAC management, NIAC External Council and NIAC Fellows for their feedback and suggestions.

The concept of airborne *WindBots* has been developed in the context of prior work in the area of surface wind-driven robotic explorers. The original idea of aerial wind-driven robots came to the PI from a discussion with JPL colleague Faranak Davoodi, the developer of the wind-driven *Moballs* concept for exploration of Mars and other windy bodies, such as Titan, as described in several publications[1,2] and subsequent patents and papers. That interaction, concepts acknowledged below, and the interactions with the co-investigators led to the novel concept of WindBots as *permanently airborne robots* (never touching a planetary surface), proposed to NIAC. We also acknowledge the earlier work and fundamental ideas of JPL colleagues Jack Jones, Alberto Behar, and collaborators from NASA Langley involved in the *Tumbleweed* rovers[3], and earlier seminal ideas from Jacques Blamont's *Mars Balls* (implemented later by University of Arizona), which (citing from the above reference) "proposed balls could be powered by the wind or could be powered and steered by an inner drive mechanism." We acknowledge the *Spherobots* of Mukherjee and colleagues[4], spherical mobile robots with various control strategies for the reconfiguration of the sphere. In terms or using wind-power to generate self-sufficient power, we acknowledge the pioneering work of Frobes et al.[5], in which the authors mention, "we introduce and study a novel tumbleweed rover design that enjoys a number of potential advantages over its competitors: 1) It employs an internal pendulum-generator system to produce electrical power as a result of being blown by the wind. This removes the need for solar panels while providing abundant power for the avionics and payload…". Ideas of exploration by groups (Tumbleweed rovers) were expressed by Southard et al [6] from which we cite: "group behavior strategies…can be used to more rapidly disperse the vehicles and to guide them toward particular targets."

© 2016 California Institute of Technology. Government sponsorship acknowledged.

[1]Design for the Structure and the Mechanics of Moballs," *NASA Technical Briefs* 36 (10), 66–68, Oct 2012, http://ntrs.nasa.gov/archive/nasa/casi.ntrs.nasa.gov/20120016261.pdf

[2]"Gone with the Wind on Mars (GOWON): A Wind-Driven Networked System of Mobile Sensors on Mars *Concepts and Approaches for Mars Exploration*, 2012, http://www.lpi.usra.edu/meetings/marsconcepts2012/pdf/4238.pdf

[3] Overview of Wind-Driven Rovers for Planetary Exploration, 43rd AIAA Aerospace Meeting 2005 http://ntrs.nasa.gov/search.jsp?R=20050041752

[4]Simple Motion Planning Strategies for Spherobot: A Spherical Mobile Robot *IEEE Int'l Conference on Decision and Control,* 3, 2132–2137, 1999, http://pirun.ku.ac.th/~fengjwp/publication/IEEE_DC1999.pdf

[5] Dynamic modeling and stability analysis of a power-generating tumbleweed rover, *Multibody Syst Dyn*, 24, 413–439, 2010, http://arrow.utias.utoronto.ca/~damaren/papers/ multitumble2010.pdf

[6]Exploring Mars Using a Group of Tumbleweed Rovers, *Robotics and Automation*, IEEE International Conference on. IEEE, 775–780, 2007

EXECUTIVE SUMMARY: MAIN FINDINGS AND RECOMMENDATION

This report summarizes the study of a mission concept to Jupiter with one or multiple Wind Robots able to operate in the Jovian atmosphere, above and below the clouds - down to 10 bar, for long durations and using energy obtained from local sources. This concept would be a step towards persistent exploration of gas giants by robots performing in-situ atmospheric science, powered by locally harvested energy. The Wind Robots, referred in this report as WindBots (WBs), would ride the planetary winds and transform aeolian energy into kinetic energy of flight, and electrical energy for on-board equipment. Small shape adjustments modify the aerodynamic characteristics of their surfaces, allowing for changes in direction and a high movement autonomy. Specifically, we sought solutions to increase *survivability* to strong/turbulent winds, and *mobility and autonomy* compared to passive balloons.

MAIN FINDINGS

We examined Jupiter atmospheric characteristics and options of WB mobility. *The optimal region both for science and operations was determined between 0.3 bar and 10 bar, within which all areas of known clouds is included. Based on the atmospheric movement, the stormy region of the Great Red Spot (GRS) and the region north-west of it, in the South Equatorial Belt, have the highest variability of wind vectors, and thus, so far, appear to be the most attractive part of Jupiter for placing a first WindBot mission.*

We examined various types of buoyancy control and energy use through static and dynamic soaring. We reviewed various solutions of aerostats, wing-based designs, an inflato-glider, reconfigurable wings, foldable and collapsible or expandable structures with various shell forms in airships. We also looked at airborne extensions of surface mobility powered by the wind (Moballs, Tumbleweed, Mars ball, Spherobot). *The lowest risk solution to providing high atmospheric mobility, covering long distances in a Jovian zone, e.g. South Tropical Zone, is the buoyant hydrogen-based inflatable design, with a diameter exceeding 70m, and with control mechanisms for enhanced mobility. Gliders with L/D factors over 70 could also potentially survive long duration flight in the target region of interest between 0.3 bar and 10 bar, provided several challenges in automated detection and navigation to obtain lift from updrafts are overcome. For exploration in stormy regions of higher turbulence (as observed at planetary scale) e.g. riding the upward currents in the eyewall of the GRS, g*liders with an L/D of only 24, could also satisfy the requirements provided they solve the localization problem and timely move towards the updrafts; a higher level of intelligent autonomy is needed in the case of the GRS. A hybrid, inflatable design with wing, or other control surface, may be potentially the solution with the highest risk yet also highest payoff.

We considered various options to harvest energy for operations. We analyzed vertical updrafts/thermals and horizontal components of the wind, and ways to convert wind energy into electrical energy. Both 1) the conversion of mechanical energy from rotors pushed by air flow, such as in autorotation, in updrafts or horizontal gusts, and 2) use of energy from vibration, were found effective. Harvesting hydrogen for fuel cells may be valuable for shorter duration missions.

RECOMMENDATION[7]

We propose to refine a mission concept to Great Red Spot, continuing the study of two alternate designs: an adaptive wing glider and a lightweight (possibly hydrogen-based buoyant) design with controllable surfaces.

[7] An Addendum to this report will be provided once new planned once new atmospheric data analysis from the Juno mission will become available.

SUMMARY QUAD CHART

1. Concept	2. Mission Scenarios
• WindBots are in-situ atmospheric explorers using winds for mobility and energy • They maintain altitude range, for year-long missions • Updrafts and horizontal gusts cause relative motion of WindBot parts (tumbling, vibrations, autorotation) which is leveraged to generate power	• Deployment of a Network of WindBots (NOW) to regions of interest in Jupiter's atmosphere • Deployed in the eyewall of the Great Red Spot (a) the WBs use anti-cyclone high wind and updraft • WindBots measure wind speeds, temperatures, and atmospheric composition
3. Main Findings	**4. Recommended Steps**
• Both aerostats and wing-based flight solutions can provide sufficient lift and control in the atmosphere, in active mode and in specific conditions of updrafts and ability to maneuver to them; a hybrid is untested but promising, see (b), (c) • Energy harvesting methods yield sufficient power for on-board operations; efficient fuel cells could reach mission duration objectives, see (d)	• Refine a Great Red Spot mission, using updated information expected from the Juno mission • Refine the analysis of two solutions: a glider (possibly with reconfigurable/inflatable wings) and a lightweight/quasi-buoyant design for which options include a hydrogen-based inflatable and a tumbling.

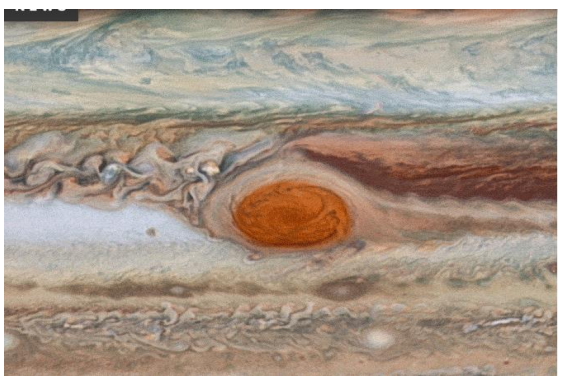

(a) Great Red Spot (center) and turblent area north-west of it

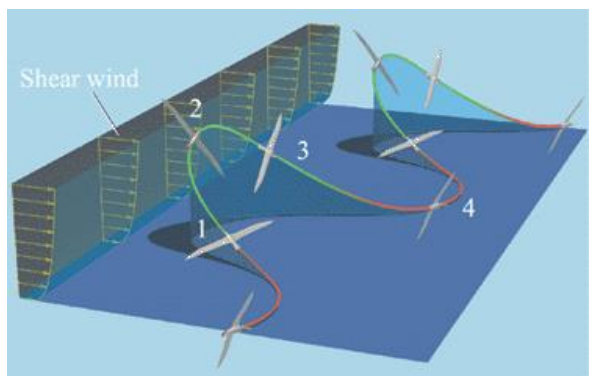

(b) Dynamic soaring

(c) Inflatable wing plane

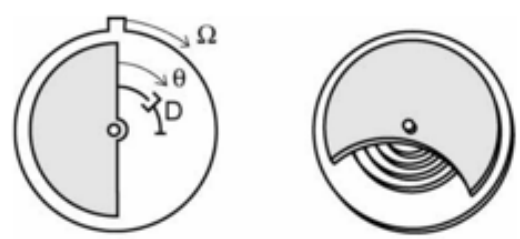

(d) Harvesting vibrational energy via a rotational generator

Table of Contents

ACKNOWLEDGEMENT IV

EXECUTIVE SUMMARY: MAIN FINDINGS AND RECOMMENDATION V
Main Findings v
Recommendation v
Summary Quad Chart vi

1 INTRODUCTION 1-1
1.1 The Need for In-situ Atmospheric Science with Long Lived Robotic Explorers 1-1
1.2 Concept, Phase I Objective, and Summary of the Approach 1-2
1.3 Organization of the Report 1-3
1.4 Benefits, Importance 1-3

2 JUPITER IN-SITU ATMOSPHERIC MISSION CONTEXT 2-1
2.1 Atmosphere Characteristics and Models – Global Circulation 2-2
2.2 Local Information 2-4
2.2.1 Galileo Probe (GP) 2-4
2.2.2 Turbulence at Aircraft-Scale 2-5
2.3 Regions of Interest 2-6
2.4 WindBot Mission Concept Science Goals and Instruments 2-8
2.4.1 In-situ Atmospheric Science, Scientific Goals for First Missions 2-8
2.4.2 Instruments 2-8
2.5 WindBot Mission Concept: Jupiter's Great Red Spot 2-9

3 MOBILITY IN THE JOVIAN ATMOSPHERE 3-1
3.1 Buoyancy Control 3-1
3.1.1 Buoyancy Control Equations 3-1
3.2 Aerostats 3-2
3.2.1 Montgolfières (Heated Gas) 3-3
3.2.2 Charlière (Hydrogen – Lighter Gas) 3-5
3.2.3 Vacuum Aerostat 3-9
3.2.4 Wing-Based Flight Control of Aerostats 3-11
3.2.5 Buoyancy Driven Winged Aerostat 3-12
3.2.6 Aerostats Summary 3-14
3.3 Wing-based Design 3-14
3.3.1 Ramjet Flyer 3-14
3.3.2 Flettner Rotor Airplane (Magnus Effect) 3-15
3.3.3 Glider 3-16
3.3.4 Autorotation Dynamics 3-17
3.3.5 Inflato-Glider 3-18

4 WINDBOT CONCEPT BODIES 4-1
4.1 Foldable – Collapsible/Expandable Structures 4-1
4.2 Foldable Structures Combined with Complex Shells in Airships 4-5
4.3 Tumbleweed 4-5
4.4 Reconfigurable Wings 4-7
4.5 Summary of WindBot Concept Mobility 4-10

5 WINDBOT CONCEPT ENERGETICS 5-1
5.1 Aeolian Energy 5-1
5.1.1 Vertical Winds (Updrafts/Thermals) for Lift and Power Harvesting 5-1
5.1.2 Horizontal Components – Wind Gradients/Cyclones/Turbulence 5-2
5.2 Converting Mechanical Energy to Electrical Energy 5-6
5.2.1 Rotational Generators 5-6
5.2.2 Converting Vibrations to Electricity 5-7
5.2.2.1 Linear Vibration Generator 5-7
5.2.2.2 Rotational Vibration Generators 5-9
5.2.3 Fluttering Generators 5-11
5.3 Turbine Generators 5-12
5.4 Thermal and Pressure Systems 5-14
5.4.1 Thermal Systems 5-14
5.4.2 Pressure Systems 5-16
5.5 Magnetic Generators 5-18
5.6 Hydrogen Harvesting 5-19
5.7 WindBot Concept Exergy 5-19
5.8 Summary of WindBot Concept Energetics 5-20

6 OPERATIONS CONCEPT 6-1
6.1 Deployment 6-1
6.2 Avionics 6-3
6.2.1 Instrumentation – Wind Measurement 6-3
6.2.2 Instrumentation – Navigation Using Magnetic Field 6-3
6.3 Automatic Detection of Thermals and Autonomous Soaring 6-3
6.4 Autonomy Challenges 6-4

7 SUMMARY AND CONCLUSION 7-1

8 REFERENCES 8-1

LIST OF FIGURES

FIGURE 1-1: SOLAR SYSTEM. BETWEEN THE ASTEROID BELT AND THE KUIPER BELT LIE THE GIANT PLANETS 1-1
FIGURE 1-1: A SCHEMATIC REPRESENTATION OF THE GIANTS AND THEIR COMPOSITION..... 1-1
FIGURE 1-2: THE GREAT RED SPOT ON JUPITER AT TWO DIFFERENT TIME MOMENTS: SHRINKAGE AND A NEW WAVE FROM ITS CENTER . 1-2
FIGURE 1-3: VISUAL MAPPING OF THE WINDBOTS MISSION FORMULATION PROCESS. 1-3
FIGURE 2-1: OBSERVED MEAN ZONAL WIND PATTERN ON JUPITER (IMAGE FROM BANGERAL ET AL. 2004). THE NOTABLE NUMBER OF JET AND BELTS, THE HIGH WIND SPEEDS AND THE CORRELATION WITH THE VISIBLE UPPER CLOUD FORMATIONS CAN BE READILY DISCERNED..... 2-1
FIGURE 2-2: PRESSURE – TEMPERATURE PROFILE OR VARIOUS ALTITUDES IN THE JOVIAN ATMOSPHERE, TWO VIEWS [106]..... 2-2
FIGURE 2-3: CHEMICAL COMPOSITION OF LOWER PARTS OF JUPITER'S ATMOSPHERE. 2-3
FIGURE 2-4: THERMAL PROFILES OF GIANTS AND CLOUD STRUCTURES OF GAS GIANTS, JUPITER AND SATURN (AFTER [19][20]) 2-4
FIGURE 2-6: EXPECTED MEAN VELOCITY DIFFERENCE WITH RESPECT TO DISTANCE FOR A TURBULENCE MODEL ON JUPITER..... 2-5
FIGURE 2-7: JUPITER ZONES AND BELTS. THE REGIONS THAT ARE PARTICULARLY INTERESTING INCLUDE THE SOUTH EQUATORIAL BELT, IN PARTICULAR WEST OF AND INSIDE THE GREAT RED SPOT [107], [108]..... 2-6
FIGURE 2-8: WARM MATERIAL RISES AND COOLS AS IT RISES. WHEN IT GETS COOL ENOUGH, THE AMMONIA FREEZES, FORMING WHITE CRYSTALS THAT OBSCURE THE NATURAL REDDISH BROWN OF THE WARMER MATERIAL. DARK BELTS (LOWER ALTITUDE AND WARMER TEMPERATURE) AND LIGHT ZONES (HIGHER ALTITUDE AND COOLER TEMPERATURE) ON JUPITER. (AFTER [104],[105]). 2-7
FIGURE 2-9: JUPITER POLAR REGIONS, BELTS, ZONES AND ANTI-CYCLONES..... 2-7
FIGURE 2-10: REGION OF INTEREST FOR WINDBOT MISSION CONCEPT WITH RELEVANT BOUNDARY ATMOSPHERIC DATA. 2-10
FIGURE 2-11: MODEL FOR CYCLONE DEMONSTRATING UPWELLING ON RIM. 2-10
FIGURE 2-12: GONE WITH THE WIND ON MARS (GOWON) CONCEPT. 2-11
FIGURE 3-1: FORCES ACTING ON POINT MASS SYSTEM ON WIND AXES. 3-1
FIGURE 3-2: SIRMA BALLOON IN JUPITER ATMOSPHERE (NASA JPL). [25]..... 3-3
FIGURE 3-3: SIRMA FLIGHT PATTERN SIMULATION WHEN UNDERGOING SOLAR HEATING (UPWARD TRENDS), AND INFRARED HEATING (DOWNWARD TRENDS) [25]. 3-3
FIGURE 3-4: SIRMA BALLOON CONFIGURATIONS ON DIFFERENT GAS GIANTS [3.4]..... 3-4
FIGURE 3-5: BALLOON DIAMETER REQUIRED TO HOLD VARIOUS MASSES BETWEEN 0.3 BAR AND 10 BAR (DENOTED BY DASHED RED VERTICAL LINES)..... 3-7
FIGURE 3-6: MASS AVAILABLE FOR PAYLOAD (ASSUMING AN ENVELOPE SURFACE DENSITY OF 30G/M^2)..... 3-7
FIGURE 3-7: INSIDE DIAMETER OF A VACUUM CHAMBER REQUIRED TO LIFT THE DENOTED MASS. THIS INCLUDES MASS OF ENVELOPE. ... 3-9
FIGURE 3-8: ICOSAHEDRON STRUCTURE [3.11]..... 3-10
FIGURE 3-9: BUCKLING MODES OF ICOSAHEDRON SHAPE OF VACUUM BALLOON. 3-11
FIGURE 3-10: LEFT SHOWS CONFIGURATION BETWEEN WING ASSEMBLY, PAYLOAD, AND BALLOON. THE RIGHT SHOWS THE DETAIL OF A POTENTIAL SINGLE-WING GUIDANCE ASSEMBLY STUDIED FOR THE DARE PLATFORM [33]. 3-12
FIGURE 3-11: SINUSOIDAL PROFILE OF FLIGHT PATH FOR UNDERWATER GLIDER AUV, SIMILAR FLIGHT PATH WOULD BE USED FOR ATMOSPHERIC APPLICATIONS [35]..... 3-13
FIGURE 3-12: BASIC CONFIGURATION USED FOR AUV TECHNOLOGY, FUSELAGE WOULD BE CONVERTED TO AEROSTAT BODY TO BE USABLE FOR ATMOSPHERIC FLIGHT [35]. 3-13
FIGURE 3-13: RAM JF-6 RENDER CONCEPT (LEFT) AND TECHNICAL SCHEME (RIGHT) [3.13]. 3-15
FIGURE 3-14: MAGNUS FORCE CREATED BY A FLUID MOVING WITH RESPECT TO A BODY WHICH IS SPINNING ALONG ONE OF HIS AXIS.. 3-15
FIGURE 3-15: PROBE CONCEPT EXTENDING CYLINDRICAL WINGS. 3-15
FIGURE 3-16: ETA GLIDER AND PERLAN 2. 3-16
FIGURE 3-17: I2000, AN AIRSHIP WITH INFLATABLE WINGS, SUCCESSFULLY TEST IN EARTH'S ATMOSPHERE [42]. 3-18
FIGURE 3-18: NON-INFLATED (ABOVE) AND INFLATED WINGS (BELOW) [42]. 3-18
FIGURE 3-19: GOODYEAR MODEL GA-468 INFLATOPLANE, 1950S [42]. 3-19
FIGURE 3-20: ILC DOVER APTERON UAV [42]..... 3-19
FIGURE 3-21: ILC DOVERS MULTI-SPAR INFLATED WING AND PACKED CONFIGURATION [42]. 3-19

FIGURE 4-1: EXPANDABLE STRUCTURES, EXAMPLE 1. CHINESE LANTERNS. FROM SMALL PACKED VOLUME TO A LARGER ONE AFTER EXPANSION. 4-1
FIGURE 4-2: EXPANDABLE STRUCTURES, EXAMPLE 2. KITCHEN DEVICE AND BIGELOW, EXPANDABLE SPACE HABITAT MODULE..... 4-1
FIGURE 4-3: OFF-CENTER SCISSOR-PAIR FOLDING PROCESS [45]. 4-2
FIGURE 4-4: ANGULATED SCISSOR-PAIR FOLDING PROCESS [45]. 4-2
FIGURE 4-5: PINERO'S TRANSFORMABLE SHELL. 4-3
FIGURE 4-6: EXPANDABLE STRUCTURE, EXAMPLE 2..... 4-3
FIGURE 4-7: EXPANDABLE STRUCTURE, EXAMPLE 3, HOBERMAN PRINCIPLE. 4-3
FIGURE 4-8: EXPANDABLE STRUCTURE, EXAMPLE 4, HOBERMAN PRINCIPLE. 4-4
FIGURE 4-9: BUCKLIBALL – 3D ORIGAMI LIKE STRUCTURE THAT COLLAPSES TO 46% ITS ORIGINAL SIZE [46]. 4-4
FIGURE 4-10: MICHAEL LEVIN'S VACUUM AIRSHIP. 4-5
FIGURE 4-11: A SYSTEM DIAGRAM SHOWING THE INFLATABLE TUMBLEWEED INTERNAL COMPONENTS. 4-5
FIGURE 4-12: A SYSTEM DIAGRAM SHOWING INFLATABLE TUMBLEWEED [47]. 4-6
FIGURE 4-13: TUMBLEWEED TEST DEPLOYMENT IN ANTARCTICA IN 2004. IMAGE COURTESY ALBERTO BEHAR, NASA JPL [47]. 4-6
FIGURE 4-14: EXAMPLE OF DEFLECTION OF A CONTROL SURFACE [49]. 4-7
FIGURE 4-15: INFLATABLE WING, ILC DOVER [42]. 4-8
FIGURE 4-17: MORPHING TENSEGRITY AIRFOIL [52]. 4-9
FIGURE 4-18: AD-1 OBLIQUE "SCISSOR" WING..... 4-9
FIGURE 5-1: UPDRAFT CORE MODEL. A SIMPLE GRAPHICAL MODEL SHOWING A PLAUSIBLE DISTRIBUTION OF UPDRAFT CORES ±5 KM FROM THE RADIUS OF MAXIMUM WIND (RMW) FOR HURRICANE ANITA AT ALTITUDE 0.5 KM [38]. 5-2
FIGURE 5-2: DYNAMIC SOARING CYCLE UTILIZING SHEAR WIND TO DEVELOP AN ENERGY-NEUTRAL TRAJECTORY [58]..... 5-2
FIGURE 5-3: SIDE GUST SOARING MAIN MODEL SCHEMES. (A) SIDE GUST SOARING SEEN FROM TOP [56] (B) VERTICAL DYNAMIC SOARING SEEN FROM SIDE WITH RELEVANT EQUATIONS [59]. 5-3
FIGURE 5-4: DYNAMIC SOARING IN DOWNDRAFTS. THIS DIAGRAM SHOWS HOW A SAILPLANE CAN GET ENERGY FROM DOWNWARD MOVING AIR [56]. 5-4
FIGURE 5-5: WINDBOTS GYROSCOPIC ENERGY HARVESTER MECHANISM. FROM LEFT TO RIGHT: POWER GYROBALL, INSIDE GYRO, AND A 3D SPHERICAL INDUCTION MOTOR, WHICH CAN BE OPERATED IN GENERATOR REGIME 5-6
FIGURE 5-6: WINDBOTS OUTER BODY CONCEPTS THAT WOULD BENEFIT FROM TUMBLING. 5-6
FIGURE 5-7: DRIVING FREQUENCIES NECESSARY TO PRODUCE 30W OF POWER FOR THE WB GIVEN VARIOUS MAXIMUM RESPONSE AMPLITUDES FOR A ONE-KILOGRAM MASS. FOR A MAXIMUM, THE SYSTEM IS DRIVEN AT THE MAXIMUM RANGE OF MOTION. 5-7
FIGURE 5-8: DRIVING FREQUENCIES NECESSARY TO PRODUCE 30 W OF POWER FOR DIFFERENT MAXIMUM DISPLACEMENTS OF A ONE-KILOGRAM MASS INSIDE OF THE SYSTEM. IN THIS CASE, THE AMPLITUDE OF THE DRIVING OSCILLATIONS IS CONFINED TO 10 CM. 5-8
FIGURE 5-9: SCHEMATIC FOR A LINEAR VIBRATION ENERGY GENERATOR [64]. 5-9
FIGURE 5-10: ENERGY AND POWER DECAY IN A DAMPED HARMONIC OSCILLATOR FOR A SYSTEM WITH ARBITRARY CONSTANTS; DECAYING FORMS AN INITIAL SYSTEM ENERGY. 5-9
FIGURE 5-11: (A) ROTATIONAL GENERATOR GEOMETRY. (B) INCLUSION OF A SPRING ALLOWS FOR RESONANCE TO BE EXPLOITED [64].5-10
FIGURE 5-12: MECHANISM OF AN AUTOMATIC WATCH [66] – A WB MAY USE A SIMILAR ENERGY HARVESTING MECHANISM. 5-10
FIGURE 5-13: FLUTTERING PIEZOELECTRIC CONCEPT [67]. 5-11
FIGURE 5-14: HYBRID HARVESTER WITH PIEZOELECTRIC AND ELECTROMAGNETIC TRANSDUCTION MECHANISMS [69]. 5-12
FIGURE 5-15: MULTI-ROTOR POSSIBLE WINDBOT DESIGN..... 5-13
FIGURE 5-16: GIMBAL TURBINE PROPOSED DESIGN. 5-13
FIGURE 5-17: DEPENDENCE OF OPERATIONAL TIME OF A CRAFT POWERED BY THERMAL RECOVERY ON VOLUME OF GAS ENCLOSED, USING ATMOSPHERIC CONDITIONS AT 10 BAR. 5-14
FIGURE 5-18: DEPENDENCE OF OPERATIONAL TIME OBTAINED BY THERMAL POWER ON PRESSURE INSIDE OF THE GAS CAPSULE, FOR A 1 M^3 SAMPLE OF GAS. NOTE THE LOGARITHMIC SCALE FOR PRESSURE; THIS RELATIONSHIP IS LINEAR. 5-17
FIGURE 5-19: DEPENDENCE OF OPERATIONAL TIME OBTAINED BY THERMAL POWER ON DENSITY OF GAS USED, FOR A 1 M^3 SAMPLE. .. 5-17
FIGURE 5-20: COMPARISON OF DIFFERENT PLANETS MAGNETIC FIELDS [72]. 5-18
FIGURE 5-21: JUPITER'S MAGNETIC FIELD. THICKER LINES DENOTE REGIONS OF STRONGER MAGNETIC ACTIVITY [73]. 5-19

FIGURE 6-1: "SKIPPING" TECHNIQUE UTILIZED TO ALLEVIATE EXTREME DECELERATION FORCES ASSOCIATED WITH HIGH VELOCITY ATMOSPHERIC ENTRY. FIGURE BASED ON NASA FIGURE PRODUCED BY CLEM TILLER. 6-2
FIGURE 6-2: PHASES OF WB DEPLOYMENT AND INFLATION (LEFT). NASA JPL PLANETARY BALLOON TESTS (RIGHT). 6-3
FIGURE 6-3: BLOCK DIAGRAM SHOWING THE KEY GUIDANCE AND CONTROL WB ELEMENTS. 6-5
FIGURE 6-4: AEROBOT AUTONOMY ARCHITECTURE [79]. 6-5
FIGURE 6-5: ILLUSTRATION OF A POSSIBLE WINDBOT AUTONOMY FUNCTIONAL DIAGRAM. 6-6

LIST OF TABLES

TABLE 2-1: LOCATION, ADVANTAGE AND DISADVANTAGE (BOTH SCIENTIFIC AND TECHNOLOGICAL) OF HAVING A WINDBOT IN DIFFERENT ATMOSPHERIC AREA ON JUPITER. 2-8
TABLE 4-1: A SUMMARY OF WB MOBILITY OPTIONS 4-10
TABLE 5-1: POWER DENSITY COMPARISON OF WIND ENERGY HARVESTING DEVICES [67]. 5-12

1 Introduction

1.1 The Need for In-situ Atmospheric Science with Long Lived Robotic Explorers

Beyond the asteroid belt lies the fascinating world of the Giants: the Gas Giants, Jupiter and Saturn, and the Ice Giants, Uranus and Neptune (Figure 1-1). Our very limited knowledge of these planets is the result of remote sensing, flybys, and telescope observation. On these giants there is no hard surface to land on, instead, the Giants have small cores characterized by very high pressure and high temperatures. The Giants are made of hydrogen, some helium, and trace amounts of other elements (Figure 1-2).

Unveiling the mysteries of Gas Giants is key to understanding the formation and evolution of our solar system [1]. These colossal planets, with volumes about a thousand times that of Earth, harbor huge atmospheric phenomena (Figure 1-3), with jets that dominate atmospheric circulation at visible levels [2].

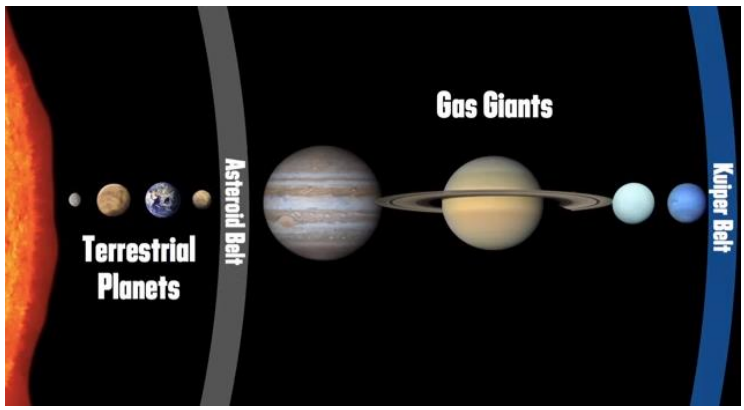

Figure 1-1: Solar System. Between the Asteroid Belt and the Kuiper Belt lie the Giant planets

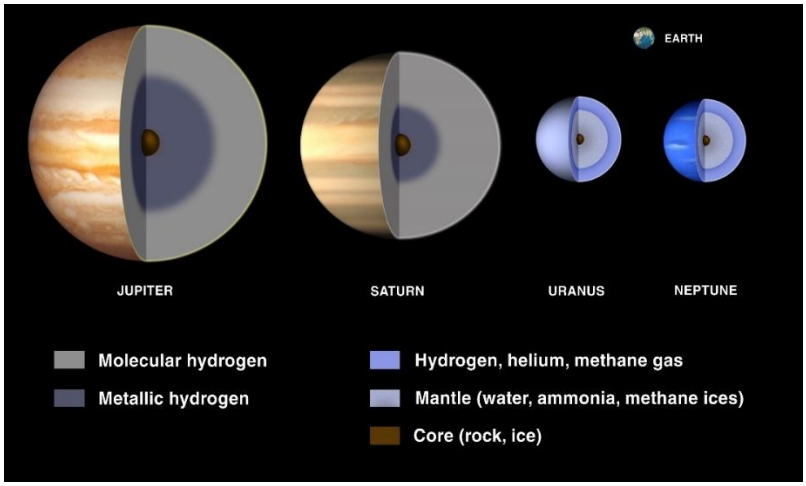

Figure 1-1: A schematic representation of the Giants and their composition.

The *Hubble 2020: Outer Planet Atmospheres Legacy program* maintains yearly reports of the outer planets, but only allows visual observation data of the upper regions of the atmosphere [3]. Thus, observations of the Great Red Spot (GRS) on Jupiter, seen in Figure 1-3, have shown the GRS is shrinking, and a new wave from its center has been identified in recent (2015) observations) [3]. However, direct

characteristics of the storm, including composition, temperature, and wind speeds below the upper levels remain almost impossible to obtain by current means.

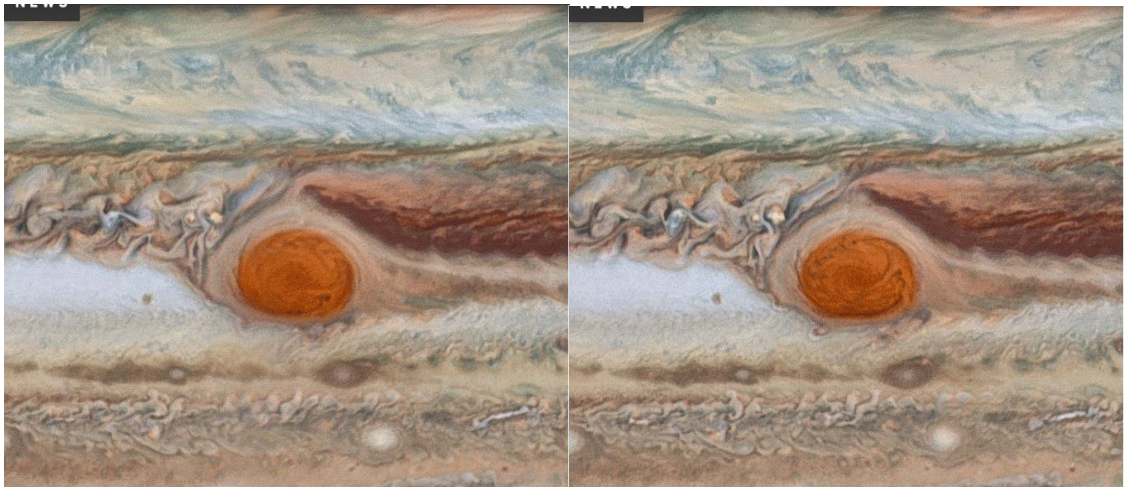

Figure 1-2: The Great Red Spot on Jupiter at two different time moments: shrinkage and a new wave from its center

The currently ongoing Juno mission will enrich our knowledge of Jupiter. Yet, despite being much closer to the planet, it still retains limitations inherent of remote sensing. To validate models and to study the layered atmospheric composition and the dynamic processes at work in the Giants' atmospheres, one needs in-situ exploration [4]. To date, the only in-situ measurements (and thus ground truth) come from the Galileo probe (GP), in its 156 km traverse through Jupiter's atmosphere [5]. GP found that the atmosphere is denser and the winds are stronger and extend deeper than expected; it did not detect an expected three-tiered cloud structure. Unfortunately, probing in a single dimension and at a single location has obvious limitations and scientists now believe the entry site may have been one of the least cloudy areas on Jupiter.

To collect data from below the upper, visual layer, with appropriate spatial and temporal resolution, special robotic explorers are required, which move and measure along three dimensions (3D), survive winds up to 170 m/s, and survive without the use of solar energy.

1.2 Concept, Phase I Objective, and Summary of the Approach

In this study we envision a persistent exploration of the gas giants with teams of multiple robots powered by locally harvested energy performing in-situ observational atmospheric science. Bumped around by gusts in the strong and turbulent[8] windstorms of the troposphere, opportunistically using upwelling currents, WindBots (WBs) use controlled aerodynamic forces for lift and direction change. Autorotation and mechanisms similar to those used in kinetic/automatic watches capture mechanical energy, converting it to electrical energy via electromagnetic generation. Unlike conventional flyers that avoid turbulence, WBs seek to leverage it. WBs 'chase' updrafts and gradients in horizontal winds, use real-time controls to adjust their surfaces, changing their aerodynamic characteristics, and advancing in the desired direction through waypoints set on high turbulence/updraft currents.

The objective of this Phase I NIAC study was to determine a mission scenario for in situ atmospheric science in a gas giant and to do a feasibility study of a WindBot.

[8] At least at the large scale, as high-level resolution turbulence is not known

To achieve this objective, we determined the optimal area of exploration both from a science and energy collection point of view. We considered what in situ atmospheric science could be performed and the necessary instrument suite needed to determine payload energy requirements and to formulate an *in-situ* mission. We focused on Jupiter, but consider WBs as a generic solution for in-situ exploration of all outer planets. Possible designs of WindBot mobility and energy harvesting systems are presented and validated.

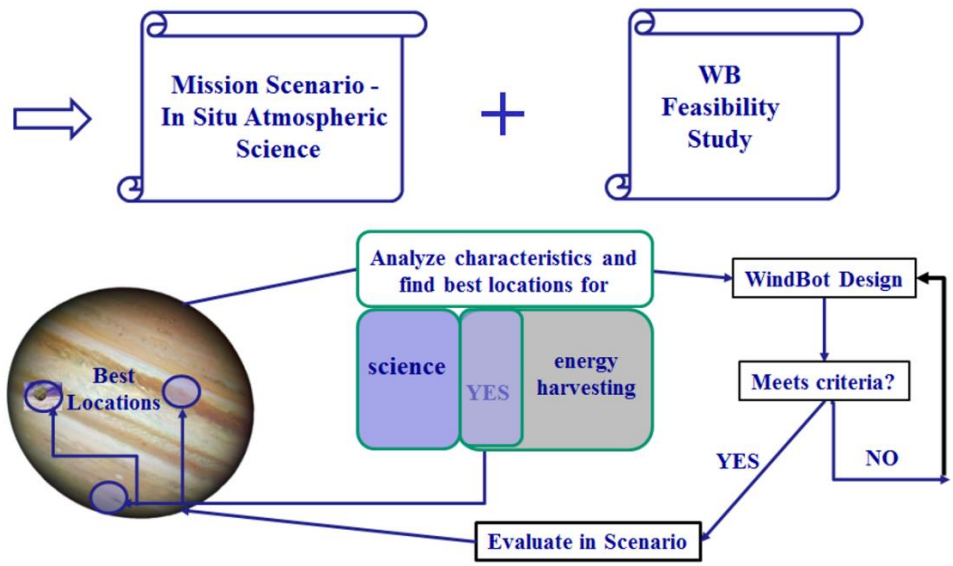

Figure 1-3: Visual mapping of the WindBots mission formulation process.

1.3 Organization of the Report

Chapter 2 provides the scientific context and motivation for a WB mission and determines optimal regions and payloads for WB missions as the intersection of regions of scientific interest and energy reservoirs – focusing on a mission to Jupiter's Great Red Spot. Chapter 3 explores buoyancy and lift generation options for WB design, focusing on maintaining mission duration, providing a measure of control for the WB, and exploring the entire proposed operating range. Chapter 4 discusses several WB body configurations and deployment, extending the mobility discussion from Chapter 3. Chapter 5 investigates energy recovery methods using active systems controlling the WB and passive systems to harvest naturally occurring wind, pressure, and thermal gradients in the atmosphere. Chapter 6 reviews autonomy architecture and control schemes to be applied to the autonomous WB. Chapter 7 presents summary and conclusions.

1.4 Benefits, Importance

This Phase I study aimed to develop *new mission concepts for in-situ observational atmospheric science* on Jupiter with persistent high-mobility WindBots, harvesting energy from the strong winds and possibly from magnetic fields, and to evaluate the feasibility of WBs. The results would apply to Saturn and other giants where in fact the winds are stronger, gravity is lower, and atmospheric composition is more favorable (less percentage of hydrogen), hence heavier components, thus easier to achieve buoyancy.

Successful WBs would enable missions of persistent in-situ exploration and the *measurement of dynamic atmospheres with high-mobility robots*. As emphasized by a National Research Council study referring to Jupiter exploration, mobility is extremely important, [6]:

> *"mobility is required to obtain the structure, composition, and wind velocity data below the clouds with the appropriate spatial and temporal characteristics."*

WBs are expected to e*stablish a basis and formulate a methodology for systematic incorporation of alternate energy-harvesting techniques in the design of planetary robots.* When perfected, alternate energy-harvesting technologies will enable new classes of missions of robotic explorers at targets deprived of solar radiation without nuclear power and enable new concepts of in-situ persistent exploration at much lower costs than the nuclear alternatives.

Exempt from the high mass, size, and cost of a nuclear power generator, *low-cost exploration solutions with small and light platforms* become possible. This will allow the deployment of many probes/WBs and the creation of distributed sensor networks to perform long-term, simultaneous measurements of synoptic and global scale phenomena o these gas giants.

WBs are expected to *open the door to in-situ science on gas giants*. Long-term observations will aid our understanding of the Jovian atmosphere, offering an exceptional opportunity to observe, study, and discover geophysical fluid dynamics in a nearly idealized setting of atmospheric circulations governed only by planetary and geophysical parameter. WBs would help answer important questions regarding the structure and composition of their atmospheres below the cloud tops, providing the key to understanding huge storms, which on Jupiter and Saturn may reach the size of several Earth diameters.

WB novelty is multi-faceted: a) As a concept of high mobility in-situ explorers of gas giants: unlike conventional atmospheric vehicles optimized for "smooth" flight, WB are highly adaptive flyers, trading smooth flights for wind energy use; b) As an in-situ energy-harvesting (self-powering) flying robot that uses wind energy and converts it to electrical energy for flight operation; and c) As an intelligent, real-time adaptive atmospheric flying robot that senses 3D wind patterns, seeking vortices, wind shear, and updrafts that can be used as energy fountains, plans its waypoints/traverse to pass by, and performs real-time control to adjust its aerodynamic properties for optimal lift and change of direction.

In contrast to Moballs, Tumbleweeds, Mars Balls which are <u>surface</u> wind-driven/powered robotic explorers (S-WDRE), WindBots, are <u>atmospheric</u> wind-driven/powered robotic explorers (A-WDRE), permanently in the atmosphere without touchdown. This is a considerable challenge as staying 'afloat' *in an unpowered craft that does not have thrust* (any harvested power is insufficient to produce sufficient thrust) in an atmosphere such as the Jovian one, as the surrounding gas is light (predominantly hydrogen) and gravity is stronger than on Earth. As opposed to the S-WDRE, A-WDRE (unless naturally buoyant) can NOT benefit of even very high winds if their velocity is constant, since once they reach the speed of the wind there is no more relative movement and thus no lift, and they would fall.

A constant (horizontal) wind, of any value, say 100 m/s would move S-WDRE and ensure a successful mission. The same wind would NOT lead to a successful mission with A-WDRE (unless performed with a naturally buoyant platform). A WindBot would need gusts (variation of wind vectors) to generate lift and stay afloat. No wind for a Moball has at most the effect of a stop in movement. No wind for a not naturally buoyant WindBot means falling into the depths of the gas giant.

2 Jupiter In-Situ Atmospheric Mission Context

The bottomless atmospheres of Jupiter, Saturn, Uranus, and Neptune in combination with the relatively high planetary rotation rates result in atmospheric circulations that are significantly more regular than Earth's. The Jovian atmosphere offers an exceptional opportunity to observe, study and discover geophysical fluid dynamics in a nearly idealized setting. Moreover, Jovian atmospheric circulations are directly governed by the planetary and geophysical parameters, in contrast with Earth's mountain ranges and ocean, which steer and alter the circulation and weather patterns [8]. In fact, the dynamics of Jovian atmospheres resemble more the geophysical spaciousness of the Earth's ocean rather than the atmosphere [9].

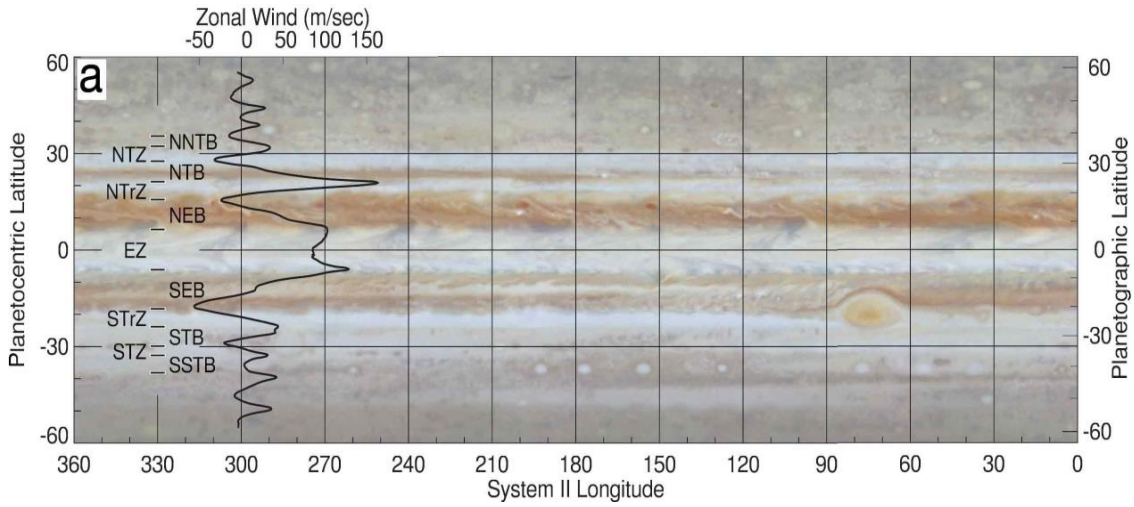

Figure 2-1: Observed mean zonal wind pattern on Jupiter (image from Bangeral et al. 2004). The notable number of jet and belts, the high wind speeds and the correlation with the visible upper cloud formations can be readily discerned.

The main characteristic of Jupiter's atmosphere is the axisymmetric zonal jet streams (Figure 2-1) and the many anticyclones forming between the jets (about 90% of the observed storms on Jupiter are anticyclones [10]), the most prominent being the Great Red Spot. Winds measurements based on the upper (visible) cloud layers show wind speeds reaching 180 m/s [11] [12].

Understanding the motion and composition of Jupiter's atmosphere has been the goal of several past missions, starting with the early exploration from Voyager I [13] and II, Galileo, the analysis of the impact from comet Shoemaker–Levy 9, and Cassini [12]. Despite the valuable data of past missions, important questions remain regarding the structure and composition of Jupiter's atmosphere below the cloud top (Marcus & Shetty 2011). As expressed metaphorically [14] current missions hope that by studying the skin of the onion we will manage to understand the onion and all of its layers. The only in situ measurements of the atmosphere were those made by the Galileo probe [15], summarized in Section 2.2.1.

On July 4, 2016 Juno successfully entered an orbit around Jupiter. This is a substantial achievement of the NASA New Frontiers Program representing the advancement of solar system exploration. The Juno Mission's primary goal is to significantly improve our understanding of the formation, evolution, and structure of Jupiter. Juno will attempt to unravel some of the mysteries – for example, it is still unknown how much water and ammonia is in the Jupiter's atmosphere, which has implications for the theories of

the formation of the solar system. The vertical profiles of Jupiter's composition, temperature, and cloud motions are poorly constrained. We don't know what the nature of Jupiter's turbulence is and how this turbulence feeds back or interacts with large-scale structures visible in the outer layers of Jupiter's clouds. Juno will shed light on some of these questions, providing an unprecedented level of details on Jupiter's structure, magnetism, and gravity.

Nonetheless, as an orbiter aimed at understanding the planet as a whole, Juno will not be able to glimpse into features that are horizontally smaller than a few kilometers [16]. A better spatial resolution of measurements may still be required for a detailed understanding of atmospheric structure and dynamics. The direct sampling of Jupiter's atmosphere, as shown by the Galileo probe [17], could fundamentally affect our understanding of Jupiter, the outer planets, and the formation and evolution of the solar system. Thus, in the end and for that reason, in-situ exploration of Gas Giants is needed that will close the observational gap by allowing us to probe the finer scales of atmospheric composition and dynamics. Furthermore, it would provide independent validation for orbital observations.

2.1 Atmosphere Characteristics and Models – Global Circulation

The Jovian cloud model currently accepted by scientists is comprised of three main layers, which are: ammonia at the highest levels (0.3–0.7 bar), the ammonium hydrosulphide (~2 bar), and the deeper water vapor clouds (5–6 bar) [18]. Figure 2-2 shows the variation of pressure as a function of temperature in the Jovian atmosphere. The main cloud layers are also depicted.

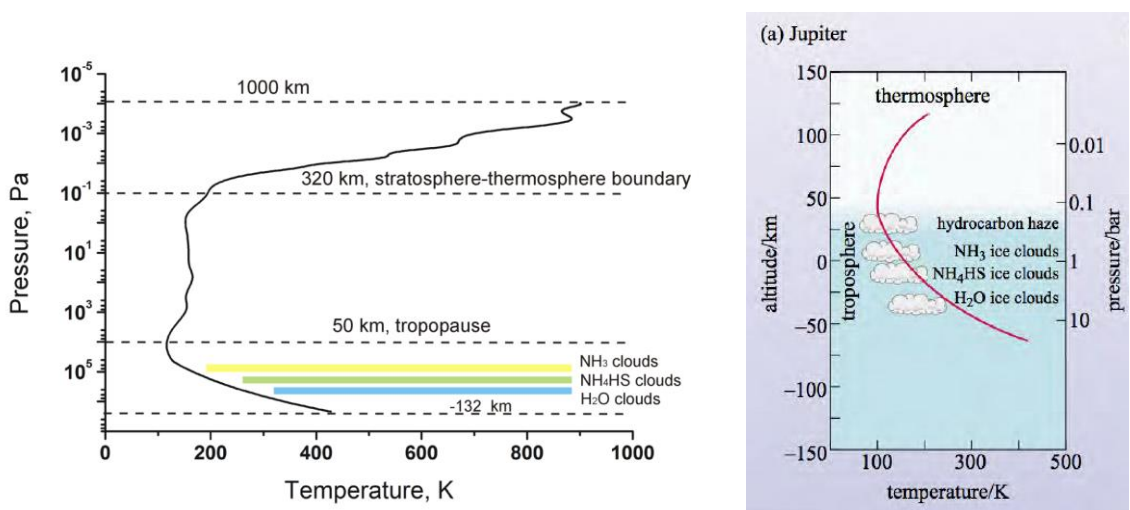

Figure 2-2: Pressure – Temperature Profile or various altitudes in the Jovian atmosphere, two views [106]

Figure 2-3 focuses on the lower parts of the Jupiter's atmosphere, illustrating the chemical composition and cloud types as one moves from the layer of molecular hydrogen upwards. As the gas density and pressure decreases, the temperature decreases with the distance from the center. The various chemical elements and their respective temperatures are mainly responsible for the colors of the visualized clouds.

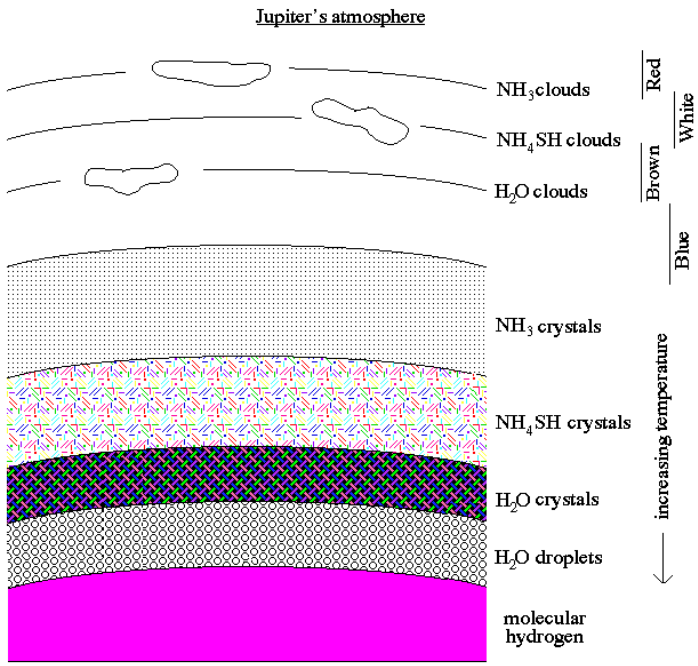

Figure 2-3: Chemical composition of lower parts of Jupiter's atmosphere.

Thermal profiles and cloud structures of the Giants are depicted in Figure 2-4 (left panel) [19] [20]. The temperatures at 1 bar differ between planets, with Jupiter being the warmest and Neptune and Pluto the coldest, but the overall temperature profiles are comparable in all of them. The three main Jovian cloud types are also present on Saturn, but due to lower temperature they are shifted towards higher pressures (Figure 2-4, middle and left panel).

With radio, we can peer through the clouds and see that those hotspots are interleaved with plumes of ammonia rising from deep in the planet, tracing the vertical undulations of an equatorial wave system," said UC Berkeley research astronomer Michael Wong. "We now see high ammonia levels like those detected by Galileo from over 100 kilometers deep, where the pressure is about eight times Earth's atmospheric pressure, all the way up to the cloud condensation levels," de Pater said. The scientists discovered that plumes of ammonia-rich gases rise to form the upper cloud layers visible from Earth — ammonium hydrosulfide clouds at a temperature near 200 Kelvin, and ammonia-ice clouds at roughly 160 Kelvin. These upwellings of ammonia swell up in wave patterns, a sign of motion deep within the atmosphere. Conversely, ammonia-poor air sinks in downwellings. Near the Great Red Spot, the researchers detected many intricate features, suggesting complex upwelling and downwelling.

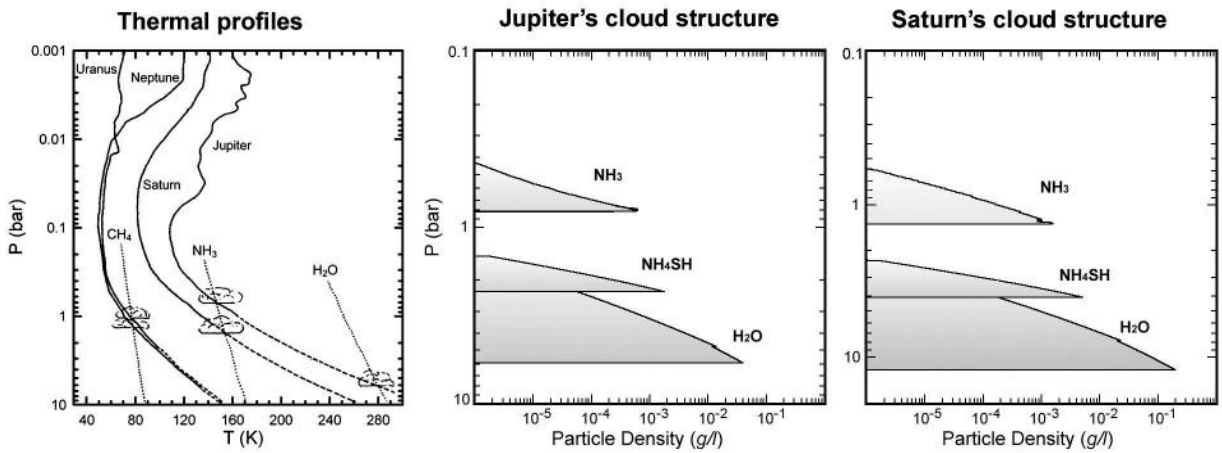

Figure 2-4: Thermal profiles of Giants and cloud structures of Gas Giants, Jupiter and Saturn (after [19][20])

2.2 Local Information

2.2.1 Galileo Probe (GP)

In 2003, the 339 kg GP, communicating through 2 L-band transmitters, and powered by lithium sulfur dioxide ($LiSO_2$) batteries with an output of 580 watts, descended 156 km through the upper layers of Jupiter's atmosphere before it stopped transmitting. Its drop was in a region termed a 5-micron hot spot, a local clearing in the clouds that is bright near the 5 µm spectral region [15] [17]. The details of the drop can be seen in Figure 2-5. The probe dropped about 24 bars before the signal ended, providing 58 minutes of local weather data; the temperature at the end of transmission was 153°C (307°F).

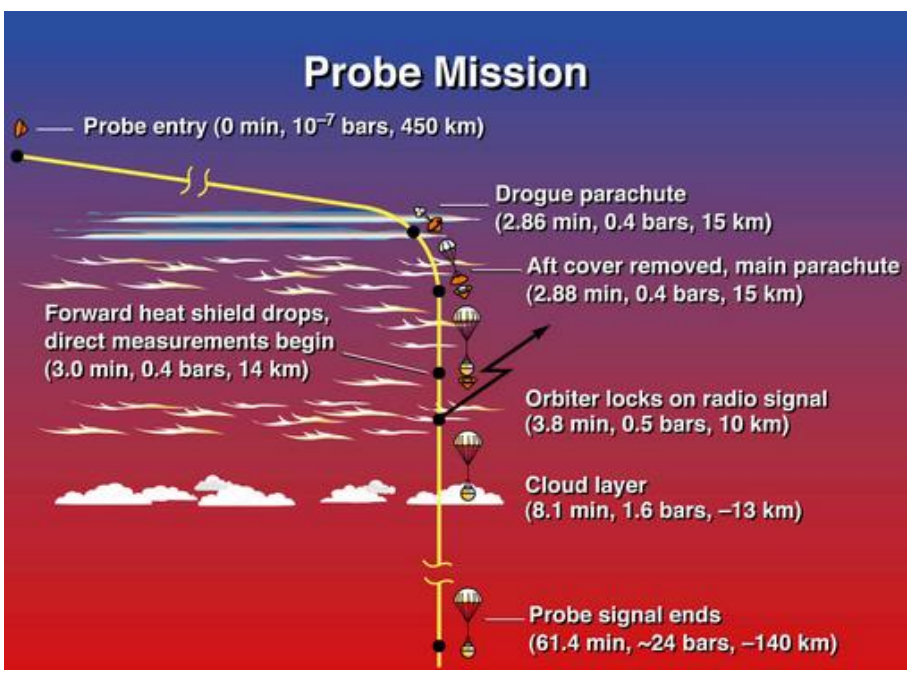

Figure 2-5: Galileo Probe entry in Jupiter atmosphere.

The probe showed the atmosphere to have a generally stable temperature stratification, and zonal winds increasing from ~80 m/s at less than 1 bar to about 180 m/s near 5 bars, after which the winds remained

approximately constant with depth. The main important findings from the descent were that the Jupiter's atmosphere was slightly hotter, more turbulent, and exhibited stronger winds than expected. It contained less helium than expected, less clouds, less lightning, and less water. As the entry point was an infrared hot spot, the findings were not representative for the general Jovian atmosphere. Many questions about the atmosphere remain unanswered. GP did not measure Oxygen content, for example. Because of the specific location of the drop, no cloud properties were observed, and the dynamic and vertical shear observations are not necessarily representative of the general Jovian atmosphere [17].

2.2.2 Turbulence at Aircraft-Scale

Virtually nothing is known about aircraft-scale turbulence on Jupiter and in this respect the scales of interest are well below the resolution of remote sensing [21]. The Galileo Probe's accelerometer data show some 1 m/s fluctuations, but because the sampling rate was low, the vertical scale is about 200 mbar, too large a distance to infer about finer scale turbulence. A conservative estimate of the largest turbulence amplitude on Jupiter is that it might be twice as strong as on Earth. This estimate is based on the fact that cumulus towers on Jupiter rise through 30 km instead of 8–10 km on Earth, in a roughly similar period of time, implying stronger vertical perturbations. These regions of active moist convection on Jupiter cover only a small fraction of the surface and their locations are well known. Jupiter's top-of-the-atmosphere solar heat flux is only 14 W/m^2, which is almost two orders of magnitude less than Earth's, so it is conceivable that there are vast stretches on Jupiter where the turbulence is negligible, at least in the upper troposphere."

However, Jupiter has an internal energy source that might be somehow contributing to convection and generation of turbulence. A turbulence theory might be used to estimate potential velocity difference with respect to distance. If we assume the Kolmogorov scaling and a uniform energy production scale, a second order turbulence structure function can be expressed as $F_2(r) = 4.82 C_k (\varepsilon r)^{2/3}$ [22]. If we further assume that $F_2(r)$ is isotropic, and dissipation rate is $\varepsilon = 10^{-5}$ m^2/s^3 [23], we can derive the mean velocity difference as a function of distance (Figure 2-6).

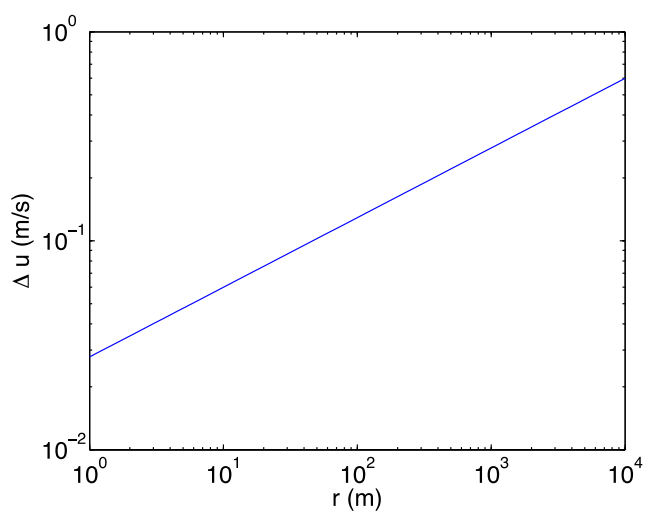

Figure 2-6: Expected mean velocity difference with respect to distance for a turbulence model on Jupiter.

The relation shows that a velocity gradient of 0.1 m/s can be expected at about 100 m. This has implications for design and requirements of in-situ explorers in areas of Jupiter that are relatively free from large sources of turbulence.

2.3 Regions of Interest

The circulation of Jupiter is largely unknown and inferred primarily from numerical modeling. The visible parts of the atmosphere are the cloud tops, which provide data on the outer layers and their dynamics. Galileo Probe vertical profiles of wind and thermodynamic properties, due to the unique entry point those profiles, are not representative for more prevalent atmospheric structures in the Jovian atmosphere, namely zones and belts. The zones and belts (Figure 2-7) are thought to be associated with vertical, in-and-out motions called convection (Figure 2-8). Upwelling warm gas results in the light-colored zones, which are regions of high pressure. As depicted in Figure 2-9, the darker belts overlie regions of lower pressure where cooler gas sinks back down into Jupiter's atmosphere. The zones and belts are therefore analogous to the high-and low-pressure systems that produce localized circulating storms on Earth, except Jupiter's rapid rotation has wrapped them all the way around the planet. Although this general convective pattern of the zones and belts was apparently supported by observations during the Voyager flybys of Jupiter, instruments aboard the Cassini spacecraft have also discovered large plumes of fast-rising gas scattered thought the belts and absent in the zones.

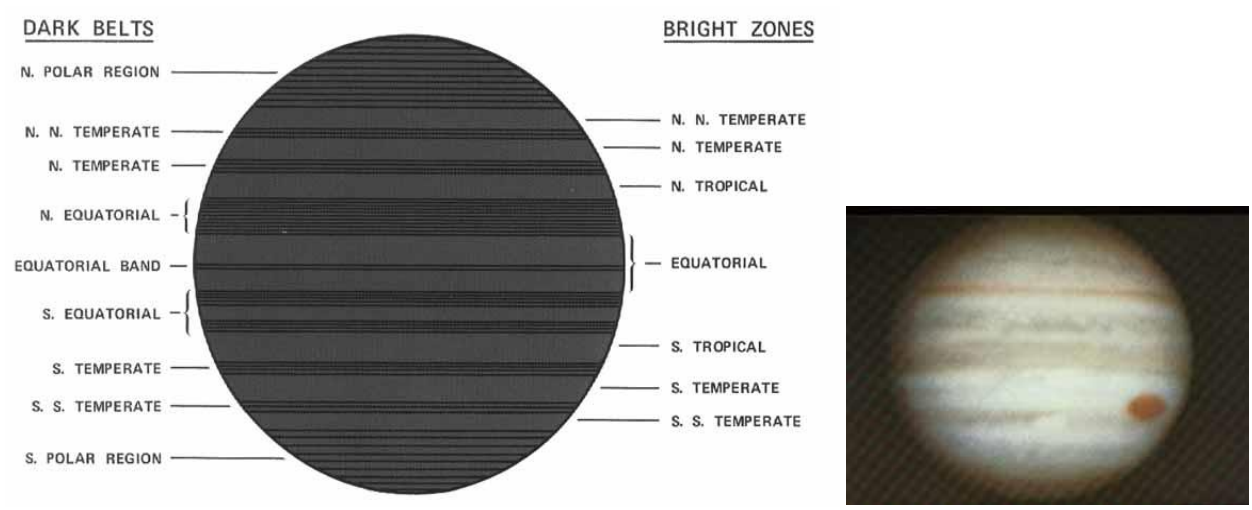

Figure 2-7: Jupiter zones and belts. The regions that are particularly interesting include the south equatorial belt, in particular west of and inside the Great Red Spot [107], [108]

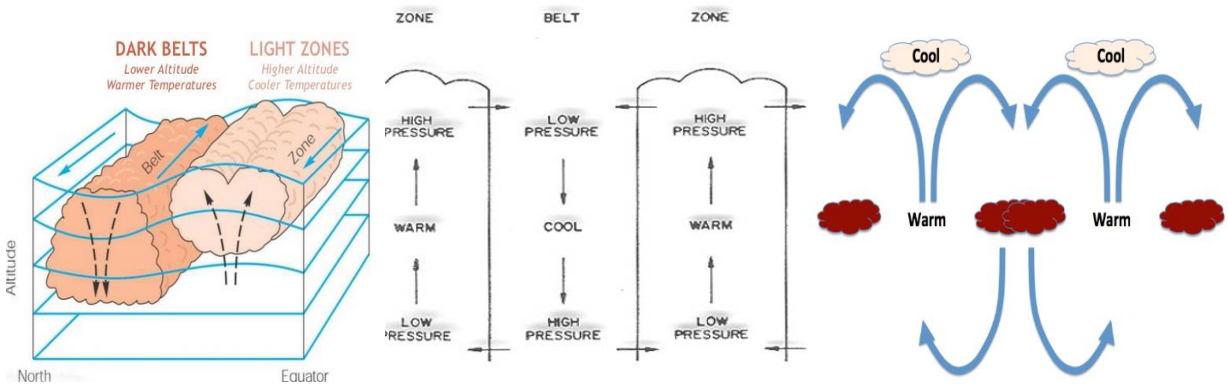

Figure 2-8: Warm material rises and cools as it rises. When it gets cool enough, the ammonia freezes, forming white crystals that obscure the natural reddish brown of the warmer material. Dark belts (lower altitude and warmer temperature) and light zones (higher altitude and cooler temperature) on Jupiter. (after [104],[105]).

Since zones and belts are most prevalent features in the Jovian atmosphere, they are natural candidates for exploration. The visible brown and white clouds are in a relatively thin weather layer (~5 bar to tropopause at ~0.1 bar, Figure 2-2). The atmosphere below the weather layer is likely convective, as inferred from numerical modeling. Traveling zonally (East-West) is much easier than meridianally. If riding in a zone (~100 m/s wind) it would take around 50 Earth days to circle Jupiter. If in a belt (~25 m/s) it would take about 200 Earth days to circle. Anticyclones (e.g. the Great Red Spot) are the most efficient way to move meridianally. Assuming the tangential velocity of 150-170 m/s in GRS, it would take about 4 days for a complete rotation and meridional displacement of ~5 degrees.

Table *2-1* summarizes advantages and disadvantages of various Jupiter atmospheric locations as far as being optimal candidates for a WindBot mission scenario.

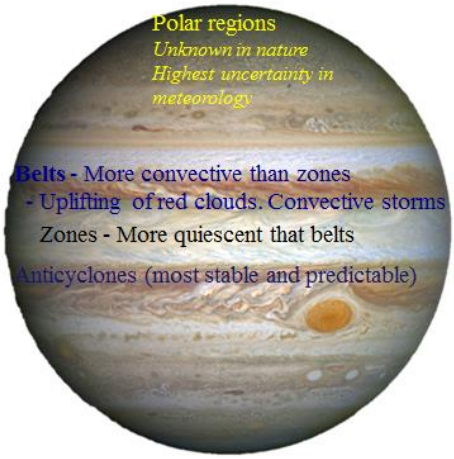

Figure 2-9: Jupiter Polar Regions, Belts, Zones and Anti-Cyclones.

Table 2-1: Location, advantage and disadvantage (both scientific and technological) of having a WindBot in different atmospheric area on Jupiter.

Location	Advantage	Disadvantage
Belts	Storms, convection, and small scale updrafts: • More interesting scientifically • Possible use of thermals for gliding	• Storms can make flight more difficult • Slower circumnavigation
Zones	• More quiescent than belts, favorable to conventional flyers • Large scale upwelling (~10^{-3} m/s) • Fast circumnavigation	• Unknown vertical structure
Anti-Cyclones	• Most stable and predictable part of the atmosphere • Vertical circulation favorable to gliding	• Significant power may be required to navigate out of the vortex
Temperate and Polar Regions	Scientifically interesting: • Data are very scarce • Important in the study of meridional energy transfer	• Least known atmospheric conditions

2.4 WindBot Mission Concept Science Goals and Instruments

2.4.1 In-situ Atmospheric Science, Scientific Goals for First Missions

Scientific goals for long-term in situ exploration of Jupiter may be summarized as follows:

- Atmospheric composition
  - Determining abundance of key elements of interests, in particular of oxygen (O), which was missing in the Galileo probe measurements.
  - Better understanding of Jupiter's composition will have considerable impact on our ideas of solar system evolution and planet formation.
- **Clouds and condensibles** (NH_3, H_2S, H_2O)
  - Due to Galileo probe's unique entry point (5 µm hot spot) no clouds and their properties were observed.
- **Dynamics and vertical shear**
  - Direct Galileo probe observations are not representative for the general Jovian atmosphere. Vertical structure and dynamics of upper troposphere might be different than in the 5 µm hot spot.
- **Thermal structure**
  - The roles of heat budget, static stability, cloud condensation in the Jovian atmospheric dynamics are largely unknown.

2.4.2 Instruments

The instruments suite should measure chemical composition (e.g., oxygen), thermal structure, observe clouds, vertical structure and dynamics of the Jovian atmosphere.

Atmospheric structure instrument group measuring temperature, pressure and deceleration

- Mass: 0.54 kg -- Power (avg): 3.8 W

Neutral mass spectrometer for measuring atmosphere composition

- Mass: 13.2 kg -- Power (avg): 13.0 W

Helium abundance detector

- Mass: 1.4 kg -- Power (avg): 0.9 W

Nephelometer for measuring cloud parameters and cloud location

- Mass: 4.4 kg -- Power (avg): 11.3 W

Net-flux radiometer for measuring solar/planetary radiative flux in the atmosphere

- Mass: 3.134 kg

Energetic particle detector

Lightning/radio-emission instrument

- Mass: 2.5 kg -- Power (avg): 3.0 W

The priority is to measure temperature, pressure, atmosphere composition, clouds parameters, energy particle detectors and lightning. One may have different instruments on different WindBots; an average science package (for a total of two or more) may be of 10 to 25 kg with 35 W each.

2.5 WindBot Mission Concept: Jupiter's Great Red Spot

Jupiter's Great Red Spot represents an exploration target of high scientific importance, as well as a fascinating subject for public engagement. The JunoCam instrument on the Juno spacecraft will take pictures of Jovian atmospheric features selected by public vote and most likely the attention will be directed at this iconic storm in Jupiter's atmosphere. Other experiments of the Juno mission such as the microwave radiometer and the gravity experiment will make observations of this perpetual, but changing, anti-cyclonic zone in an effort to understand its structure, formation and evolution. For years the Great Red Spot has shrunk continuously with variable rates and also became more circular, while its color has become more orange than red. A WB in-situ mission could be the only way to understand why this fascinating phenomenon is present and how it is evolving.

A WBs mission to Jupiter would operate in the 125km vertical region between 0.3 bar and 10 bar. The WB vertically profile this region, gathering data on the thermal and atmospheric structure as well as the wind speeds and compositions, per the scientific goals outlined in Section 2.4.

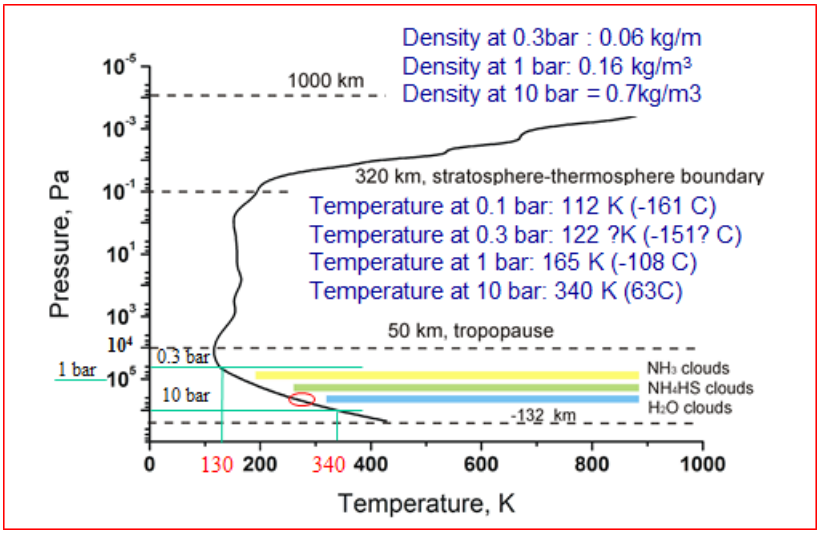

Figure 2-10: Region of interest for WindBot mission concept with relevant boundary atmospheric data.

The Great Red Spot offers atmospheric stability as well as the potential for large updrafts. Cyclonic updrafts have been observed on Earth and explored in Section 5.1 for their ability to maintain altitude of a WB. Similar structures are predicted in the Jovian equivalent, further substantiated by the high levels of ammonia in the GRS, typically indicative of upwelling [2]. The WBs would remain on the rim of the GRS, flying around the center with a period of approximately four days to take advantage of the updrafts.

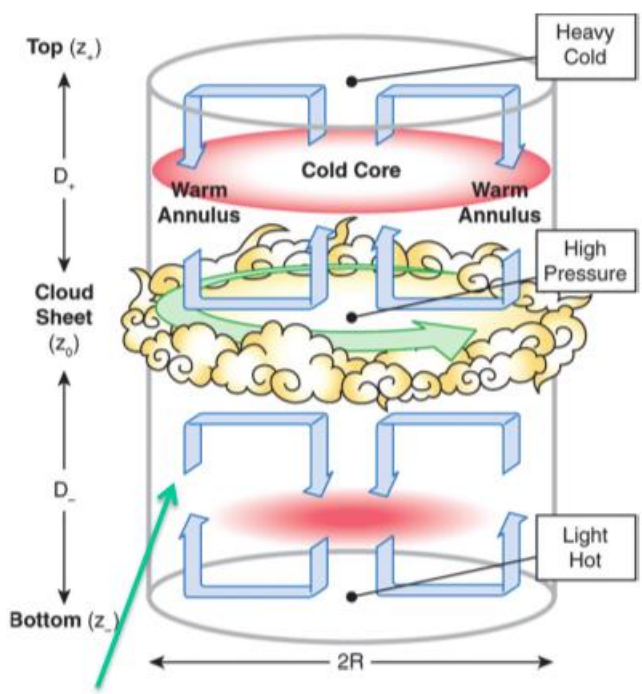

Figure 2-11: Model for cyclone demonstrating upwelling on rim.

An example of a network of wind-driven mobile sensors is “Gone with the Wind on Mars” (GOWON), proposed for studying the surface of Mars using a wind-driven network of mobile sensors. GOWON was envisioned to be a scalable, 100% self-energy-generating and distributed system that allows in-situ

mapping of a wide range of phenomena in a much larger portion of the surface of Mars compared to earlier missions [24]. The GOWON concept is illustrated in Figure 2-12. For more details and for design aspects of the Moballs see published papers and patents [93-96]

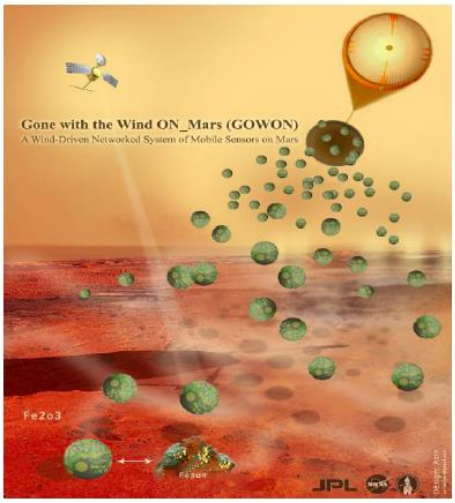

Figure 2-12: Gone with the Wind on Mars (GOWON) concept.

In a notional Jupiter-scale Network of Windbots (NOW) the distances between WB would be quite large, of the order of kilometers or more. NOW would deploy several WBs into the GRS, operating in different regions to provide a spatial distribution of simultaneous measurements. NOW would remain in the atmosphere for approximately one year, gathering power using in-situ resources. From the technologies discussed in this report, a combination of a buoyancy-driven aerostat and vibrational generator would comprise the WB deployed on Jupiter. The buoyancy-driven aerostat provides the greatest level of control without the need for long, extended systems or excessive power used for control. In addition, it is the technology that most readily may vertically profile the atmosphere.

Vibrational generators are chosen to provide power due to their self-contained mechanism without the need for external components as well as ability to rapidly store incident energy and produce a steady stream of electrical power. They may also scale their power most readily for the size of the mission.

3 Mobility in the Jovian Atmosphere

We consider two main design approaches (and hybrids from their combination) to maintain altitude within a range: aerostats and wing-based aerodynes. This chapter provides a high-level analysis for a number of alternatives, estimating feasibility based on preliminary calculations, discusses advantages and disadvantages and needed work and simulations needed to further evaluate feasibility.

3.1 Buoyancy Control

We examine buoyancy control in the context of Figure 3-1 which illustrates the forces acting on a WindBot when simplified as a point mass system.

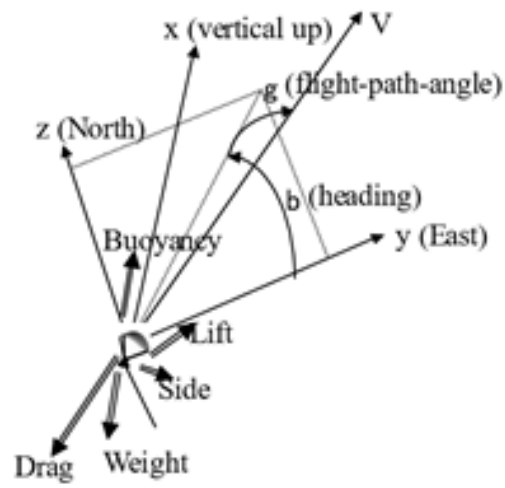

Figure 3-1: Forces acting on point mass system on wind axes.

The equation for buoyancy (where *B* is the buoyant force, ρ_a is the atmospheric density around the WB, *V* is the volume occupied by the WindBot, $\boldsymbol{m_p}$ is mass of the payload, and *g* is the gravitational acceleration characteristic of the planet is given below, see insert):

$$\frac{B}{g} = m_p + \rho_a(V_0 + \delta V)[1 - \frac{M_g T_a}{M_a T_g}(1 + \frac{\delta p}{p_a})]$$

3.1.1 Buoyancy Control Equations

Buoyancy is given by:

$$B = \rho_a V g$$

At the equilibrium of the forces along the vertical axes, buoyancy equals the gravitational force (weight), we obtain:

$$\frac{B}{g} = \rho_a V = m_e + m_g + m_p$$

$$m_e + m_p = \rho_a V - m_g = \rho_a V - \rho_g V = (\rho_a - \rho_g)V$$

where m_e is mass of the balloon envelope, m_p is mass of the payload, and m_g is the mass of the gas inside the envelope.

Invoking ideal gas thermodynamics, we obtain:

$$m_e + m_p = V\left(\frac{p_a M_a}{RT_a}\right) - V\left(\frac{p_g M_g}{RT_g}\right) = V\left(\frac{p_a M_a}{RT_a}\right)(1 - \frac{p_g M_g T_a}{p_g M_g T_g}$$

The total pressure is the ambient pressure plus the super pressure δp. The total volume is $V = V_0 + \delta V$, so we obtain:

$$\frac{B}{g} = m_p + \rho_a(V_0 + \delta V)[1 - \frac{M_g T_a}{M_a T_g}(1 + \frac{\delta p}{p_a})$$

There are several control variables for buoyancy: the volume differential $\boldsymbol{\delta V}$, the pressure differential $\boldsymbol{\delta p}$, the gas molecular weight $\boldsymbol{M_g}$, the gas temperature $\boldsymbol{T_g}$, mass of the payload, $\boldsymbol{m_p}$ leading to the following buoyancy control modes:

- Buoyancy control based on $\boldsymbol{\delta V}$: this type of control would rely on changing the volume – implicitly the geometry of the envelope. This change can take place by pulling risers, or by inflating and deflating internal "ballonets";
- Buoyancy control based on $\boldsymbol{\delta p}$: this type of control would rely on varying the pressure of the gas inside the envelope. Commonly done for super pressure balloons;
- Buoyancy control based on $\boldsymbol{M_g}$**:** this type of control would rely on changing the properties of the gas, possibly by a phase-transition. This could also be performed by including a vent at the top of the balloon envelope to vent off extra gas.
- Buoyancy control based on $\boldsymbol{T_g}$**:** this type of control is based on changing the gas temperature. This can be accomplished through the use of heating elements inside the gas chamber, or through use of radiative heating from the sun or infrared radiation from Jupiter.
- Buoyancy control via $\boldsymbol{m_p}$***:*** This type of control requires weight shedding; it is also known as ballast control. This takes the form of dropping available weight to increase buoyancy potential through payload mass being decreased.

In addition, the control mechanisms will increase payload and power consumption of the WB.

3.2 Aerostats

One way to achieve buoyancy is to use a buoyant that is lighter than the atmospheric gas outside the envelope. On Earth, a common choice is to use helium or hydrogen balloons or airships. An alternative is to use heated gas balloons, as when ambient atmospheric gas is heated (according to ideal gas laws, other parameters held constant), the gas becomes less dense than that the one in the surrounding environment, thus generating lift. A different way to reduce density is to extract the gas creating vacuum chambers. For reference, the density on Jupiter at 1 bar is 0.16 kg/m^3 (at T = 165 K) compared to 1.20 kg/m^3 on Earth (at T = 293K).

Airships can achieve directional mobility like an airplane, using control surfaces. This provides a way to navigate the atmosphere with a directional drive mechanism – at the price of power consumption. A different way, potentially more efficient energetically is to use a tethered winged system that can provide lateral mobility. A few alternatives are analyzed in the following.

3.2.1 Montgolfières (Heated Gas)

Montgolfière aerostats generate buoyancy through the isobaric heating of ambient gas within a balloon envelope. A simple example of this design is a hot air balloon. Because of power and fuel constraints it quickly becomes unfeasible to bring fuel to burn, or electrically heat the gas inside the envelope. Passive heating provides the best solution to keep such a system sustained in the atmosphere.

Solar Infrared Mongolfière Aerobots (SIRMAs) are an example of passive heating, using a combination of lower planetary infrared heating during the night and solar heating during the day [25], as depicted in Figure 3-2 and detailed in a previous JPL study [25]. For a Jupiter mission in which: a) Floats at about 0.1 bar during the day; b) Descends to about 0.2 bar at night (Figure 3-3), and c) uses a ~50km long tether to float payload beneath cloud layer, the SIRMA balloon would have 60m diameter and weight 112 kg of total floating mass to support a 10 kg payload (see Figure 3-4 for other planets payload masses).

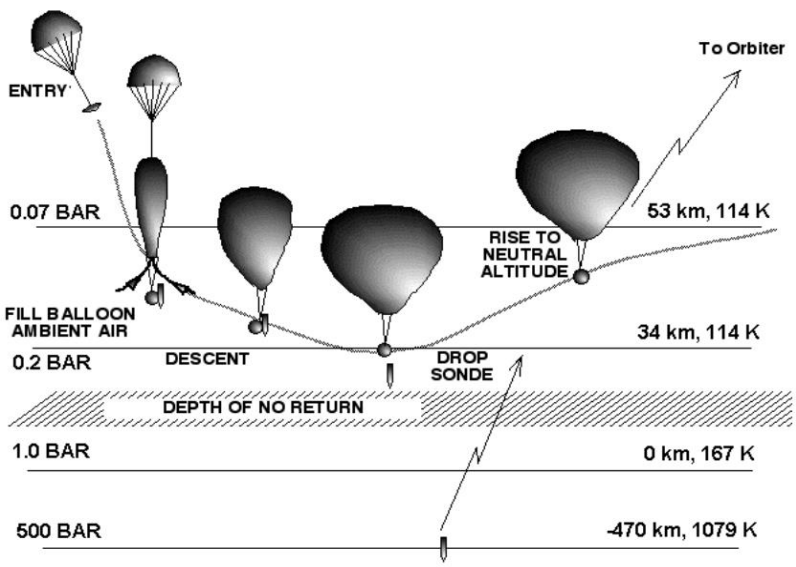

Figure 3-2: SIRMA balloon in Jupiter atmosphere (NASA JPL). [25]

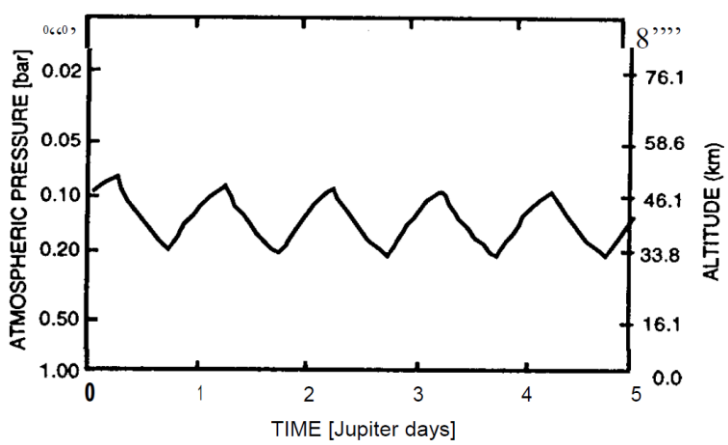

Figure 3-3: SIRMA flight pattern simulation when undergoing solar heating (upward trends), and Infrared heating (downward trends) [25].

There is a point of no return, below which the balloon will not rise again with the Sun. This occurs because the thick atmosphere limits solar radiation deeper in the atmosphere.

The SIRMA envelope material requires a material that has a high ratio of absorptivity to emissivity, maximizing radiative energy absorbed and stored by the balloon. The material used in [25] was a combination of a different top and bottom. The top of the baloon was mylar with Kevlar scrim, and had a 6-µm Titanium coating to maximize solar absorptivity (0.95), while minimizing radiative emissivity (0.2). The bottom half of the balloon was tailored primarily to gather all available IR radiation and took the form of a carbon coated black surface with high absorptivity (0.95) and emissivity (0.95). **The balloon had a diameter of ~60m with an interior temperature of 120±5 K, and an envelope mass of 85kg.**

This system utilized two 50km long PBO (polybenzoxazole) high-tensile strength tethers to carry scientific payload of up to 10kg beneath the cloud layer. This SIRMA design was partially based on a concept tested in the late 1970s through the 1980s for in-situ data collection of the upper stratosphere of earth. The concept proved to be extremely effective, with one flight lasting 69 days while carrying a payload of 50 kg. The balloon envelope was composed of aluminized Mylar on the top hemisphere of the balloon and a transparent polyethylene on the bottom [26].

Initial filling and heating of the balloon is a problem that requires future work. The main concern is that the incident Solar/IR radiation is only sufficient to maintain altitude of the baloon. This means that as the balloon descends and fills with ambient gas, it may not have enough time to gather enough heat to generate adequate buoyancy. A potential solution for this problem utilizes heating from atmospheric entry to heat the gas inside the balloon envelope, providing a temperature stimulus before Solar/IR heating can begin to take effect.

Planet	Solar AU	System wt., kg	Diameter, m	Atmospheric molecular wt.	Axis Inclination
Jupiter	5.20	112.2	60.1	2.25	3°
Saturn	9.54	219.7	86.1	2.10	27°
Uranus	19.18	278.1	97.4	2.64	82°
Neptune	30.06	842.4	171.6	2.62	29°

Assumptions: Daytime float altitude = 0.1 bar
Balloon envelope = 6-micron polymer composite with 50% weight margin
Science payload = 10 kg

Figure 3-4: SIRMA balloon configurations on different Gas Giants [3.4].

An advantage of using the Montgolfière balloon concept is the balloon is filled with ambient atmospheric gas, mitigating the need for a heavy pressure vessel to house pure hydrogen gas. This greatly reduces payload weight (and for example maximizes instrumentation potential as well as lowering costs associated with payload delivery.) This type of hot air balloon is relatively robust and pinholes and punctures do not rapidly and disruptively affect the performance, since the balloon is filled with ambient gas.

Montgolfière can perform buoyancy control by venting off hot gas or by changing the volume of the envelope to decrease buoyancy. Positive buoyancy would be achieved through internal heat beyond the equilibrium temperature.

3.2.2 Charlière (Hydrogen – Lighter Gas)

A Charlière uses an inside gas that is less dense than that of the surrounding ambient. As the Jovian atmosphere is composed primarily of hydrogen, a large quantity is required to keep even a relatively small payload aloft. Jupiter's atmosphere estimates range from 86–90% hydrogen. For the following calculations, it is assumed that the atmospheric composition is a simple 90% Hydrogen, 10% Helium model. This allows for a safety factor to be implemented into the design consideration.

Assuming an initial overall WB mass target of 40 kg (as the sum between structural mass and payload mass) , the balloon diameter and resultant effective payload mass for different locations in the Jovian atmosphere are tabled in Table 3-2, while the equations used to generate the table are found in the following insert [27]**.**

Charlière Analysis

The following analysis is for a zero-pressure balloon configuration assuming inside pressure and temperature conditions are equal to those outside of the balloon. Other factors such as changes in atmospheric density, and radiative heating are not included. Further calculations and models are required to understand the full effects of the radiation-rich environment on buoyancy characteristics such as internal temperature. In addition, an atmospheric composition of 90% hydrogen and 9% helium is assumed.

Considering the gravity independent equation of buoyancy it is possible to determine total mass payload available from total envelope volume (V), and densities of the Jupiter atmosphere (ρ_a) and Hydrogen gas (ρ_{H_2}):

$$m_{total} = V(\rho_a - \rho_{H_2})$$

To determine atmospheric density as well as hydrogen gas density, the ideal gas equation must be used. This requires the temperature and pressure to be known.

$$pV = nRT$$

Where n represents the mole number, defined as mass (m) over molecular mass (M).

To simplify calculations, the ideal gas constant (R) and the molecular mass (M) are equated to one value: the specific ideal gas constant (R_{sp}). The values of R_{sp} for Hydrogen and Helium are 4124 ($\frac{J}{kg \cdot K}$) and 2077 ($\frac{J}{kg \cdot K}$) respectfully.

$$R_{sp} = \frac{R}{M}$$

The ideal gas equation then takes the following form.

$$pV = mR_{sp}T$$

To further simplify calculations, density is found from mass and volume.

$$\rho = \frac{m}{V}$$

The resulting ideal gas equation takes the following forms in pressure, then in density. From here Density of Hydrogen gas and Helium gas can easily be found with given temperature and pressure.

$$p = \rho R_{sp} T$$
$$\rho = \frac{p}{R_{sp} T}$$

The atmospheric density is calculated from the 90% Hydrogen, 9% Helium model using the following equation.

$$\rho_a = \rho_{H_2}(0.9) + \rho_{He}(0.09)$$

From here, total envelope volume required for a given total mass can be determined.

$$V = \frac{m_{total}}{\rho_a - \rho_{H_2}}$$

Because volume is now known, surface area and envelope diameter can be found. By using envelope material mass per square meter, envelope weight can be found. Envelope mass can be subtracted from total mass, giving a value for weight available for a payload.

To lift 40kg the above equations result in a volume of 693 cubic meters of hydrogen payload, and a resulting mass of **500kg**. The 40kg being the combined mass of structure/envelope and payload, operation at higher pressure allows for a heavier payload as illustrated in Table 3-2.

Table 3-2: Balloon diameter and resultant payload mass for different locations in the Jovian atmosphere

Pressure [bar]	Diameter [m]	Volume [m^3]	Structure/envelope [kg]	Payload [kg]
10	11	693	12.12	27.88
7	12	888	14.3	25.7
4	13.6	1312	18.55	21.448
1	18.6	3405	35.02	4.97
0.5	21.8	5416	47.71	**−7.718**

Working at higher pressure maximizes the payload. As the table illustrates somewhere between 1 and 0.5 bar of Jovian atmospheric pressure, it becomes impossible to sustain a 40 kg system at altitude. Figure 3-5 illustrates the relationship between different balloon diameters and the mass it can lift, for the pressure range of interest, between 0.3 bar and 10 bar.

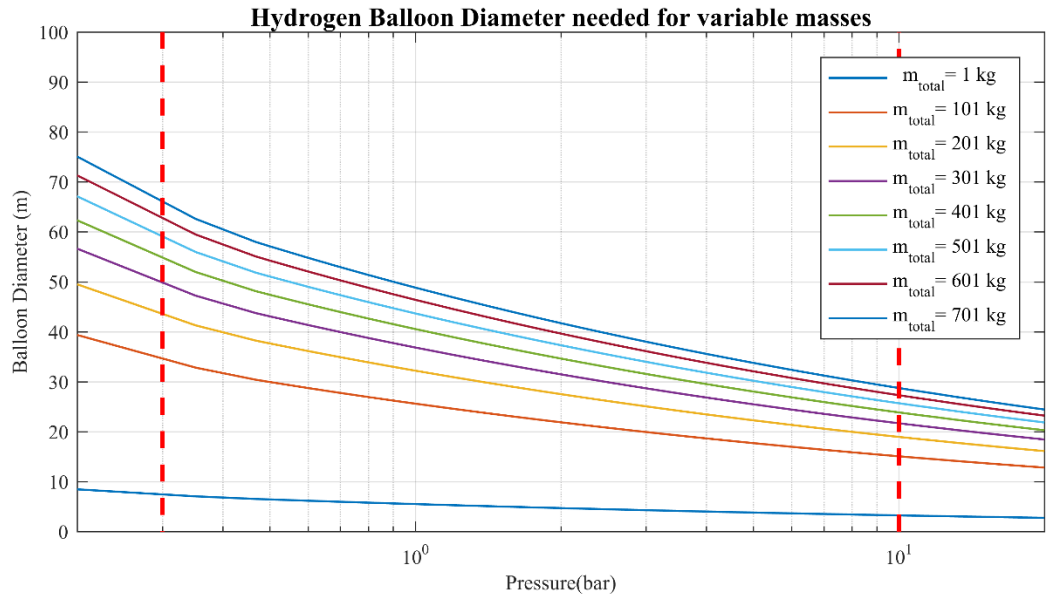

Figure 3-5: Balloon diameter required to hold various masses between 0.3 bar and 10 bar (denoted by dashed red vertical lines).

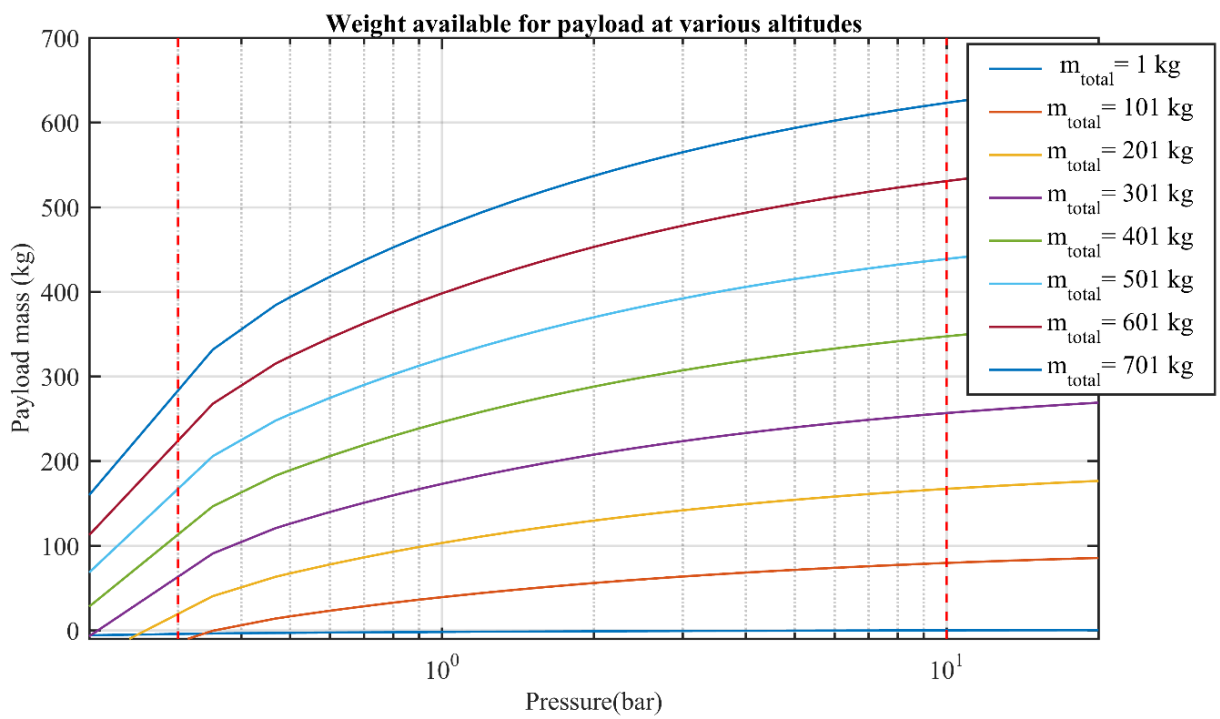

Figure 3-6: Mass available for payload (assuming an envelope surface density of 30g/m^2).

If the mass of 500 kg of hydrogen is stored at 700 bar and 200 K the tanks would be of 6 m^3. The mass of the hydrogen that needs to be brought to Jupiter outweighs the mass of the WB (40kg, without the hydrogen). One requires ~13 kg of hydrogen for every 1 kg of WB total mass (includes envelope and payload).

Several methods may be used to reduce the amount of hydrogen the spacecraft must bring from Earth, for example one could heat the hydrogen, either using an active system or a hybrid Charlière-Montgolfière system. Alternatively, the WB could inflate the balloon during descent if it could process hydrogen out of the atmosphere.

Types of Charlières include:

Zero-pressure balloons (ZPBs): balloons at ambient pressure, as discussed above. Common use in terrestrial weather balloons. Flight pattern is subject to cycling from day to night due to change in radiation environment.

Super-pressure balloons (SPBs): Useful for applications requiring stable flight altitude. Needs future work to investigate ability to stay aloft even with higher internal pressures in the Hydrogen-rich environment.

Rozière balloons: Hybrid Montgolfièr/ Charlière concept. Feasible given a consistent heat source. Potentially useful for maximizing lift without the need to package extra hydrogen gas.

Zeppelins: Advantage lies in control surfaces and navigational abilities. Provides benefits of aerostats with control of airplanes/gliders. If enough electrical power is available, navigation is feasible. However, driving props is a major power consumer and increases weight of the craft. This design also has a large envelope weight, reducing payload potential.

The balloon detailed in this section require a zero-pressure variation. Super-pressure balloons were considered, but may not be feasible due to increase in internal gas density associated with pressurizing hydrogen, considering that hydrogen comprises almost the entire atmosphere. Further calculation is necessary to determine what operational pressure and volume gas are required to hold a payload and to better understand how a super-pressure balloon could work at different Jovian altitudes.

The flight pattern of a zero-pressure design is susceptible to changes in environmental conditions, such as heating-cooling cycles from solar energy and atmospheric changes between regions of the atmosphere. Future simulations to understand how the cycles on Jupiter would affect balloon endurance and flight patterns will be performed.

Common means of buoyancy control for a Charlière are primarily ballast mass oriented, but also include ballonets.

3.2.3 Vacuum Aerostat

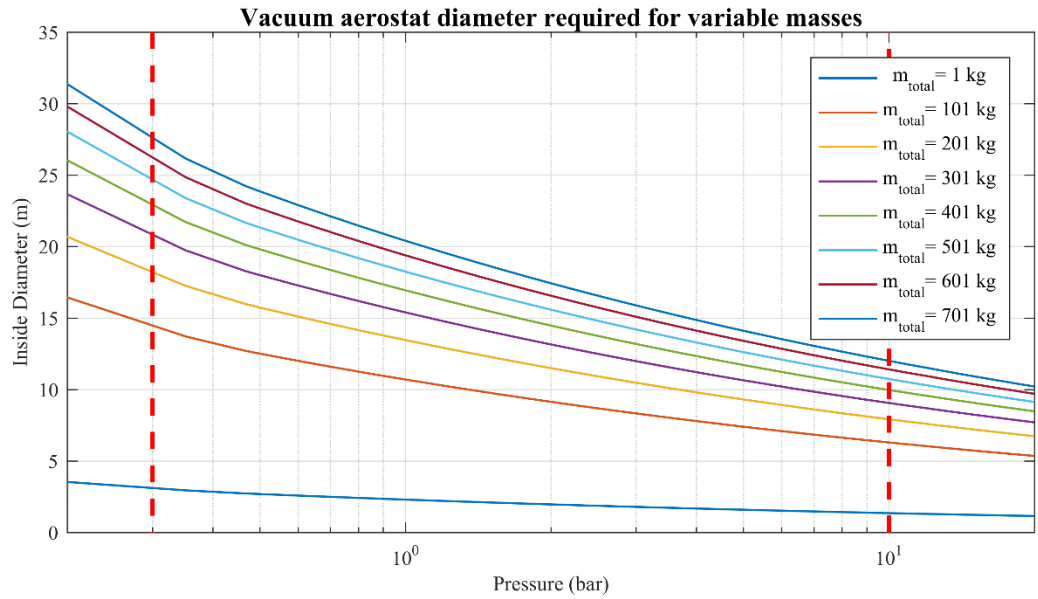

Figure 3-7: Inside diameter of a vacuum chamber required to lift the denoted mass. This includes mass of envelope.

In a hydrogen-dominated atmosphere, one could consider a vacuum balloon type WB [28] (see insert).

Vacuum Aerostat

The operating principle behind a Vacuum Aerostat is that because there is no mass within the structure's envelope, thus displacing pure mass, creating a theoretically efficient means of lift creation. The mass displaced by the vacuum envelope must be equal to the mass of the balloon in an area of the atmosphere in which the ambient Jovian atmospheric pressure will not buckle the structure of the vacuum envelope skin, which presents the largest design challenge of this consideration of technology.

The basic buoyancy equation is:

$$B = \rho_a V g$$

Modified for terms on a mass-density basis:

$$\frac{B}{g} = \rho_a V = m_e + m_p$$

Simple volumetric relation based on mass, density (Valid for spherical model):

$$V = \frac{4}{3}\pi r^3$$

Then, equating vacuum balloon interior radius required to total mass, atmospheric density:

$$r = \sqrt[3]{\left(\frac{m_e + m_p}{\rho_a}\right)\frac{3}{4\pi}}$$

At 0.3 bar (cloud layer) with an atmospheric density of ~0.07 kg/m^3, a 100 kg total mass would require a vacuum envelope with an inside diameter of ~14 m.

The main challenge with a vacuum solution is the buckling due to the external pressure. A homogeneous spherical shell buckles under atmospheric pressure for any known material, as no material has the needed specific stiffness of 4.5×10^5 m^5/(kg s^2) for a Poisson ratio (ν) of 0.33 [29]. A sphere with thin outer and inner layers interconnected by a core layer provides enough specific stiffness to resist buckling due to an atmosphere of pressure while allowing for positive buoyancy using commercially available materials [29].

Recent studies found that a grid-stiffened structure theoretically could achieve positive buoyancy using current materials, specifically carbon fiber struts and a Zylon membrane. Geodesic approximations of a sphere perform a bit worse than a sphere but still could achieve positive buoyancy, with Weight/Buoyancy ratio of 0.94. An icosahedron achieves better performance than more complicated shapes due to symmetry and sparse structure [30]. The structural response of an icosahedron type LTAV is characterized by large displacements, where membrane behavior dominates the icosahedral skin response, generating geometric stiffening in the overall structure.

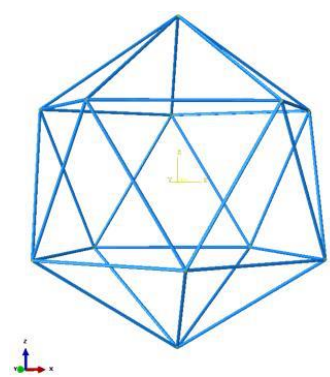

Figure 3-8: Icosahedron structure [3.11].

Figure 3-9 demonstrates some buckling modes. These deflections have no more than 4% reduction in buoyancy. This structure is theoretically feasible but currently has not been developed into a working prototype [31]. Dynamic analysis of the structure using finite elements of the icosahedron structure revealed that chaotic motion is present in the frame of the icosahedron under certain loads and boundary conditions [32].

Buoyancy control through the vacuum aerostat is somewhat limited considering the chamber would most likely be rigid. Main forms would most likely include a dispensable mass ballast that would be dropped for a buoyancy increase.

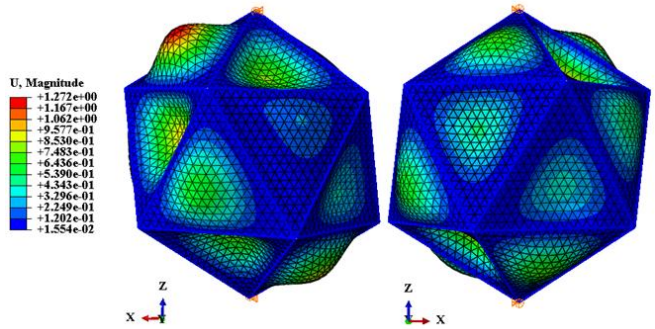

(a) Mode 1: P_{crit} = 6.98 *Pa*

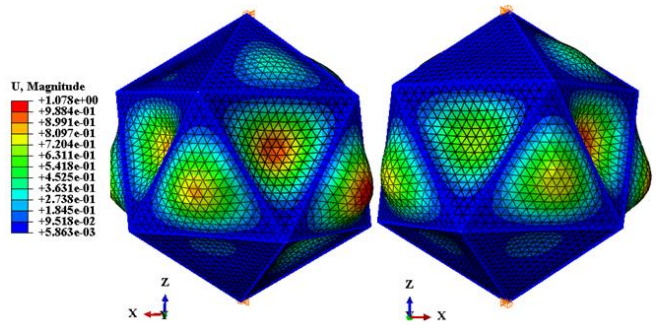

(b) Mode 2: P_{crit} = 7.26 *Pa*

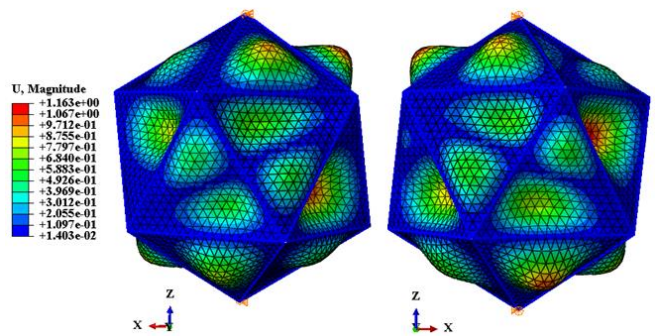

(c) Mode 14: P_{crit} = 20.5 *Pa*

Figure 3-9: Buckling modes of icosahedron shape of vacuum balloon.

3.2.4 Wing-Based Flight Control of Aerostats

Most designs of Aerostats lack the ability to achieve flight control (aside from varying buoyancy). Zeppelins can have directional control through the use of a thrust system to power the craft through the air, utilizing horizontal and vertical stabilizers to control flight paths. This requires a thrust system with large power requirements, making it less appealing to power-aware Jovian WBs.

A potential solution to achieve low-power lateral flight control is to utilize a tethered wing assembly with the Aerostat (as shown in Figure 3-10). A Balloon Guidance System (BGS) was studied as part of the DARE platform introduced in a previous NIAC study. This BGS would utilize potential wind gradients between

the balloon envelope and the wing to tension the tether and to allow for steering control with the wing. The assembly would effectively "drag" the balloon from side to side through the wind currents. [58] The level of control achieved, although not as good as that of an airplane, allows steering to areas of interest within the atmosphere. The balloon would drift with the wind, but the steering would allow navigation within the wind current, subject to relative wind velocity.

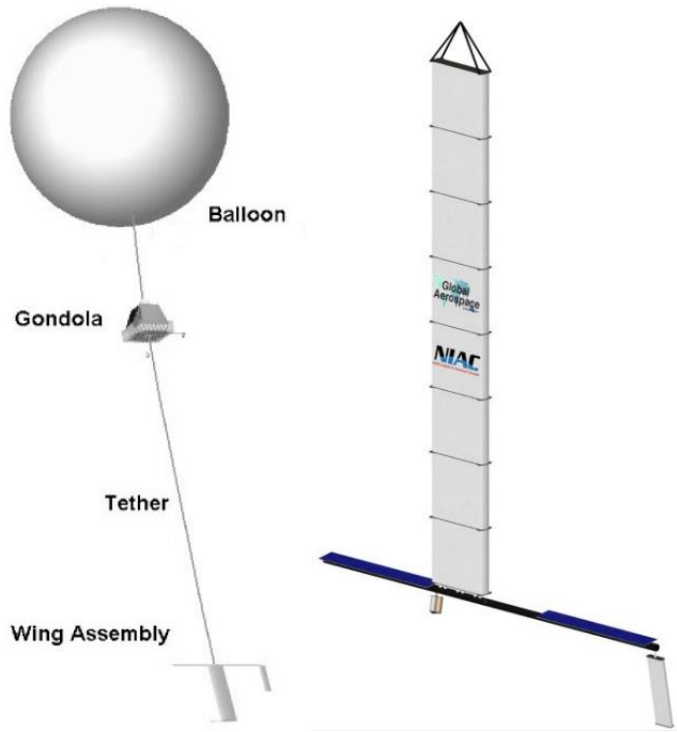

Figure 3-10: Left shows configuration between wing assembly, payload, and balloon. The right shows the detail of a potential single-wing guidance assembly studied for the DARE platform [33].

The BGS platform can be used on any type of aerostat, giving use to all outlined solutions for an aerostatic WB. Having been successfully tested, this system is indeed a viable solution for guidance control for a WB under understood conditions. While this platform has been studied extensively for applications for Mars and Venus, work is required for applications for Jupiter to determine maneuverability and navigation potential [33]. These future studies would require scaling design parameters and relating to the Jupiter environment.

3.2.5 Buoyancy Driven Winged Aerostat

The descending motion of a winged glider induces airflow over its airfoils resulting in horizontal movement. Typical gliders descend through the atmosphere, a device with buoyancy control may glide in both ascending and descending modes. This technology has been used extensively in autonomous underwater vehicles (AUVs), achieving long duration gliding and navigation by actively controlling buoyancy characteristics. While negatively buoyant, they glide down to a prescribed depth, where they become positively buoyant and glide back up to the surface (Figure 3-11). These AUVs take advantage of thermal gradients within the ocean to power their buoyancy engines and actuate the gliding motion. Underwater gliders use active controls to power themselves for hours, over extended duration (several months and thousands of kilometers [34]).

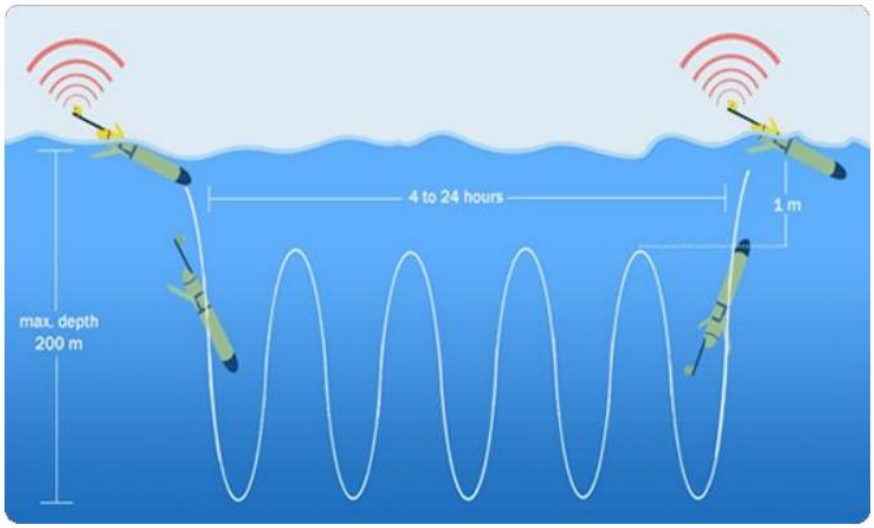

Figure 3-11: Sinusoidal profile of flight path for underwater glider AUV, similar flight path would be used for atmospheric applications [35].

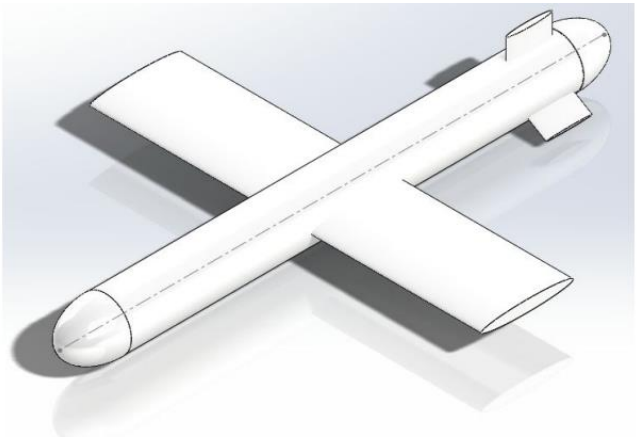

Figure 3-12: Basic configuration used for AUV technology, fuselage would be converted to Aerostat body to be usable for atmospheric flight [35].

One can imagine an aerostat-glider hybrid designed for long duration flight; the aerostat to provide the buoyancy. The aerostat would be built into a rigid, lightweight body, much like a zeppelin. Wings mounted to the side of the zeppelin produce horizontal motion as the zeppelin's buoyancy is changed and the craft either ascends or descends. This passive drive system gives mobility to the WB lacking in other aerostatic devices. In addition, the wings allow the WB to have control over attitude and heading in the atmosphere, enabling targeting of specific regions which could be harvested electrical energy (Fig. 3-12).

A buoyancy-driven aerostat would be able to perform vertical sampling of the atmosphere while having significantly lower power consumption than a powered craft. Depending on the method of actuation, it appears feasible within the power levels that a WB could store during a glide (downwards) before recharging and being lifted again (by an updraft). Possible methods of achieving buoyancy control include storing a heavy gas in a rigid vessel at pressure and using it to displace the buoyant gas or a thermal system taking advantage of incident solar heating (Montgolfière) or the natural thermal gradient in the atmosphere. Flight ranges for the vehicle would be carefully chosen to prevent collapse of the vehicle at high pressures.

While extensive work for buoyancy-driven gliders has been undertaken for underwater applications, a similar concept for autonomous atmospheric flight has yet to be tested. Such a proposed vehicle but for a planet with dense atmosphere (Titan), Shape Change Actuated, Low Altitude Robotic Soarers (SCALARS) [99] was proposed as an appealing alternative to more conventional vehicle technology. SCALARS are buoyancy driven atmospheric gliders with a twin-hulled, inboard wing configuration. The inboard wing generates lift, which propels the vehicle forward.

3.2.6 Aerostats Summary

Atmospheric gas aerostats use ambient gas to fill the balloon envelope, forgoing the need to bring hydrogen. The aerostat passively generates lift when heated by solar radiation or from planet infrared emission. The up-down cycles have a limit which when exceeded the balloon is no longer able to come up. Its payload is relatively reduced payload. Previous studies examined operation at higher altitudes to capture more from solar incident radiation – did not take in consideration operation below clouds (proposed operation was above a limit of 0.2 bar).

Charlière aerostats provide a reliable lifting mechanism that may be deployed within the WB operating range. Brining pure hydrogen to Jupiter is costly, as the mass of hydrogen needed is roughly an order of magnitude more than the WB mass. It would also be moving up and down as an effect of heating or cooling from the sun or planetary IR radiation

Vacuum aerostats might be the best theoretical alternative for buoyancy, yet buckling is a challenge to current materials and though solutions appear possible they are still to be practically demonstrated.

3.3 Wing-based Design

Several wing-based designs are evaluated in the context of operation on Jupiter.

3.3.1 Ramjet Flyer

A ramjet design or Jupiter was covered in a previous NIAC study [21]. A ramjet relies on a jet engine that uses the movement of the aircraft through the atmosphere to draw in air for combustion. A modified Miniature Reactor Engine (MITEE) nuclear rocket engine operates as a ramjet in planetary atmospheres [36]. MITEE is a compact, ultra-light-weight thermal nuclear rocket which uses hydrogen as the propellant. High-pressure gas is heated by a thermonuclear reactor and passes through a nozzle, which accelerates the flow, and the reaction to this acceleration produces thrust. Figure 3-13 illustrates the concept [21]. The nuclear ramjet could operate for months because the Jovian atmosphere is a virtually unlimited source of propellant, the MITEE nuclear reactor is a (nearly) unlimited power source, and since there are few moving parts, wear should be minimal.

The ramjet used a high speed (1.5 Mach) flight at altitude of 0.1 bar pressure – higher than the proposed altitude for WB; it relied on nuclear power. It appears to be a feasible flier for high altitudes and high speeds, yet not aligned with the WB concept and mission.

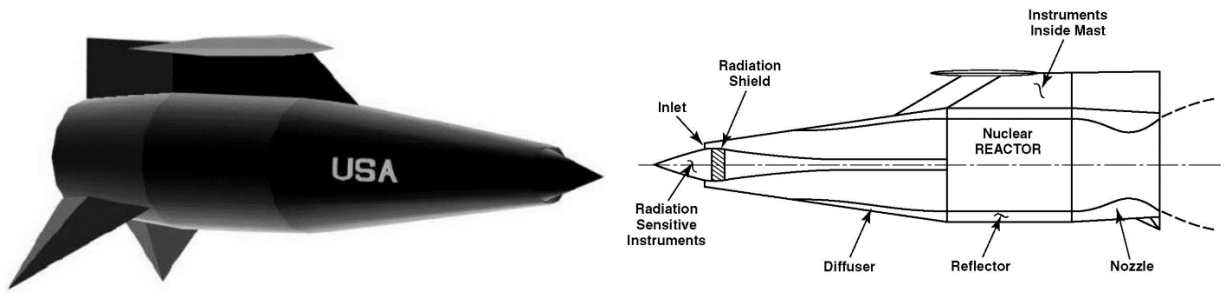

Figure 3-13: RAM JF-6 render concept (left) and technical scheme (right) [3.13].

3.3.2 Flettner Rotor Airplane (Magnus Effect)

A Flettner (rotor) airplane produces lift using rotating cylinders as wings, exploiting the Magnus effect (Figure 3-14) – the upwards force created by the fluid moving with respect to a body spinning along one of its axes, a differential velocity being provided by a propeller or a fan inside the fuselage.

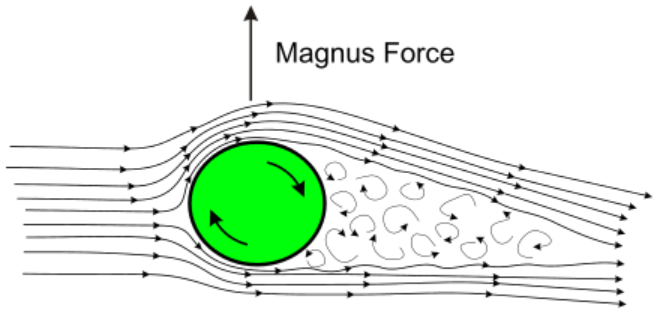

Figure 3-14: Magnus Force created by a fluid moving with respect to a body which is spinning along one of his axis.

To reduce the volume, the wings (cylinders) would be compacted inside the body during transport, and then deployed – by inflation, e.g. with high pressure hydrogen. The cylinders would be driven by a Brushless Direct Current (BLDC) motor inside the fuselage. The torque exerted by those engines is counterbalanced with the lift exerted by the cylinders, thus the center of mass should be behind the wings, closer to the tail.

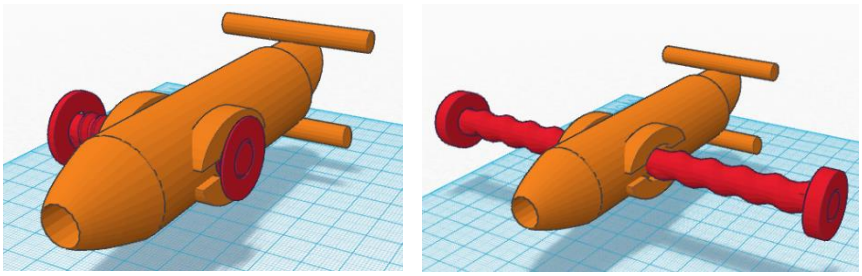

Figure 3-15: Probe Concept extending cylindrical wings.

Kutta-Joukowski theorem states that the lift produced by Magnus effect is equal to $L = \rho\Gamma v = 2\rho v\pi\omega r^2$, where Γ is vortex strength (circulation) and v is ambient flow velocity acting perpendicular to the cylinder.

Some advantages of this concept are:

1. The spinning wing produces more lift than a static airfoil wing at low relative velocity. For example, for a relative velocity of 5.5 m/s, air density of 0.5 kg/m^3 and same surface of 10 m^2 a Magnus effect probe with cylinders rotating at 500 rpm (52 rad/s) would give on Jupiter 37.8 kg of lift, while a conventional airplane with a lift coefficient of 1.2 would lift only 3.7 kg;
2. The gyroscopic effect of the spinning cylinders enables the stability of the probe during updrafts and turbulences;
3. Altitude control may be obtained easily through spin control or forward velocity;
4. Can take heavy loads (Since the Magnus effect works with the square of the radius, doubling the wing radius quadruples the lift to 151.2 kg.)

The disadvantage of this solution is the high amount of power (around 2–3 kW) needed to spin the rotors and for the forward propulsion, although the values are significantly less than that of Ramjet. An adequate energy harvesting mechanism needs to be developed before this concept can be considered feasible for WBs. Another setback is the plane's inability to stay afloat and glide in case of motor shut-off.

3.3.3 Glider

Gliders, or sailplanes, are aircraft with standard aircraft parts, construction, and flight control systems, but without engine – an attractive solution because of the minimal needs for power. Figure 3-16 illustrates one of the best performing commercial gliders with lift over drag ratio of 70 (ETA, left). It also illustrates PERLAN 2, Perlan 2 aircraft is made from composites has 83.83 ft (25.55 m) span wing and a aspect ratio of 27:1.

Figure 3-16: ETA glider and PERLAN 2.

Gliders are always descending relative to the air in which they are flying [37]. To maintain altitude range over long duration missions they use updrafts to increase altitude. On Jupiter, as on Earth, thermal gradients create updrafts. They can also trade the potential energy difference from a higher altitude to a lower altitude to produce kinetic energy.

Two kinds of updrafts are considered: updrafts in jets, specifically using upwelling in bands and updrafts in storms.

The first one is found along Jovian zones and belts. Zones are colder than bands and there is upwelling. Updrafts may be as far as 10,000 km away (estimate in discussions with Prof Ingersoll). Assuming a glide ratio of 80 (very high but theoretically possible), when the WB glides to an updraft from another one 10,000 km away, it would drop 125 km in altitude, the equivalent of the drop from 0.3 bar to 10 bar. After

the drop, using an updraft of 1 m/s, the WB ascend again to the 0.3 bar region (125 km up). There are a lot of assumptions in this scenario, including that the updraft is present for the entire column of air at all altitudes at a given point or within a region where the glider maneuvers, but in general, a glider solution seems possible.

The second type of updrafts are those associated with storms, such as the GRS. To make up for the lack of data about the GRS, an analogy with tropical cyclones on Earth is used to make assumptions. It is possible for a single cyclone to contain several updrafts and for a single updraft to contain several cores [38]. To maintain consistency with these, we estimated that the GRS (30000 km by 12000 km) may have updrafts of 1m/s minimal strength 3000 km apart. [38]). The drop in altitude that needs to be regained is only 37.5 km with the given L/D ratio. Or, if allowed to drop 125 km column, the WB would need a glide ratio of only 24.

This updraft-hopping strategy to stay aloft implies the ability to detect and reach zones of upwelling wind. At least theoretically, this has been examined and shown possible [38] and some recent UAVs flights have proven it on Earth tests as well.

The maximum recorded on Earth glide ratio of 71 was produced by a glider with a wingspan of 30.9 meters. The force needed to sustain flight is three times greater in Jupiter's high gravity.

To achieve similar performance on Jupiter, it requires the same drag mitigation techniques used on Earth, including smooth skin layer, aerodynamic shape, as well as winglets and other design features to reduce induced drag [39]. Long thin wings like those used in high glide ration terrestrial gliders improve lift.

Assuming no turbulence, a glider of aspect ratio AR = 35, total mass of 112 kg, L/D = 40, wing loading = 3 kg/m2, and operating with a coefficient of lift = 1.2 was analyzed for this study by Prof William Engblom, at the 10 bar and 0.3 bar limits of the WB operating range. In the upper limit, the minimum updraft to keep altitude needs to be 1.2 m/s and in the lower limit 0.3 m/s. These numbers are within reason for GRS.

3.3.4 Autorotation Dynamics

Another mechanism examined for use by a WB was autorotation, i.e., the rotation induced on an object moving through fluid – the use of winds to stay afloat [40]. An autogyro, or gyroplane, uses an unpowered rotor in a state of autorotation to develop lift, turning the rotor by forcing moving air through the rotor disc [41]. Assuming the WB can modulate its lift as a rotorcraft, an endurance assessment was carried out, which led to the determination of the endurance (in hours of steady flight) as a function of the system mass (Figure 3-17). The system mass was parameterized as motor mass, battery mass, and payload mass, assuming a power to weight ratio of 2 kW/kg, a 11 kWh/kg battery efficiency (Li battery), a rotor diameter of 10 m, and a typical disk loading of 20. Preliminary results indicate endurance levels of up to 10 hours with a payload mass of 50 kg. While useful for extending the lifetime of a descending probe, the vertical autorotation is not a feasible solution for long endurance WBs.

A possible design with a number of rotors placed along axes in different directions, and pushed by the wind in different directions, may use autorotation not only along the vertical – and hence determine forces that would contribute to WB movement, possibly in a controlled way if the blades have adjustable controls.

3.3.5 Inflato-Glider

Hybrids combining buoyant and wing aerodynamics are a promising yet unexplored area: at extremes are inflatable gliders and winged balloons, which combine buoyancy given by inflatables and control and lift provided by wing surfaces.

Prototypes of inflatable wing gliders have been flown on Earth (Figure 3-17 to 3-21) with an early prototype deployed in the 1950s. Another airship, I2000 [41], had the skeleton of the wings made of inflatable tubes, surrounded with crushable foam to provide the airfoil cross-section. The deployment time was ~0.3s [42]. To maintain suitable wing strength and stiffness, nitrogen gas pressurization at 1380–1725 kPa (200–250 psi) was required.

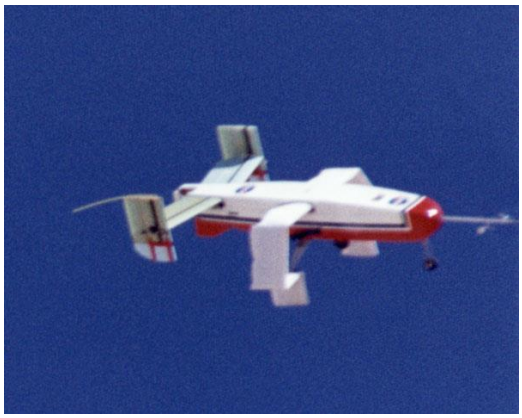

Figure 3-17: I2000, an airship with inflatable wings, successfully test in Earth's atmosphere [42].

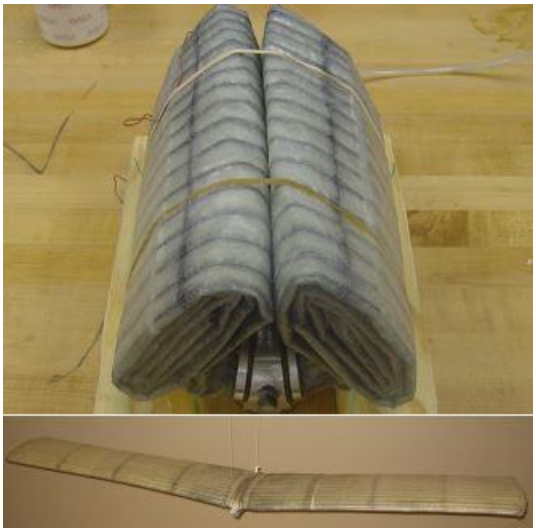

Figure 3-18: Non-Inflated (above) and inflated wings (below) [42].

Figure 3-19: Goodyear Model GA-468 Inflatoplane, 1950s [42].

Figure 3-20: ILC Dover Apteron UAV [42].

More recently, the University of Kentucky created and tested two variants of inflatable wing gliders: inflatable only wings that require constant pressurization to maintain shape and inflatable/rigidizable wings. In the pressurized version, pressure was maintained by gas injections to counter losses. The equivalent density in pressurized wings is increased, which reduces buoyancy. In one experiment the design pressure was 186 kPa (27 psi), though the wing has been successfully flight tested at values down to 52 kPa (7.5 psi) with sufficient wing stiffness for low speed applications [42].

Figure 3-21: ILC Dovers multi-spar inflated wing and packed configuration [42].

Volume reductions of over 60% have been demonstrated for the inflatable wings technology.

4 WindBot Concept Bodies

WindBot bodies would serve multiple roles, providing the overall structure that houses all subsystems; it is what keeps the WB in the atmosphere for the mission. As the volume to transport the WB to Jupiter is constrained, we explore a variety of concepts that allow compact packing, such as through folding mechanisms presented in the following section.

4.1 Foldable – Collapsible/Expandable Structures

People have used foldable structures since at least as early as 200 BC, and over years these have been used for a wide variety of applications, such as architecture and human habitat construction, solar panel arrays and other space applications, art, etc; some examples are given in Figure 4-1 and Figure 4-2.

Figure 4-1: Expandable Structures, example 1. Chinese lanterns. From small packed volume to a larger one after expansion.

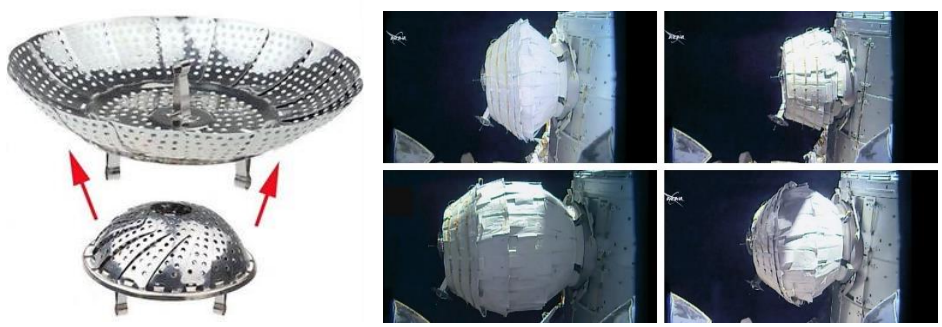

Figure 4-2: Expandable Structures, example 2. Kitchen device and Bigelow, expandable space habitat module.

The main advantages of collapsible structures are packing efficiency and reduced weight. Non-rigid, variable shapes for WB bodies would benefit from better packaging efficiency, important because large flyers need to be compressed at launch. Moreover, shape and volume change provide additional benefits during atmospheric flight. A foldable structure provides opportunities for expanding and actuating control surfaces.

There are two general approaches to foldable structures, distinguished by the shape of the rigid bars and the position of the scissor hinge: the off-center scissor-pair (OSP) developed by Pinero [43] (Figure 4-3) and the Angulated Scissor-Pair (ASP) discovered by Hoberman [44] (Figure 4-4). Each structure relies on three key components: bar, scissor pair, and differentiation of components. Bars are rigid components with fixed length. Scissor-pairs are composed of a pair of identical bar components. Differentiation of components is the manners by which rigid bars are connected through the position of the scissor-hinge assembly and edge-pivots [45]. Optimized collapsibility and structural performance are needed should

this approach be implemented in WBs. A scissor-pair defines a single-degree-of-freedom (SDF) foldable mechanism. The SDF property enables the control of the folding process through the propagation of rotations from one scissor-pair to the next one and vice versa. This principle of propagation is essential because it reduces the control mechanism to one variable, the rotation of only one component.

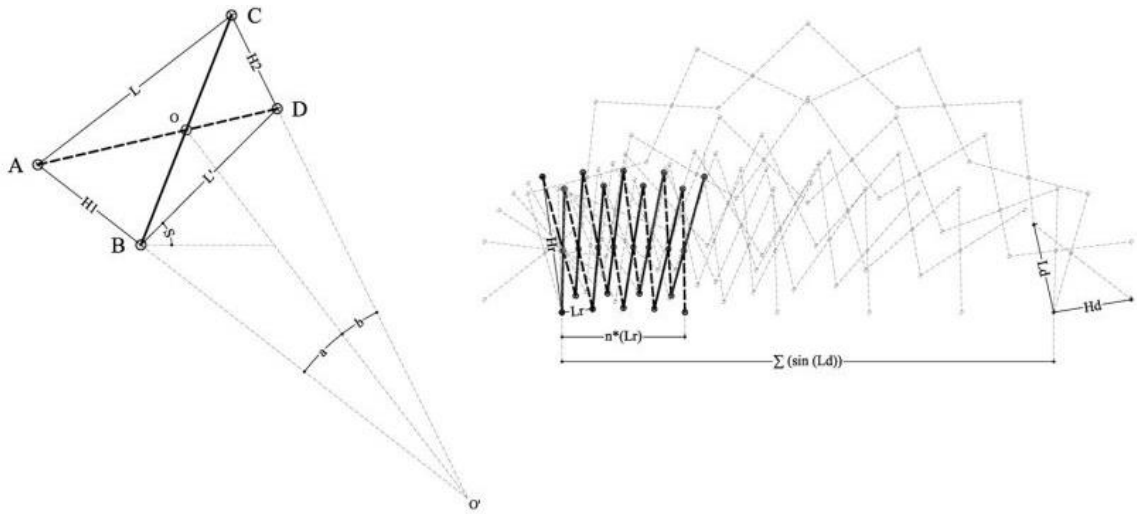

Figure 4-3: Off-center scissor-pair folding process [45].

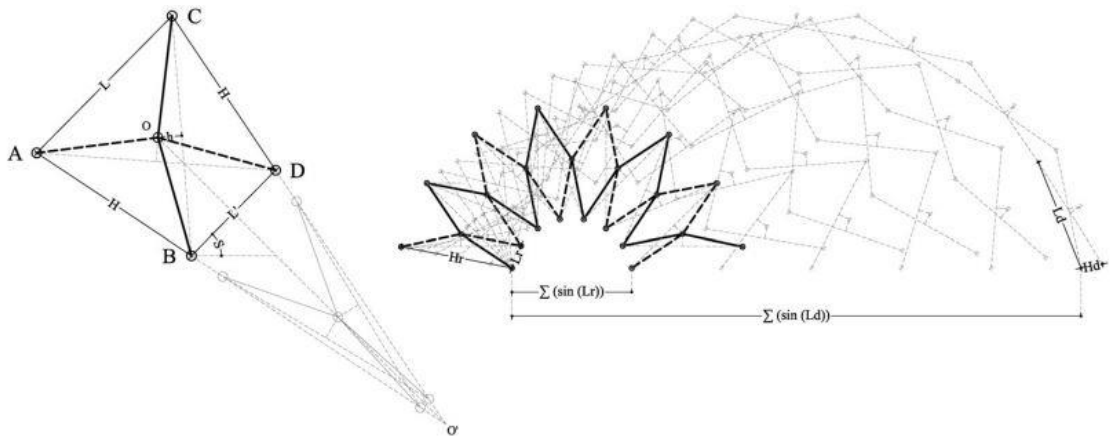

Figure 4-4: Angulated scissor-pair folding process [45].

The main difference is that in ASPs straight bar components are substituted by angulated ones. Now, the system is able to achieve different slopes and curvature, yet the overall shape during folding remains constant [45]. This property generates a homogeneous transformation between retraction and deployment in which all in-between configurations are scaled versions of each other. This scaling transformation offers great advantages since the variation and propagation of heights and lengths are invariable. Thus, it is possible to add components in three-dimensional configurations such as domes, spheres and other types of volumes [44]. The original Hoberman sphere expands its diameter from 9 inches to about 30 inches in diameter, increasing volume by a factor of ~30. Figure 4-5–Figure 4-8 offer examples of man-made structures illustrating this principle.

If the "skeleton" components of such a structure are covered with a material that provides enough encasing to maintain some outside shape and house sensors, it can be made buoyant and turned into a balloon-like polyhedral probe with rigid edges.

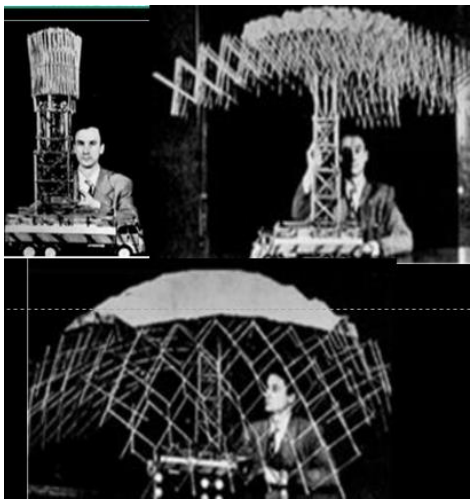

Figure 4-5: Pinero's transformable shell.

Figure 4-6: Expandable Structure, example 2.

Figure 4-7: Expandable Structure, example 3, Hoberman principle.

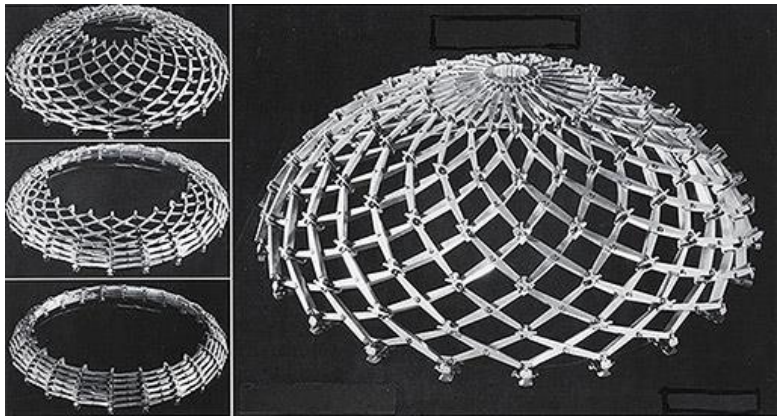

Figure 4-8: Expandable Structure, example 4, Hoberman principle.

Entirely forgoing the folding bars and thus achieving the collapse only by the cover material is also possible and can yield a design similar to Figure 4-9 [46]. The top three images show the Hoberman-like sphere and the bottom three are the Buckliball at corresponding stages of collapse.

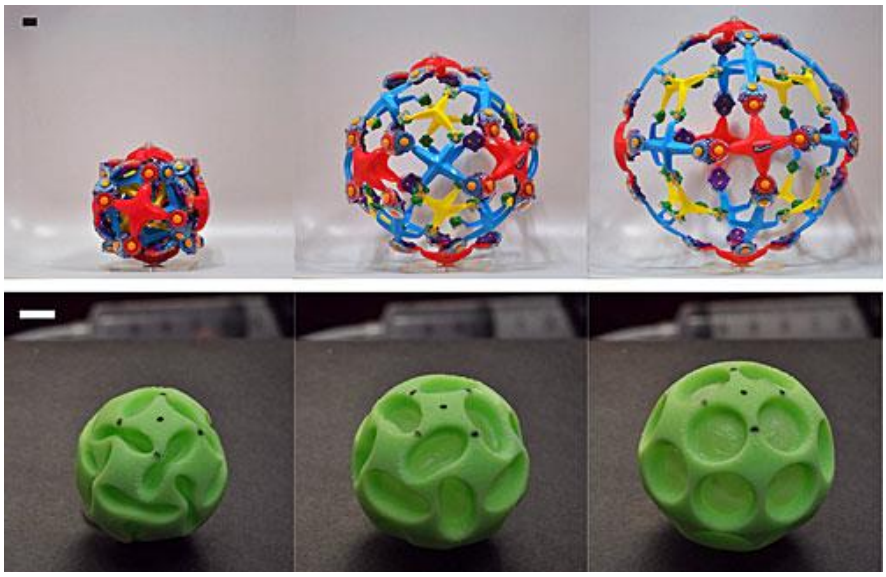

Figure 4-9: Buckliball – 3D origami like structure that collapses to 46% its original size [46].

A Buckliball pictured in Figure 4-9 is a unique structure made of soft rubber with no moving parts inside. The bars forming the skeleton of a traditional collapsible structure are substituted by 24 “dimples” on its surface. Sucking air out induces distributed loading, causing buckling and collapse of the ligaments between the dimples until the ball is 46% of its original size. This technology relies on a single pressure impulse and takes advantage of a reversible buckling-induced collapse. A WB of this design would be confined to a small volume during interplanetary transport. Upon removal of a constrictive shell after insertion into atmosphere, the structure will expand and fill with ambient gas, proceeding to operate as a balloon.

4.2 Foldable Structures Combined with Complex Shells in Airships

Combining foldable structures with complex shells provides new variable buoyancy solutions, such as Michael Levin's vacuum airship, seen in Figure 4-10.

Figure 4-10: Michael Levin's vacuum airship.

The concept of a balloon-like floating body that has separate compartments allows for WindBots to be mobile by means of changing pressure inside chambers by a system of valves. Advantage of such structures is their ability to maneuver and potentially change shape, if material with correct rigidity is chosen. There exists an inflatable wing design that relies on splitting the wing into chambers which are inflated separately to allow more control over the morphing. Section 4.4 of this chapter describes the morphing mechanism in more depth.

4.3 Tumbleweed

Tumbleweeds are inflatable wind-directed robots that have been well tested in extreme terrestrial environments by NASA JPL [47]. They house sensors inside their inflated interior which also provides mechanical and thermal protection and gather data on their environment as they tumble.

A system diagram showing the Inflatable Tumbleweed internal components is reported in Figure 4-11.

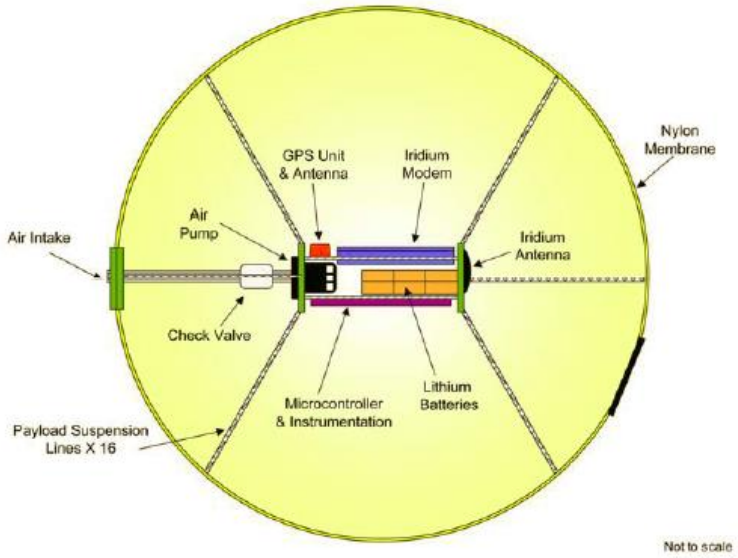

Figure 4-11: A system diagram showing the Inflatable Tumbleweed internal components.

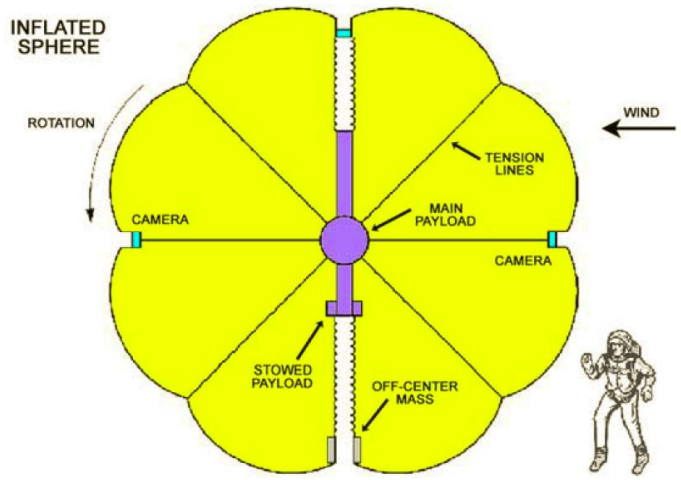

Figure 4-12: A system diagram showing Inflatable tumbleweed [47].

An example of a Tumbleweed concept refers to a ball 1.5 meters in diameter which has the capability to roll over sand dunes, boulders, and even bushes [47]. In its current state, a tumbleweed is optimized for long-range autonomous operations in remote and hazardous environments. The design stresses simplicity, robustness, lightweight, low volume (for spacecraft delivery), and low power [48].

The Tumbleweed can carry 20–30 kg of payload for hundreds of kilometers. It is propelled by winds and does not have control over its direction of travel. Tools for the mission are housed inside an inflated membrane. If surroundings are cold, the components can remain warm from heat generated by running electronics and an internal air pump [48]. A Tumbleweed concept has been tested in Antarctica and performed well over the course of eight days (Figure 4-13). It covered over 130 km in less than 48 hours. Due to its success, the Tumbleweed design has been proposed as an explorer of Mars's polar ice caps.

Figure 4-13: Tumbleweed test deployment in Antarctica in 2004. Image courtesy Alberto Behar, NASA JPL [47].

The main challenge of basing a Jupiter WindBot on the tumbleweed design, or any previously proposed wind-propelled surface rolling or hopping designs is making it airborne – all previous designs rely on wind energy compensating for work against friction or other work in *movement on or bouncing off the surface, and not providing for a force that is larger than the gravitational force at all times.*

4.4 Reconfigurable Wings

A WB design may have reconfigurable wings that change properties in flight depending on local conditions. The price to pay is reduced reliability due to moving parts and additional weight. Instead, one would gain adaptability to changing air currents for potential improved maneuverability, possibly lift and possibly energy harvesting. Changing airfoil benefits to taking advantage of different densities to maximize lift.

Lift is given by

$$L = C_{lift}\frac{\rho v^2 A}{2}$$

drag by

$$D = C_{drag}\frac{\rho v^2 A}{2}$$

Mach number by

$$M = \frac{v}{speed\ of\ sound}$$

and Reynolds number by

$$Re = \frac{\rho v l}{\mu}$$

Mach and Reynolds number change with altitude. Airfoils are optimized to perform in a narrow set of conditions. Lift and drag will have very different values at different M and Re, thus an airfoil's efficiency – its L/D – will vary dramatically. By altering the shape of the wing, the L/D ratio can be changed and the airfoil can improve its performance in a wider range of conditions. Modern aircraft wings commonly rely on control surfaces like flaps and slats, ailerons, and their derivatives such as flaperons for changing camber and thus maximizing L/D at different velocities. Morphing wings replicate the effect of control surfaces by changing their cross section and thus providing a simpler and more lightweight mechanism to achieving advantageous shape.

Typical value for deflection of ailerons, surfaces responsible for roll control, is $\delta A = \pm 20$ degrees [49]. On average deflection angle of most common aircraft rarely exceeds 30 degrees (Figure 4-14).

Figure 4-14: Example of deflection of a control surface [49].

The main difference between reconfigurable wings and deployable wings is that the latter are actuated at the beginning of WindBot's in situ mission and then remain rigid, while the former are actuated at any point during flight when conditions favoring a different shape arise. The inflatable wing has been discussed in Chapter 3 and is an example of a deployable wing.

One can conceive hybrids which are deployable/inflatable as well as reconfigurable/adaptable. Traditional movable control surfaces used on rigid wings (of multiple components, connected with rigid enough

interfaces) are not feasible on inflatable wings. However, it is possible to actively manipulate their shape, e.g. roll control has been successfully achieved by wing warping [42]. Smart materials (e.g., nitinol) and mechanical actuation are primary existing methods of changing the camber. An effective increase in angle of attack of 3° was demonstrated. If the deflection is measured from the first deformation point (approximately 0.75c), the effective flap deflection is approximately 16°, which is comparable to values achieved through standard control systems. Figure 4-15 shows an example of inflatable morphing wing.

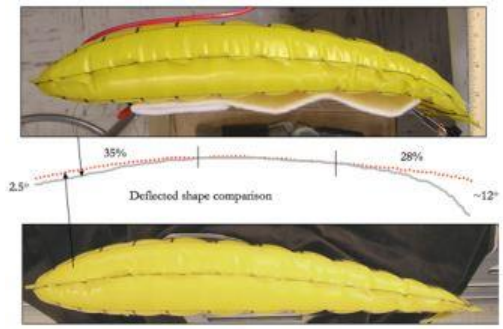

Figure 4-15: Inflatable wing, ILC Dover [42].

Rather than employing a plethora of actuators to locally deform an otherwise stiff structure, an alternative approach is to draw energy from a few remotely located actuators and distribute the energy to the structure through some intermediary mechanism. The primary design methodology employed in this effort utilized distributed compliance rather than distributed actuation [50]. Localized strain, if distributed properly over a compliant structure, can improve wing control surfaces while being less complex and power-requiring than inflatable morphing wings. ACTE (Adaptive Compliant Trailing Edge) bendable flap technology eliminates gaps in a wing for a seamless surface (Figure 4-16).

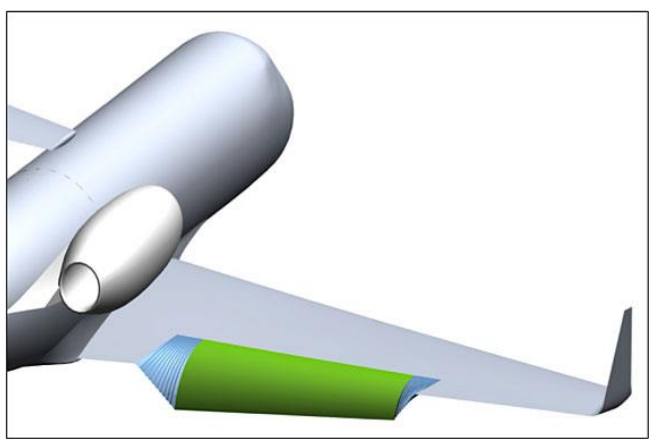

Figure 4-16: ACTE flap technology [51].

A few small strains on the mechanism can bend the wing's flaps and trailing edge from -9° to + 40°, according to FlexSys, the company researching this technology. At zero-degree angle of attack, the compliant flap achieves nearly a 75% increase in L/D compared to the plain hinged flap and 25% decrease in drag [50].

Achieving wing morphing by changing a wing cross-section can be done by using *tensegrity airfoils*. Tensegrity structures are configurations of axially-loaded members (sticks and strings) stabilized by string tension [52]. They can be extremely light weight and may require little energy for control, which makes

tensegrity structures excellent candidates for morphing wing WindBots. Figure 4-17 illustrates a sample transition from one airfoil shape to another.

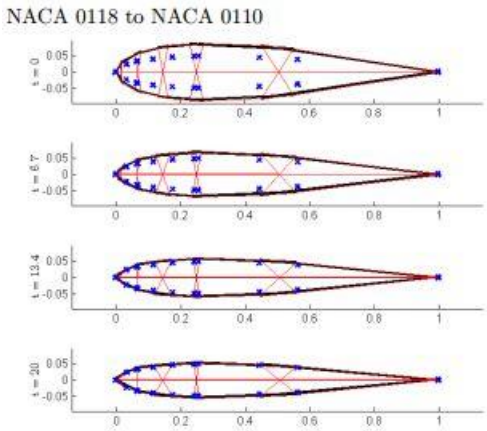

Figure 4-17: Morphing tensegrity airfoil [52].

Another parameter that can inrease WindBot's performance is variable sweep angle. Variable sweep wings allow the aircraft to take advantage of a wider range of speeds and be more packageable. A scissor wing that has the ability to pivot about the fuselage is the simplest way to implement the variable sweep characteristic without making the craft heavier. AD-1, depicted in Figure 4-18, was a craft with pivoting wings that has been constructed and tested in flight over 70 times. The wing remains perpendicular to the fuselage during slow flight and changes up to a 60 degree angle as speed increases. Incorporating this characteristic into WindBot winged design may improve its performance during speed changes but it is not naturally aligned with previously discussed morphing wing techniques and by itself does not outweigh the benefits of having wings that change profile [53].

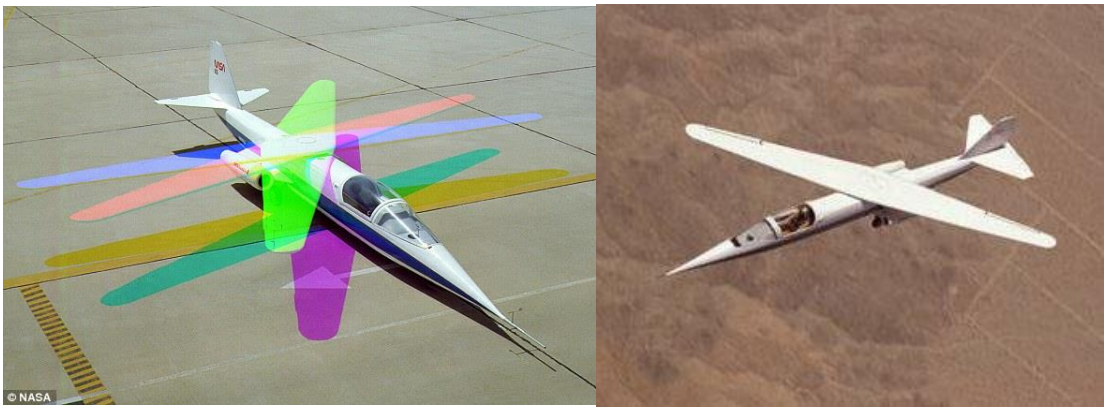

Figure 4-18: AD-1 oblique "scissor" wing

4.5 Summary of WindBot Concept Mobility

Table 4-1 summarizes the mobility alternatives examined for WBs.

Table 4-1: A summary of WB mobility options

	Buoyancy capability	Buoyancy control modes	Tolerance to wind gusts	Lateral maneuverability	Ease of packaging	Ease of deployment
Montgolfière	Low to medium; very dependent on ambient conditions	Medium; limitations in descending below the cloud layer	Low; limitations due to buoyancy loss through convection and susceptibility to tear	Low to medium with Balloon Guidance System; none without it	High due to absence of gas tanks	Medium; requires heating before EQ altitude
Charlière	Medium to high due to hydrogen	Medium due to ballonets, ballasts, temperature control	Low to medium due to a large envelope (though smaller than Montgolfière)	Low to medium with Balloon Guidance System; none without it	Low due to gas tanks; need 13 kg of H per 1 kg payload, unless can harvest hydrogen	High; uses gradual inflation upon descent
Vacuum	High with proper structure design	Low; mainly through ballasts	Medium; smaller envelope size and rigid structure decrease susceptibility to tear	Low to medium with Balloon Guidance System; none without it	Very low due to rigidity and large size of the vacuum chamber; may be feasible with a deployable vacuum chamber	Low; technical problems with deployable pressure vessels not fully addressed
Buoyancy Driven Winged Aerostat	Tuned to be neutrally buoyant	Adjusts buoyancy above and below neutral to actuate flight	Ability to control pointing of glider, still susceptible to large wind gusts	Good lateral maneuverability, but less than a standard glider	High, as the entire system is inflated upon entry	High, requires one inflation event
Ramjet	None	n/a	Very high due to large mass and speeds	Poor (some) due to air intake at high speeds	None	Requires assisted launch, i.e., catapult
Flettner (Magnus)	None	n/a	Depends on design	Some due to rudder (omitted in present model)	Medium (rotors are retractable)	Little to no test data exists
Glider	None	n/a	Medium	High; requires autonavigation mechanism	None for entirely rigid structure	High, well-tested platform

	Buoyancy capability	Buoyancy control modes	Tolerance to wind gusts	Lateral maneuverability	Ease of packaging	Ease of deployment
Autorotation	Low	Depends on design	Medium but unfavorable for the rotor	High due to blade pitch; requires a comprehensive control algorithm	Depends on design	High, eject from mothership
Inflatoglider	Possible	Valve system	Medium due to inertia of the craft	High; requires a comprehensive control algorithm	High; volume reduction of over 60%	Medium, requires UV light and certain temperatures
Foldable Structures	Possible if filled with buoyant gas	Valve system	Provides no resistance; travels with wind	No control over direction of travel	High; volume reduction by a factor of 30	Requires actuation mechanism
Foldable + Shells	Strong – similar to aerostat	Valves and multiple chambers	Medium	Medium; fins can be added for control	High	Similar to aerostat
Tumbleweed	Possible if filled with buoyant gas	Depends on design	Provides no resistance; travels with wind	No control over direction of travel	High	Medium, previously tested on Earth
Reconfigurable	None	n/a	Depends on design, medium to high	High; requires a comprehensive control algorithm	Medium to high (for inflatable wings)	Requires actuation mechanism

5 WindBot Concept Energetics

Long duration missions with multiple WBs implies reliance on harvesting energy in-situ, for staying in the atmosphere, to measure and communicate data. Solar power below clouds, for Jovian missions, is challenging, and in this report we did not determine attenuation for different altitudes. We are not ruling out the use of solar power in the upper part of the atmosphere. With ~50 W/m^2 above clouds, in context of possible advances in solar cells, assuming an ambitious 50% efficiency and ultralight photovoltaics, one could consider ~25 W/m^2 as a possibility in the future; this would clearly be a useful power source, which could potentially convert energy and beam to a WindBot below clouds. Either large inflatables having photovoltaics on their envelope or receiving energy from a transmitter from above clouds are not impossible scenarios but were not analyzed; for Saturn and for other giants this option appears less feasible. On the other hand, these bodies have other forms of energy in their atmospheres, which may be captured and used, and this was the focus of this section.

5.1 Aeolian Energy

Wind gradients and updrafts, where available, have promise for maintaining WB aloft and operational. The information to date is scarce – more data is expected from the Juno mission.

5.1.1 Vertical Winds (Updrafts/Thermals) for Lift and Power Harvesting

Updraft cores in the eyewall of anti-cyclones may be the most promising source of energy for Jupiter WBs. Figure 5-1 illustrates a simulated system of updraft cores in the eyewall of a terrestrial cyclone. Persistent UAV flight within this region has been proposed and simulated [38]. Previous research and analysis of direct flight observations of mature terrestrial hurricanes has found that the updraft cores covered about 55% of the eyewall regions with speeds of 4.5 m/s at 500 m. Poh & Poh demonstrated that persistent flight is viable in such an environment. Using a glider with a glide ratio of 20.7 and a wing loading of 117.06 Nm^{-2}, 300 m of altitude loss was registered during the gliding phase between cores, over a distance of 2.9 km. This simulation accounted for the regions of downdraft between cores.

Very long duration soaring flights have been observed in terrestrial environments by various avian species. Frigate birds have been observed to use oceanic thermals in soaring flight to routinely fly for periods of 14 days or more, with very low energy expenditure. In addition, they can use these thermals to travel up to 4000 m above the sea, giving them exceptional gliding distance [54].

Due to the similarities in structure between Jovian and terrestrial storms, it may be hypothesized that Jovian cyclones would provide regions of updrafts in which a glider could fly. Updrafts and thermals are likely present outside of cyclones and would provide another source of lift to a craft seeking to explore the atmosphere beyond cyclones. Most terrestrial gliders use updrafts and thermals created by terrain features and heating of the surface [55]. There are additional methods of using updrafts and downdrafts to gain small amounts of energy for a glider. These methods require very precise control and knowledge of state of the vehicle to execute properly [56].

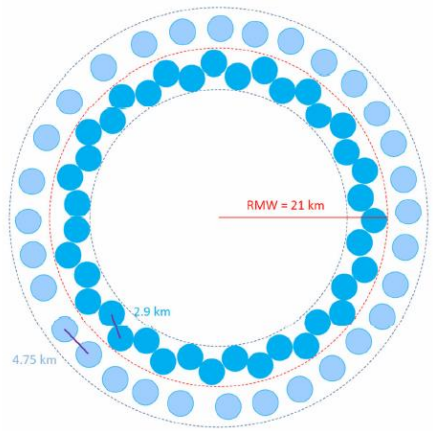

Figure 5-1: Updraft Core Model. A simple graphical model showing a plausible distribution of updraft cores ±5 km from the radius of maximum wind (RMW) for Hurricane Anita at altitude 0.5 km [38].

To use updrafts one needs to detect them from a sufficient distance such that the move towards them uses minimal energy. While algorithms have been constructed and simulated for glider flight planning based on available wind energy [57], there is still a need for sensors to detect long-range wind shear. One possible technology is Terminal Doppler Weather Radar (TDWR), which is used around airports to detect wind shear. The operational range of this radar is on the order of hundreds of kilometers, which somehow limits its use in WBs. However, if these updrafts do not significantly change their position in relatively short timeframes, e.g. those in the eyewall of the GRS, an initial detection is the most important part after which shorter range detectors may be sufficient, provided that WBs have good means for self-localization.

5.1.2 Horizontal Components – Wind Gradients/Cyclones/Turbulence

A WB glider could use shear winds (Figure 5-2) as well as wind gradients to enable dynamic soaring. By pushing against wind gradients with the wing, the WB can harvest power from the air equal to the velocity of the air times the force generated by the wing. Dynamic soaring depends on moving the glider through wind gradients. Also, as turbulence develops on sharp wind gradients, dynamic soaring often results in large vibrations in the glider [56]. While this is an effect which human flight tries to avoid, rapid oscillations of the glider could be used to generate power. Energy generated through dynamic soaring manifests itself as kinetic energy, which may be used to sustain altitude.

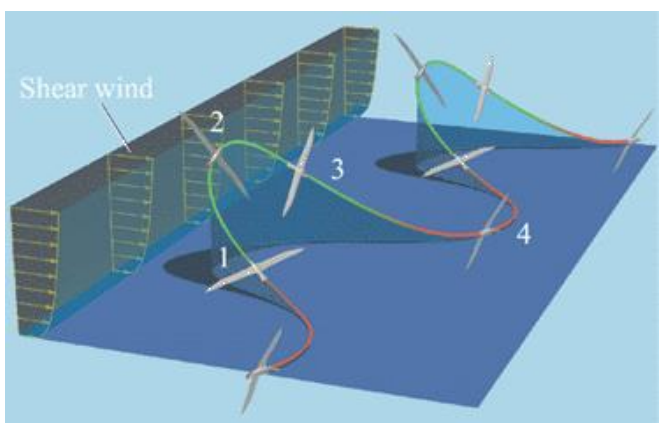

Figure 5-2: Dynamic soaring cycle utilizing shear wind to develop an energy-neutral trajectory [58].

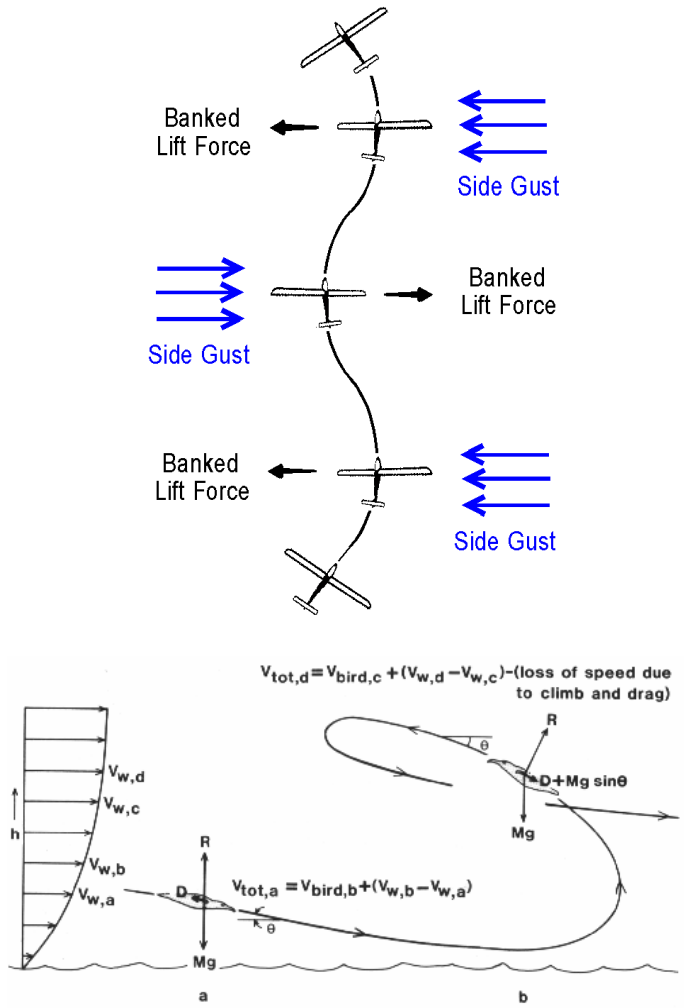

Figure 5-3: Side Gust Soaring main model schemes. (a) Side gust soaring seen from top [56] (b) Vertical dynamic soaring seen from side with relevant equations [59].

Figure 5-3 provides a flight-model description for dynamic soaring. In Figure 5-3(a), the glider takes advantage of horizontal winds, banking away from side gusts to gain energy. The banked lift force pushes the glider sideways and upward, gaining energy. Figure 5-3(b) illustrates vertical dynamic soaring. As the glider approaches the ground moving with the wind, its groundspeed remains constant while its airspeed and lift increase. This allows the glider to turn and rise, further increasing the airspeed. At a height where the winds are constant, the process slows down and the glider turns again to repeat the process [59]. Dynamic soaring makes use of energy-neutral trajectories to sustain flight, replacing energy lost to drag with energy gained from moving air.

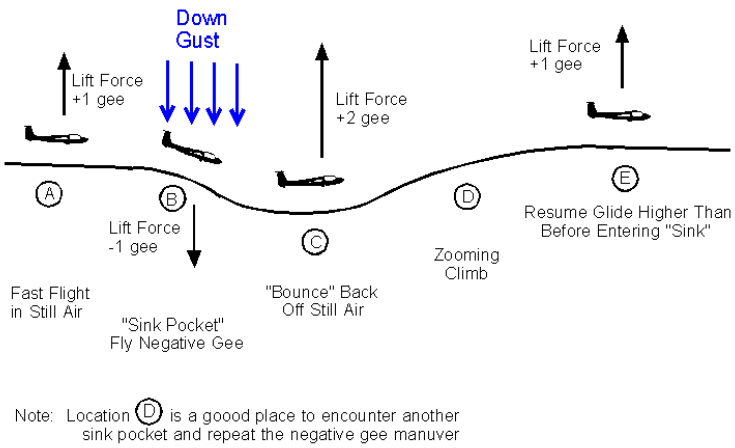

Figure 5-4: Dynamic soaring in downdrafts. This diagram shows how a sailplane can get energy from downward moving air [56].

Figure 5-4 illustrates techniques which may be used to gather energy when a WB encounters a downdraft. By riding the downdraft downwards, the WB may use its gained kinetic energy to bounce off still air underneath and gain energy relative to the beginning of the maneuver [56]. On Earth, typically, a maneuver of this type would last approximately two seconds, necessitating a high degree of sensing and control on board the flyer. There is needed power to operate the control surfaces of the craft, and which also depends on the selection of actuation/motors. For typical RC craft on Earth, the power demand does not exceed 1 W, however, power consumption for dynamic soaring may be higher due to the need for frequent maneuvering. This power would not be recovered through dynamic soaring and would require the glider to have another source of energy.

Energy Use Through Static/Dynamic Soaring

The energy rate of the WindBot soaring in the wind can be expressed as follows:

$$\frac{\dot{E}}{m} = -V_a \frac{D}{m} - gW_z - V_a \begin{bmatrix} \cos\psi_a \cos\gamma_a \\ \sin\psi_a \cos\gamma_a \\ -\sin\gamma_a \end{bmatrix}^T \begin{bmatrix} \frac{\partial W_x}{\partial x} & \frac{\partial W_x}{\partial x} & \frac{\partial W_x}{\partial x} \\ \frac{\partial W_y}{\partial x} & \frac{\partial W_y}{\partial x} & \frac{\partial W_y}{\partial x} \\ \frac{\partial W_z}{\partial x} & \frac{\partial W_z}{\partial x} & \frac{\partial W_z}{\partial x} \end{bmatrix} \begin{bmatrix} \dot{x} \\ \dot{y} \\ \dot{z} \end{bmatrix}$$

In this equation, m is the vehicle mass, V_a is the vehicle velocity relative to the wind, D is the aerodynamic drag, g is the gravitational acceleration, $[W_x\ W_y\ W_z]$ are the components of the wind speed in the inertial frame, $[x, y, z]$ are the inertial components of the vehicle's position vector, ψ_a is the heading angle, and γ_a the climb angle. The first term is the power loss due to drag. The power loss due to (parasitic) drag is proportional to the cube of the airspeed.

The second term is the static soaring term; that is, it represents energy gained or lost from vertical motion of the air relative to the fixed inertial frame. As seen from the equation, this term is only affected by the magnitude of the vertical wind; positive values of W_z (downdrafts) result in energy loss and negative values (updrafts) result in energy gain. Since this term is only a function of the wind magnitude, flying at minimum sink (minimizing drag) will result in the fastest energy gain from rising air; a fact well-known to glider pilots. This is also the only term which results in energy change from a uniform wind field.

The third term is the dynamic soaring term and represents energy gained or lost due to wind gradients. This term is more complicated, as it is affected by airspeed and climb angle as well as the wind gradients. It is not instantly apparent from this equation the speed and/or climb angle that will maximize energy gain from a wind gradient, since the required lift and drag are functions of airspeed and climb angle. An interesting result of this equation is that wind energy can be gained from any wind gradient with the appropriate selection of a climb angle. Using dynamic soaring, the vehicle could be kept in flight for a long time in a persistent manner, and with no thrusting power, provided that it has the capability to sense, map, and track either a static thermal profile, or a dynamic gust event with adequate resolution.

The WindBot could have the ability to estimate the local wind vector using an air data sensor and an inertial sensor. Assume that the air data sensor measures the speed and direction of airflow relative to the center of mass of the WindBot, and the inertial sensor measures the acceleration and speed of the vehicle in a fixed inertial frame. While airspeed and inertial measurement units are common on UAVs, air angle measurements are not. One method for estimating air angles is an alpha-beta vane system, which records the wind direction around two perpendicular axes each using a lightweight wind vane and potentiometer. An alternative system is a multi-hole pressure sensor which estimates the air angles by calculating the pressure at different orientations to the wind and solving for the wind direction [60].

5.2 Converting Mechanical Energy to Electrical Energy

In autorotation under an updraft, a lateral wind gust, or while tumbling, mechanical energy of a rotor can be harvested. Also, vibration during atmospheric movement may be harvested as mechanical energy and converted to electrical energy to provide power for instrumentation, controls, and propulsion.

5.2.1 Rotational Generators

Gyroscopes are currently used to harvest ocean wave energy through forced oscillation. The gyroscope is placed on a buoy, which is oscillated by the action of wave energy. As the waves move the buoy, the gyroscope resists changes in its motion. When the oscillation frequency and gimbal rotation frequency of the gyroscope is synchronized, the gimbal rotates, allowing the generation of energy. The power gyroball shown in Figure 5-5 operates on this principle. This method could be utilized by a WB to produce energy; the naturally induced oscillation due to turbulence provides the driving force for the gyroscope motor. An array of three gyroscopes would allow turbulence incident in any direction to drive at least one motor, maximizing energy output [61]. However, it is unknown whether turbulence could provide a large, consistent oscillation to produce power.

Another internal method of energy production would be to use a spherical induction motor in generator mode. These motors use inductors to drive spheres of copper in any direction [62] [63]. Run in reverse (generator regime), they could theoretically take any rotational input and turn it to electricity. A speculative design involving a spherical motor would be to place the instruments in the center sphere of the WB. A light outer shell containing aerodynamic elements and the inductors would be free to rotate around the sphere when impacted by gusts of turbulence, creating electricity.

Figure 5-6 depicts possible WindBot outer body concepts shaped as 3D rotors. These body designs would optimize the WB's tumbling in the atmosphere, increasing the efficiency of an internal generator.

Figure 5-5: WindBots gyroscopic energy harvester mechanism. From left to right: power gyroball, inside gyro, and a 3D spherical induction motor, which can be operated in generator regime

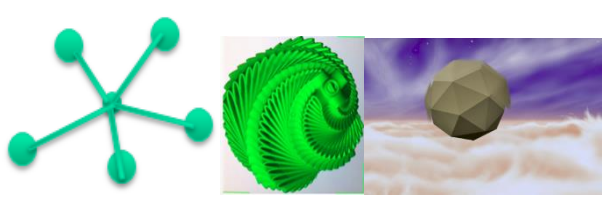

Figure 5-6: WindBots outer body concepts that would benefit from tumbling.

Work needs to be done to validate 3D motors as efficient generators and convert them to a design usable for a WB. Using current technology these designs are likely to be heavy, but in principle this can be improved. Completely contained inside of the WB, these would have minimal atmospheric exposure.

5.2.2 Converting Vibrations to Electricity

Vibration of the WB body through turbulence is a form of mechanical energy that can be recovered through linear or rotational vibration generators. This section explores designs for rotational and linear generators as well as conducting preliminary exploration of power available through these means.

5.2.2.1 *Linear Vibration Generator*

A linear vibration generator consists of a spring, mass, damper system. When the body is vibrated, the mass vibrates on the spring. The damping force is provided by a generator, which removes energy from the system as electrical energy. The maximum achievable power for a linear system is

$$P_{max} = \frac{m\omega^3 Y_0 Z_1}{\pi}$$

where ω is the driving frequency, Y_0 the driving amplitude, and Z_1 the maximum range of motion inside of the apparatus [64]. To provide 30 W of power to the WB, a one-kilogram mass would have to be oscillated along a one-meter distance at a frequency of 4.53 Hz.

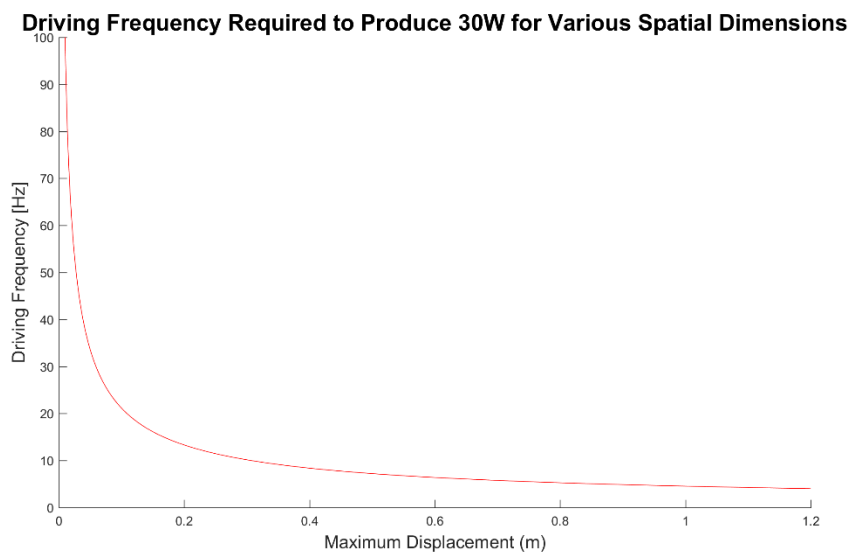

Figure 5-7: Driving frequencies necessary to produce 30W of power for the WB given various maximum response amplitudes for a one-kilogram mass. For a maximum, the system is driven at the maximum range of motion.

Figure 5-7 illustrates the benefits of increasing the maximum range of motion of the device. The minimum frequency of oscillation decreases significantly with increases the amplitude of movement – especially below 10–20 cm.

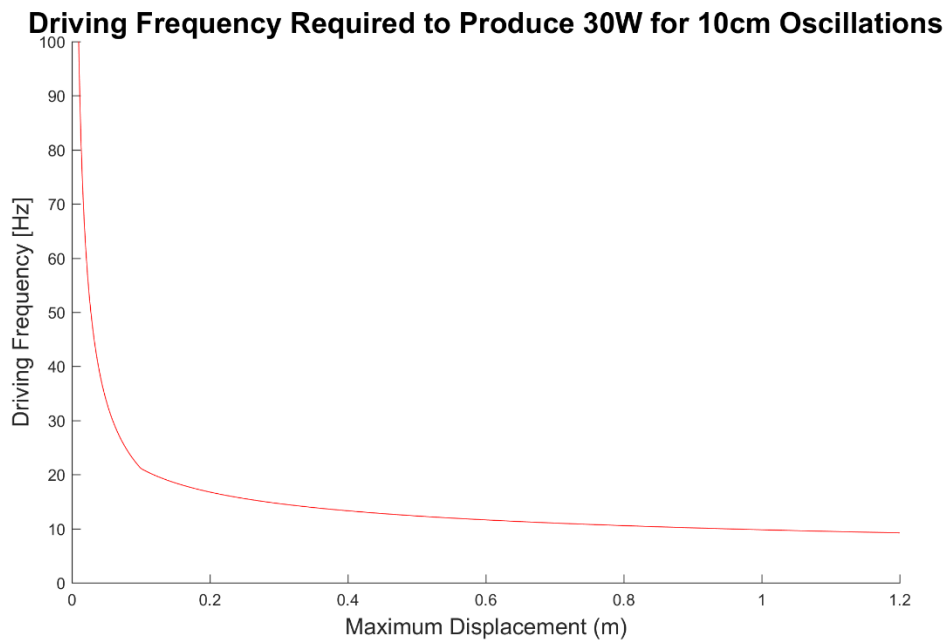

Figure 5-8: Driving frequencies necessary to produce 30 W of power for different maximum displacements of a one-kilogram mass inside of the system. In this case, the amplitude of the driving oscillations is confined to 10 cm.

Atmospheric, small scale turbulence may drive a device at a variety of different amplitudes and frequencies depending on the geometry of the WB as well as the conditions inside of the atmosphere, which are not well defined. Figure 5-8 demonstrates that even when the amplitude of the driving oscillations is confined to not exceed 10 centimeters, the device still requires diminishing driving frequencies with increased displacement. For a one-kilogram mass with 10 cm oscillations, a travel length between 20 and 40 centimeters requires a driving frequency of approximately 10 Hz, potentially reachable for a WB and within a reasonable length. The driving frequency may be further lowered by increasing the mass of the oscillator.

The maximum power increases with mass, meaning it responds poorly to miniaturization. In addition, low frequency driving oscillations do not generate nearly as much power as high frequency, yielding poor power density. This calculation assumes that the mass travels its maximum allowable length and that the oscillatory input is driven at a regular frequency. A system placed in turbulence would be able to sustain some oscillations due to the random motions imparted on the system and would then oscillate at the damped natural frequency associated with the system. There is no current characterization of the power available from turbulence harvested in this method. For a damped oscillator, the power removed from the system at a given time, t,

$$P(t) = \frac{b}{2m} k Z_1^2 e^{-\frac{b}{m}t}$$

where b and k respectively represent the damping and spring constants of the system. Turbulence would likely add energy to the system through induced oscillation before the system was completely damped, increasing the recoverable power. Further improvements to the power of the system would be to tune the resonant frequency of the device to the mean driving frequency, creating high amplitude responses. Figure 5-9 demonstrates a schematic model of this type of linear vibration generator. Figure 5-10 illustrates the energy and power decay curves for an underdamped harmonic oscillator. To achieve steady

power, turbulence would need to continuously force the generator, adding energy to the system. An array of three linear generators along each axis would allow maximum use of incident turbulent energy. In addition, plans for an efficient linear generator based on a concept of multiple masses placed in series may be found in [65].

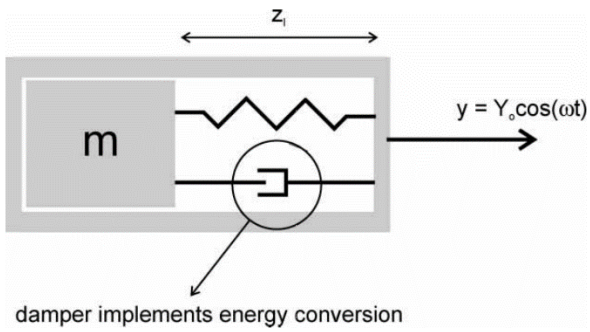

Figure 5-9: Schematic for a linear vibration energy generator [64].

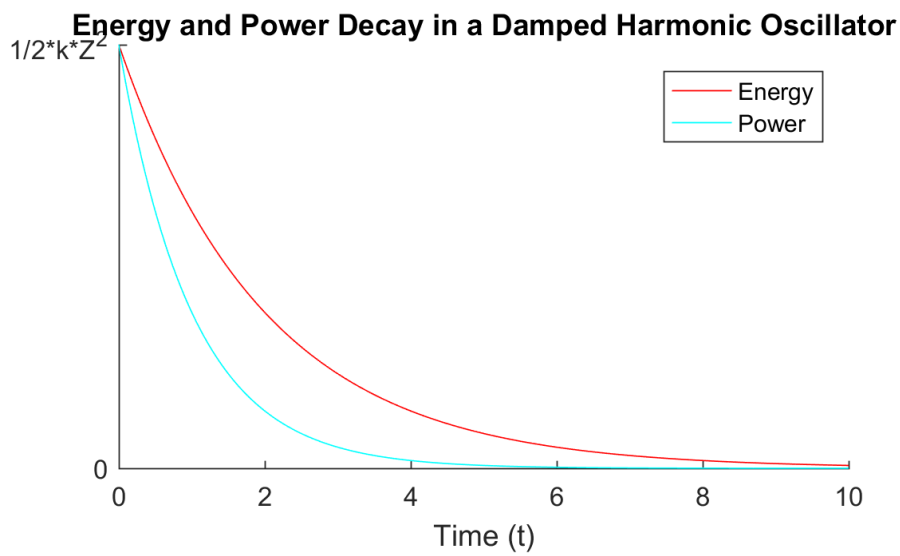

Figure 5-10: Energy and power decay in a damped harmonic oscillator for a system with arbitrary constants; decaying forms an initial system energy.

5.2.2.2 *Rotational Vibration Generators*

It is also possible to harvest vibrational energy through a rotational generator. A rotational generator offers two improvements over a linear generator. First, it may harvest both rotational and linear oscillations, and second it presents no maximum displacement beyond which the mechanism may take in no more energy. The mass of rotational generators is contained in a semi-circular disk mounted on a central axis. The semi-circular geometry makes possible the harvesting of energy through linear excitations. Figure 5-11(a) shows an example of a rotational generator geometry. When the frame holding the disc is moved linearly, the central axis exerts a torque on the disk, leading to oscillation. A rotational excitation will also exert a torque on the mass, again causing oscillation. These oscillations may be harvested by a generator to produce electrical power [64].

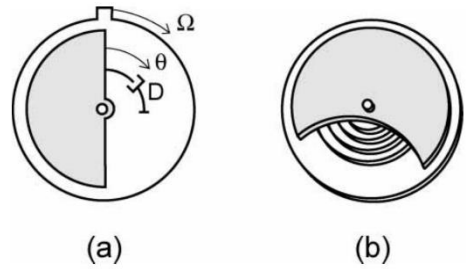

Figure 5-11: (a) Rotational generator geometry. (b) Inclusion of a spring allows for resonance to be exploited [64].

The maximum power output for a rotational generator excited linearly is the same as for a linear generator. In most cases, the power output for a rotational generator is much higher working from linear excitation than that produced by angular excitation. However, little analysis has been done for large amplitude rotation, which may be the result of turbulent winds. In addition, the design of a WB body could further increase the amplitude of induced rotations [64].

There may be potential for increased energy gains using a resonant generator. This geometry connects a spring to both the mass and the frame, as in Figure 5-11(b). The limiting factor on power in this system is the parasitic drag in the mechanism itself. The addition of resonance may increase the power generated from rotational excitation by many factors but comes with an extreme sensitivity to driving frequency, which will not be constant in a turbulent environment.

It is also possible to harness a gyroscope to function similarly to the rotational generator. If the parasitic drag is sufficiently lowered on a gyroscopic generator, it may exceed the power produced by a linear vibration generator, even while considering the power input to keep the gyroscope spinning. A generator of this form would only be able to harness rotational excitation, but this may be maximized for a WB as discussed above. In addition, a gyroscopic generator would not be constrained to a single frequency, allowing broadband response to excitation frequencies [64].

Further development of a gyroscopic generator would be necessary before use in a WB. This would include designing a low parasitic drag system as well as the exact mechanics of the power storage and harvesting mechanism. Rotational vibration generators have been in use for several decades in automatic watches. These watches collect energy through a non-resonant rotational generator and store it in a spring, which delivers the power necessary to drive the watch. The same mechanism could store the mechanical energy of the random excitations of a WB before delivering this power to a gear train to continuously drive a generator at high speeds. An example of an automatic mechanical watch mechanism is provided in Figure 5-12.

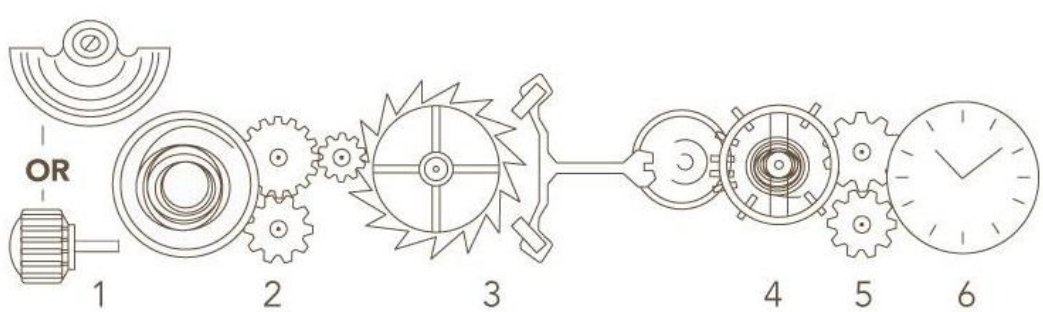

Figure 5-12: Mechanism of an automatic watch [66] – a WB may use a similar energy harvesting mechanism.

In [38], the motion of the rotational generator of an external knob winds a spring. This spring releases energy via a gear train to the escapement in Figure 5-12 (2), which delivers regulated amounts of energy (3). The energy drives the balance wheel back and forth at a constant rate (4) which is then transferred through another gear train to turn the watch hands at precise times. This mechanism could be adapted for use as a continuous electrical generator from irregular input motion.

Vibration mechanisms appear promising, with theoretical power outputs on the scale of those needed by WBs. Both linear and rotational mechanisms benefit from extra mass; assigning as much mass as possible during design will be critical for the WB. These mechanisms have decent power density. Based on COTS 30W generators, the generator will likely not exceed 3 kg in current technology and will likely be smaller due to custom sourcing. No more than 5 kg would likely be necessary for the additional mechanisms and structure, bringing the total mechanism to around 8 kg for 30 W of power. The characterization of the energy recoverable from turbulence using these methods on Earth would provide an estimate for their operational abilities on Jupiter.

5.2.3 Fluttering Generators

Piezoelectric materials provide another potential source of WB energy harvesting. By applying a strain to the piezoelectric material, a current is produced, resulting in power for the WB. One proposed method of producing energy via piezoelectrics is a fluttering generator. This generator works by exposing two thin strips of piezoelectric material, fastened at one end, to an incident wind. When the wind velocity is sufficiently high, aeroelastic flutter causes the piezoelectric strips to vibrate, inducing strain in the material and producing power. This effect may be amplified by adding more strips of piezoelectric material to the system. While the power produced by one strip is small, the individual components are light and could be replicated across the vehicle to generate meaningful power [67].

Figure 5-13 illustrates a potential piezoelectric fluttering concept, arranged in the optimal configuration for flutter. This arrangement lowers the initial wind velocity required for flutter, increasing its effectiveness in a broader range of applications.

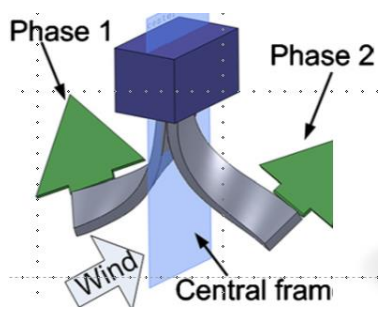

Figure 5-13: Fluttering Piezoelectric concept [67].

Other piezoelectric concepts involving the deflection of beams were explored, including hybrid designs which included piezoelectric elements as well as induction mechanisms to make use of the deflection oscillations [68] [69]. An example of one of these hybrid harvesters may be found in Figure 5-14. However, these designs, summarized by energy density in Table 5-1, produced power on the order of microwatts, too low for the WB power needs, which are projected to be around 30W for instrumentation alone.

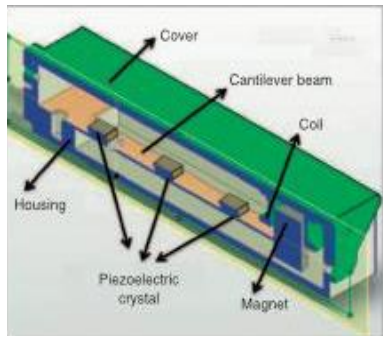

Figure 5-14: Hybrid harvester with piezoelectric and electromagnetic transduction mechanisms [69].

Table 5-1: Power density comparison of wind energy harvesting devices [67].

Device	Configuration	Dimension (mm)	Peak power	Power density: Per weight (mW/kg)	Per volume (mW/cm^3)	Per swept area (W/m^2)	Per cost (mW/U.S.$)	Cut-in speed (m/s)
Small windmill	Bimorph	60×20×0.6	5 mW	77.2	0.579	0.13	0.021	2.4
Galloping beam	Bimorph	100×38×1.54	1.14 mW	74	0.556	Unknown	Unknown	2.5
Windbelt (micro)			5 mW	Unknown	Unknown	1.28	Unknown	2.7
Tan's harvester	Bimorph	76.7×12.7×2.2	0.16 mW	9.94	0.075	Unknown	Unknown	~3
Flaglike harvester	Bimorph	203×279×0.5	10 mW	Unknown	0.347	Unknown	0.033	~4.5
Devices presented in this paper								
Parallel-flow long stalk	Unimorph	72×16×0.205	0.02 mW	34	0.09	0.001	0.003	1.5
Cross-flow long stalk	Unimorph	72×16×0.205	0.21 mW	343	0.871	0.013	0.034	1.5
Cross-flow short stalk	Unimorph	41×16×0.205	0.26 mW	576	1.928	0.046	0.069	4
Cross-flow double-layer long stalk	Bimorph	72×16×0.41	0.61 mW	472	1.300	0.039	0.051	4
Cross-flow narrow-short stalk	Unimorph	41×8×0.205	0.14 mW	415	2.036	0.024	0.037	2.8
Typical commercial wind turbine								
VESTAS V52-850KW			850 kW	27 000	Unknown	400	~300	4

5.3 Turbine Generators

The theoretical power generated by a wind turbine is

$$P_{turbine} = C_p A \rho v^3$$

where A is the area of the blades, ρ the density of the fluid, v the velocity of the fluid, and C_P the coefficient of power. For an ideal wind turbine, $C_P = 0.59$ [70]. In winds more than 100 m/s, a static wind turbine in Jupiter's atmosphere would need approximately four square centimeters of coverage to produce 30 W of power. However, for a passive WB moving with the wind, power generation would depend on wind gradients.

Unfortunately, there is no characterization of available small-scale wind gradients in Jupiter yet. These gradients would manifest as gusts or sudden changes in wind direction which could play on a WB and cause turbines to rotate. On Earth, for wind speeds around 100 m/s, the differential between sustained winds and gusts is approximately 20 m/s [71]. In this case about 30 W of power can be produced with blades of about 12 cm, 2cm width; this would be scaled up for Jupiter density.

A heavier-than-air WB would make further use of turbines as it falls through the air. This could include a glider based design, with a propeller mounted on the body undergoing autorotation as the device glided through the air. The deployment of a ramjet on a glider or other WB design allows the incident, apparent wind to be compressed and sped up, further increasing the power produced by a turbine.

Figure 5-15 illustrates a concept for WB turbine placement. By placing turbines at different locations on the body, the WB ensures at least one will be incident to an incoming gust of wind. Additionally, a side gusts will spin the turbines, increasing the effective area presented to the wind beyond the size of any one turbine. This design would require a complex system to translate the turning of the turbines to driving a generator, in lieu of having one generator per turbine due to weight considerations.

Figure 5-15: Multi-rotor possible WindBot design.

Another potential turbine design is illustrated in Figure 5-16. This design incorporates a gimbal turbine, which may be spun regardless of the incident angle of the wind. A gimbal turbine would offer a WB the advantages of a multi-rotor design in allowing the capture of wind energy in all directions and reduce the complexity of the design, but would need to be large to have an equivalent exposed area.

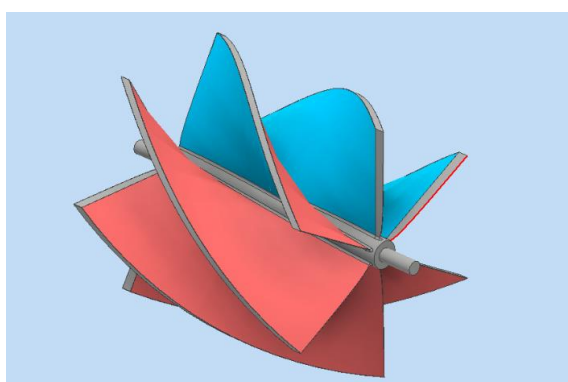

Figure 5-16: Gimbal turbine proposed design.

Another possibility for a turbine based design would be the inclusion of a mechanical system like that described in Figure 5-12. This would allow random gusts to store energy in an internal spring, while the mechanism feeds power to the generator at a constant rate, ensuring continuity of operations and relaxing the needs for battery technology.

Turbine technology is currently the most proven of all the technologies discussed and the inclusion of a turbine system in parallel with other technology would allow increased power generation as well as a

diversity of sourcing. The mass of the turbine would likely be on the same order as the vibrational generators when the supporting structure is accounted for. However, more work on the power harvested by a turbine from small scale velocity gradients is needed before the power density may be fully characterized.

5.4 Thermal and Pressure Systems

A WB traversing through the proposed operational range of Jupiter's atmosphere will undergo pressure changes from 0.3 bar to 10 bar and temperature changes from about 120 K to 300 K. The gradients in temperature and pressure present a potential source of energy. The following assumes a series of ascents and descents.

5.4.1 Thermal Systems

To harvest energy from Jupiter's thermal gradients, a WB may capture a supply of air at 10 bar on its initial descent. This air would be at atmospheric pressure and would be thermally insulated from its environment. Once the WB has made the ascent through its operational range, it may harvest the thermal energy stored in the captured air. One possible method for harvest explored here is to use the stored air as a heat source to power a heat engine.

From analysis presented in the insert, a WB operating under ideal circumstances would produce enough power from Jupiter's thermal gradient to power instrument operations for a period of several hours, depending on the volume of the WB. This information is summarized in Figure 5-17. A volume of one or two cubic meters would yield enough power for about two hours of operation. The WB would need to actively traverse the region between 10 bar and 0.3 bar, which would likely require some input of power, lowering the operational time. Many assumptions were made in this calculation to provide for the best case scenario. Coupled, these assumptions likely might reduce the power retrieved, perhaps by an order of magnitude. In addition, at minimum a pressure vessel withstanding 10 bars as well as the thermal gradient would weigh about 50 kg. A well-insulated vessel would likely weigh significantly more than that.

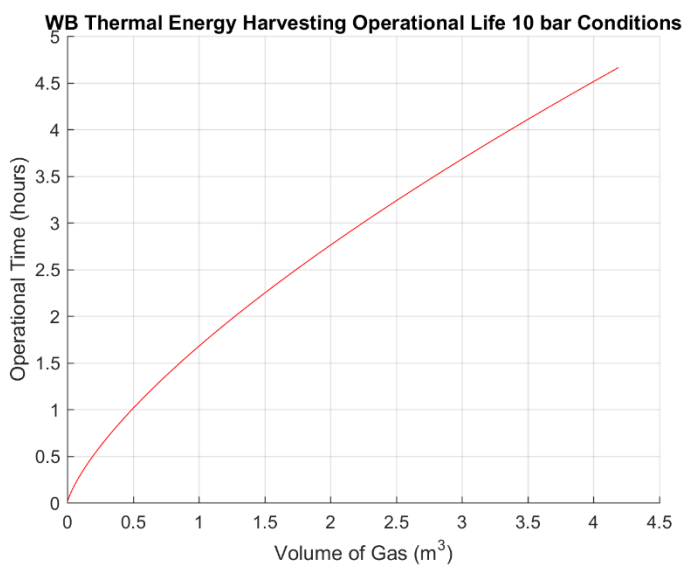

Figure 5-17: Dependence of operational time of a craft powered by thermal recovery on volume of gas enclosed, using atmospheric conditions at 10 bar.

Thermal Analysis

Throughout this analysis, numerous assumptions are made to simplify calculations. These assumptions always ere on the side of a "best-case" for power generation.

A pressure vessel of radius R, surface area A, and volume V captures a supply of Jovian air at a pressure of P_1, density ρ, specific heat c_v, and temperature T_h. The air has a coefficient of convection, h, in the vessel. The vessel is well insulated such that the rate of heat transfer out of the vessel during transport $\dot{Q} = 0$. Upon reaching an environment where the ambient temperature is T_c, the gas is exposed to the ambient and loses heat. Assuming that the gas follows a lumped parameter model, which is the best-case for this application, its temperature follows

$$T(t) = T_c + (T_h - T_c)e^{-\frac{t}{\tau}}$$

where $\tau = \frac{\rho V c_v}{hA}$. From the First Law of Thermodynamics, the rate of heat transfer out of the gas, $\dot{Q}_h$ is given by

$$\dot{Q} = mc_v\dot{T}$$

where m is the mass of the gas and is given by the ideal gas law as $m = \frac{PV}{\bar{R}T}$. The heat transfer out of the gas may be used to harvest work using a heat engine. The work obtainable by a heat engine is given by

$$\eta = \frac{\dot{W}}{\dot{Q}_h}$$

where η is the efficiency of the engine. The maximum obtainable efficiency for a heat engine is given by the Carnot cycle, which has an efficiency of $\eta = 1 - \frac{T_c}{T(t)}$. By taking the integral of $\dot{W}$, the total energy harvestable by the heat engine may be found to be

$$E = \int_o^\infty \dot{W} dt$$

In this integral is the assumption that all the energy produced by the heat engine is stored as electrical energy, even for the very high amounts of power produced at the beginning of the transfer, which would be unattainable by modern battery technology. Finally, the operating time of the WB using this energy recovery method may be obtained by dividing the total energy E by the operational power, P_{op}. For the results given, the following constants were used:

$$\rho = 0.32\ kg\ m^{-3}$$
$$P_1 = 10^6\ Pa$$
$$P_2 = 3 * 10^4\ Pa$$
$$c_v = 10.16 * 10^3 J\ K^{-1}$$
$$T_h = 300\ K$$
$$T_c = 120\ K$$
$$h = 1\ W\ m^{-2}\ K^{-1}$$
$$P_{op} = 30W$$

The value for h is at the low end of free convective heat transfer coefficients but was chosen to optimize the power generated. The volume chosen was arbitrary but chosen to be a fair spatial dimension for a WB. Section 5.4.1 refers to simulation results.

5.4.2 Pressure Systems

A WB utilizing a thermal system as described above could also take advantage of the natural pressure gradient in Jupiter's atmosphere. Upon capturing a supply of warm air at 10 bar, and after using heat from it while up, at 0.3 bar, the gas would still above atmospheric due to its higher density. By using this pressure differential to drive a stream of air past a turbine, the energy stored in the gas may be captured for use by the WB. To determine the energy available in a compressed gas, the following relation is used:

$$E = P_{max} V \ln \frac{P_{max}}{P_{min}}$$

Using the values in the insert for the pressure of Jupiter's atmosphere for a cubic meter of compressed gas, a WB could harvest enough power for about 32 hours of instrument operation at 30 W. This represents a significant amount of power, but much of the available energy would be wasted through harvesting losses. As atmospheric conditions are fixed, the only control over energy available is the volume of the container, which scales linearly. However, a spherical pressure vessel capable of withstanding the pressure and temperature stresses and hold a cubic meter of gas would weigh, in current technology, around 50 kg.

Additional arrangements of both the thermal and pressure systems could yield greater power returns. Both systems may also be run from the top down, capturing colder, low pressure air and using it at 10 bar to drive a heat engine and for its pressure gradient. However, this system would be less efficient than on the passage up, due to the lower pressure of gas at 0.3 bar. Another model would be to keep the original supply of gas captured at 10 bar and forgo pressure harvesting. The WB could then make use of both the up and down thermal gradient to capture power via a heat engine. Furthermore, a canister of high pressure gas may be sent with the WB. This would remove the need for a mechanical system for air capture as well as increasing the maximum thermal energy in the gas, increasing the power obtainable through this method. The power gained with increasing pressure is linear. Operational time supplied by thermal power for various densities and pressures with one cubic meter of gas are summarized in Figure 5-18 and Figure 5-19.

First order approximations of thermal and pressure power recovery yields promising results as a method for powering the instrumentation aboard a WB. Further analysis should be done to close simplifying assumptions and determine a more accurate figure for the obtained power. WB designs which could traverse from 10 bar to 0.3 bar with minimal power input should be explored as a necessary design element to enable this technology.

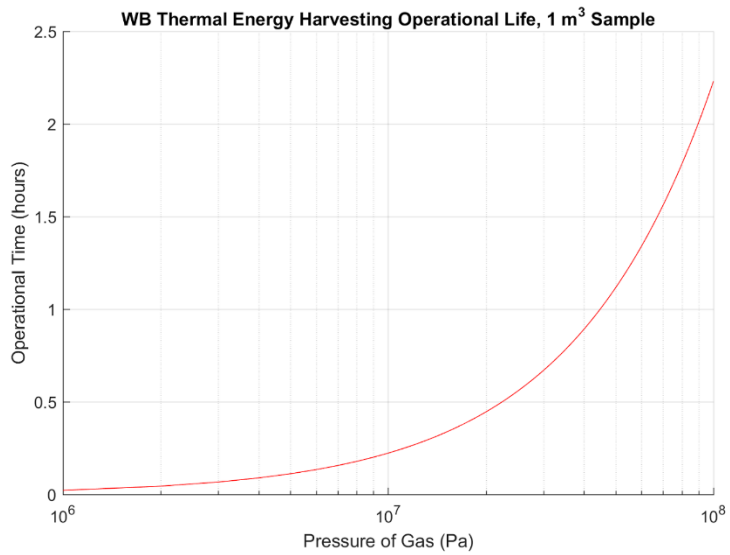

Figure 5-18: Dependence of operational time obtained by thermal power on pressure inside of the gas capsule, for a 1 m³ sample of gas. Note the logarithmic scale for pressure; this relationship is linear.

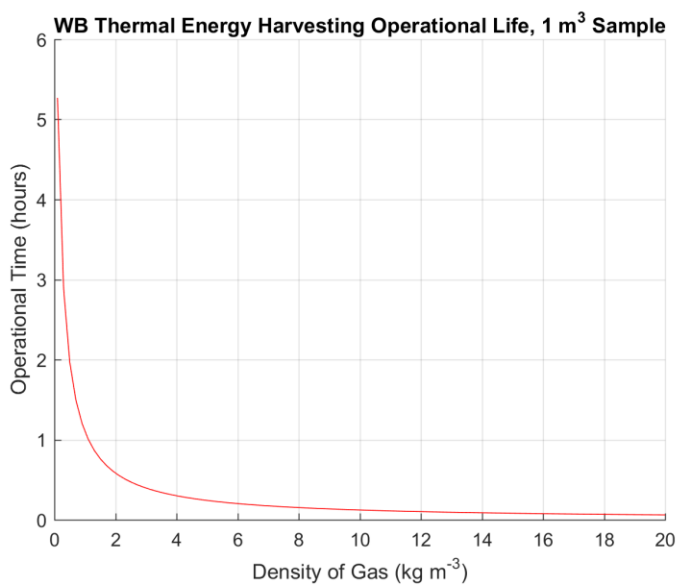

Figure 5-19: Dependence of operational time obtained by thermal power on density of gas used, for a 1 m³ sample.

5.5 Magnetic Generators

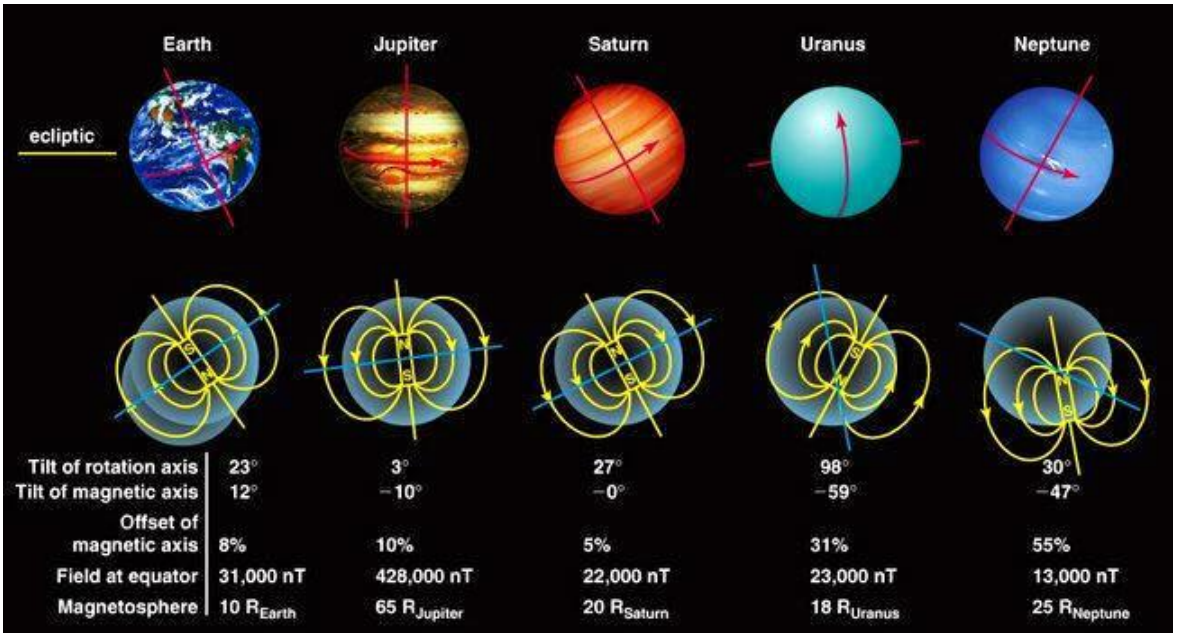

Figure 5-20: Comparison of different planets magnetic fields [72].

Jupiter has the strongest magnetic field of any of the planets, as illustrated in Figure 5-20. It may be possible to harvest energy from this magnetic field, for example by making use by phenomena characterized by Faraday's law. Running a wire of length L at a velocity of $\vec{v}$ through a magnetic field of strength $\vec{B}$ generates a voltage, V, of

$$V = (\vec{v} \times \vec{B}) \cdot L$$

Running a current I through the wire in turn generates power,

$$P = VI$$

For a WB flying at the equator, where its velocity and field lines would be roughly perpendicular, and with a velocity of $125\ m/s$ relative to the corotating magnetic field, a $100\ m$ tether would be sufficient to generate $\sim 5\ V$. This induced emf would be sufficient to generate $5\ W$ of power with a $1\ A$ current. Drag forces on the wire would be orders of magnitude higher than magnetic forces acting on the same wire.

Studies of tether power sources for Jupiter have focused on orbital vehicles [7]. These vehicles can make use of the plasma ring around the orbit of the moon Io, to close the circuit with their tether and power the spacecraft. A WB would have to carry a loop of wire to close the circuit, potentially requiring shielding on one side. This will double the weight as well as drag on the WB, both detrimental to the vehicle's longevity in the atmosphere. Additional care would need to be taken to ensure a lightning strike on the exposed tether would not overwhelm the WB's electronics and systems.

Magnetic tether methods may have promise, due to their relatively high power density of $4\ W/kg$. However, their additional drag dynamics may render them unsuitable to the WB. In addition, these calculations assume the tether hangs directly underneath a WB moving along the surface at peak wind velocity. If the tether becomes strung out behind the WB, like the tail of a kite, the power will fall off

dramatically; the WB will produce no power if it is traveling with the field lines, or in the N–S direction. For a WB circling the Great Red Spot, this will leave much of its mission unpowered.

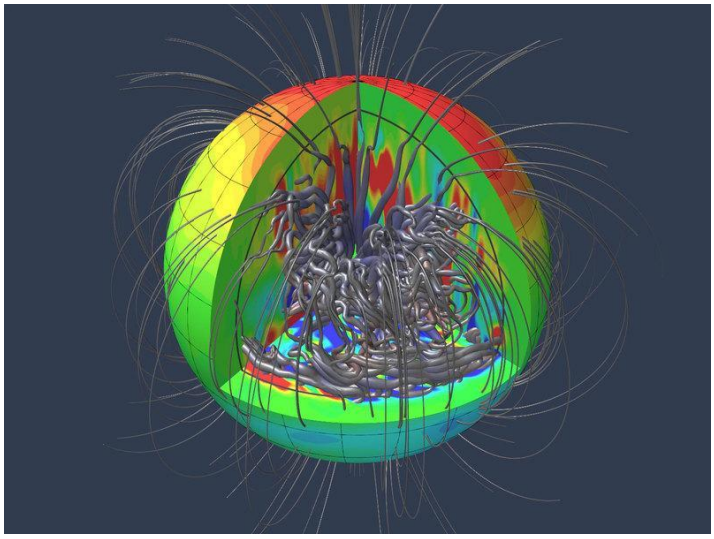

Figure 5-21: Jupiter's magnetic field. Thicker lines denote regions of stronger magnetic activity [73].

5.6 Hydrogen Harvesting

As atmospheric hydrogen is plentiful on Jupiter, it can provide a ready supply for a fuel cell to produce power for a WB. A COTS 30W fuel cell requires hydrogen at 0.5 bar and 300 K to operate at peak efficiency, which can be matched in Jupiter's atmosphere. At this efficiency, using 0.42 L/min, approximately 35 kg of oxygen are required to continuously power the WB for a period of six months. This mass would be feasible for a WB to carry inside of the atmosphere and optimization of the fuel cell and its efficiency could yield smaller masses of oxygen or longer operational times. A downside to this technology is the limitation in mission duration – while power is ensured throughout the operational lifespan, there is no possibility of mission extension past exhaustion of the oxygen reserves.

Fuel cells were not covered in the study due to their dependence on a limited resource. However, these preliminary calculations warrant their inclusion in a subsequent study – or missions of fixed (perhaps months) duration.

5.7 WindBot Concept Exergy

All energy methods considered in this chapter are evaluated based on First Law energy analysis. While these methods provide a reasonable first pass at the total energy contained in a system, they do not account for entropic losses due to real environments and energy transfers necessary to turn environmental energy into electrical energy. For a more complete model accounting for the Second Law, exergy analysis of the energy harvesting methods is necessary.

Exergy analysis has been successfully applied to studies on Earth; however, little has been done on this analysis for space and non-terrestrial planets. Delgado-Bonal et al. (2016) applied exergetic methods to the Martian environment for flat-paneled solar panels. Exergetic methods improve on energy methods by accounting for environmental factors acting during the energy conversion processes. Delgado-Bonal et al. (2016) demonstrate that there is an order of magnitude exergy efficiency difference between operating a solar panel on the Martian surface and operating a panel 1.6 m above ground.

Further work on WB will include exergy analysis for those energy harvesting methods shown to be viable through first-order analysis, such as vibrational and wind systems, to further determine the feasibility of these systems in a WB application.

5.8 Summary of WindBot Concept Energetics

Type	Electrical Power	Benefits	Drawbacks	Operational Life at 30 W	Continue for Further Study
Aeolian	*N/A*	*May be applied to vehicle; primary reliance on GNC algorithm, not mechanism*	*Requires fine control of vehicle attitude and ability to navigate through atmosphere*	*N/A*	*Yes, Phase II should investigate methods of detecting updrafts*
Vibrational	*30–50 W*	*Power may be obtained at any level of the atmosphere, can rapidly store wind gradient energy and provide a constant stream of power, good power to weight ratio, applicable to Earth-based systems*	*No knowledge of small-scale wind gradients, a more stable platform produces less energy*	*Determined by oscillatory response of flyer and small-scale wind gradients*	*Yes, Phase II should investigate extending these mechanisms to WB scales and dynamic modeling to determine power for different wind gradients*
Fluttering	~10 mW	Power due to boundary layer over WB, few moving parts and no mechanism development	Produces very small amounts of power, low power to weight ratio	Determined by small scale wind gradients	Without improvement in piezo technologies, this mechanism is not worth pursuing
Thermal	30 W	Very passive system, encourages vertical sampling of atmosphere	Large weight to contain hot gas, low operational life	About 2 hours for 50kg of shell weight	No, this method is infeasible for WBs
Pressure	30 W	Passive system, encourages vertical sampling	Large weight to contain pressurized gas against pressure gradient	Ideally about 30 hours for 50 kg of shell weight, but will be less under actual conditions	No, this method is infeasible for WBs
Magnetic	30 W	Constant power, no mechanism or moving parts	Has not been investigated for in-atmosphere power, tether must remain constantly weighted, loop must remain circularized and closed, large drag	N/A	Further investigation of closed-loop tethers could prove beneficial but should not be prioritized
Fuel Cell	*30 W*	*Continuous, guaranteed power supply*	*Outside of WB mission plan for in-situ resource harvesting, puts an end date on mission, must transport heavy fuel*	*Using a COTS fuel cell and 35 kg of oxygen, can sustain for about 6 months*	*Custom fuel cell efficiencies should be explored to reduce mass and extend mission time*

6 Operations Concept

This section describes the functional aspects of the WB concept in operation: deployment, instrumentation, wind measurement, navigation using magnetic field, avionics, autonomy/algorithms, and autonomy challenges.

6.1 Deployment

The phases of WB Entry, Descent, and Deployment (EDD) (developed and tested at NASA JPL) include:

- Atmospheric Entry, accounting for high G forces and extreme temperatures potential
- Parachute deployment
- WindBot deployment
- WindBot inflation (if appropriate)
- Parachute release
- Inflation system release, ascent to float altitude

A challenge with deployment of such a system is mitigating atmospheric entry acceleration shock. When the Galileo probe was deployed into the Jovian atmosphere in 1995, the probe experienced deceleration forces as high as 230 g. These acceleration fields produce enough force to destroy any hardware that has not been extremely ruggedized. Recent developments in aeroshell technology may provide a solution to mitigating these strong deceleration forces, the Low Density Supersonic Decelerators (LDSD) tested in 2014 demonstrates deployable technology to create a higher-drag entry vehicle that could serve a role in Jovian WindBot deployment, and if used correctly could alleviate extreme deceleration environments [74].

The technique of atmospheric entry will also determine the overall intensity of deceleration encountered. The greatest deceleration forces will be encountered if an entry angle is steep, effectively increasing the atmospheric density gradient, resulting in a shorter deceleration distance and in turn increasing forces induced on the WB aeroshell. On the other hand, if the angle of entry is shallow, aerobraking can be used to gradually slow the body of the craft, thus mitigating extremely high shock forces. Some techniques of aerobraking involve “skipping” through the atmosphere as shown in Figure 6-1 to slow the craft to suborbital speeds in preparation for final entry into the atmosphere. The primary disadvantage of using this type of entry technique is the precision guidance system required to properly execute such a complex maneuver. It has yet to be implemented in spaceflight.

The parachute deployment also serves as a potential point of acceleration shock. When the parachute opens, the induced drag increases drastically. This is why some descent systems utilize a drogue chute to initially slow the vehicle and pull out the primary chute. System parachutes could be utilized to more gradually slow the payload to a speed appropriate for WindBot deployment. In the case of an ambient gas aerostat, the envelope must be filled during the descent. If designed correctly, as the aerostat envelope fills with gas, it may be able to be used as drag inducing mechanism. This means as the envelope is deployed, it will increase with percentage of inflation, so that if the envelope is filled gradually with ambient gas when it is descending the payload will gradually slow to an equilibrium altitude. Some balloons inflate in sections, utilizing package stitching to inflate the envelope one section at a time. Similarly, if an inflatable glider is chosen as a WB, it would have to be suspended under a parachute to take loading off its wings so that internal pressure needed to inflate the wings before rigidization occurs can be minimized and there is no need for heavy gas tanks supporting the process.

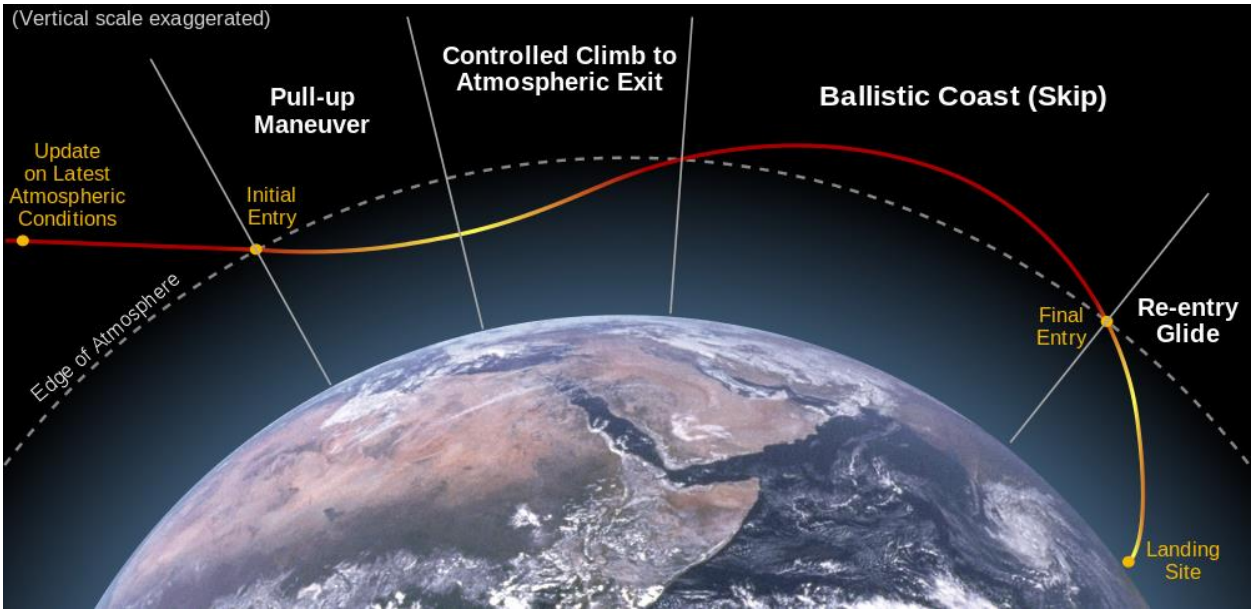

Figure 6-1: "Skipping" technique utilized to alleviate extreme deceleration forces associated with high velocity atmospheric entry. Figure based on NASA figure produced by Clem Tiller.

When the WB deploys, the lift mechanism, the lift mechanism (buoyant or wing) must be able to handle the speed at which it is deployed; the faster the deployment speed, the higher the induced shock on the structure, thus the stronger the mechanism must be. A glider concept must be deployed in conditions that will not compromise flight dynamics. For instance when WB experience extreme turbulent conditions during flight (like those may be encountered during package free-fall) a stall or death spiral has the potential to occur. A small retro rocket package could slow a package to a point to allow for effective glider deployment.

The WindBot with all associated systems is packed inside the aeroshell, which is deployed from the orbiter. After entering into the atmosphere, the aeroshell and the heatshield separate and the parachute deploys. A few seconds after reaching the terminal velocity, the surface package container opens and the WindBot deploys. Some moments after start of the inflation the parachute releases, and the WB with the inflation system continue to descend. The inflation system is released when the inflation process is completed and the WB and the parachute reach sufficient separation. After that, the WB starts to ascend to the float altitude. First, the WB inflates in a vertical attitude, and then turns into a horizontal orientation for stability. In this initial phase, several problems exist requiring new technology effort:

1. Shock alleviation mechanism needed to mitigate blimp envelope stresses during deployment;
2. Dynamic stability of WB during inflation and delivery to the float altitude;
3. Safety of the WB floating during inflation.

The first is dependent on EDD procedure and the latter two are dependent on the design of the WB.

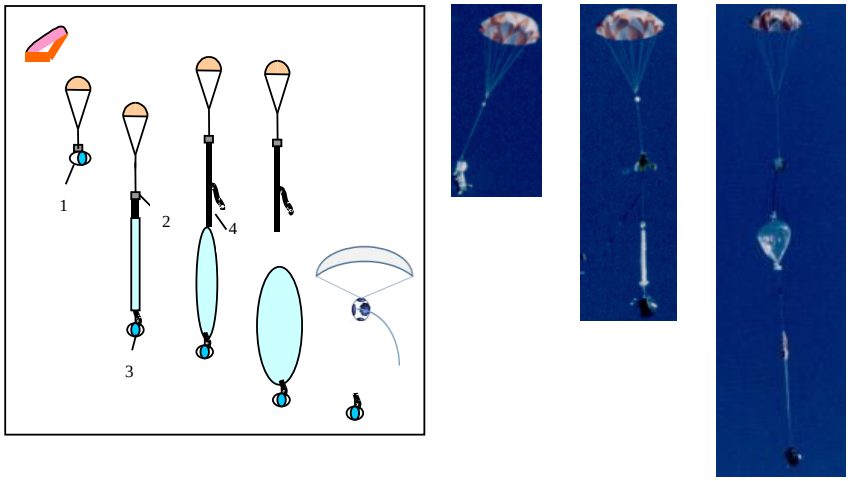

Figure 6-2: Phases of WB deployment and inflation (left). NASA JPL planetary balloon tests (right).

6.2 Avionics

Autonomous operation requires an intelligent, adaptive atmospheric flyer that senses 3D wind patterns, seeks vortexes, wind shear, and updrafts that can be used as energy fountains, plans its waypoints/traverse to pass by them, and does real-time control to adjust its aerodynamic properties for optimal lift and change of direction. To be able to determine how to move toward the energy reservoirs, the WB will need intelligent autonomy. It will need to sense the surrounding wind patterns at a distance; we will examine solutions, such as, the Laser Doppler Velocimeter [75], and how can this be scaled. The WB will include gyros and accelerometers for attitude stabilization, wind velocity/pressure probes, and a triaxial magnetometer.

6.2.1 Instrumentation – Wind Measurement

The WB could have the ability to estimate the local wind vector using an air data sensor and an inertial sensor. Assume that the air data sensor measures the speed and direction of airflow relative to the center of mass of the WB, and the inertial sensor measures the acceleration and speed of the vehicle in a fixed inertial reference frame. While airspeed and inertial measurement units are common on UAVs, air angle measurements are not. One method for estimating air angles is an alpha-beta vane system, which records the wind direction around two perpendicular axes each using a lightweight wind vane and potentiometer. An alternative system is a multi-hole pressure sensor which estimates the air angles by calculating the pressure at different orientations to the wind and solving for the wind direction [60].

6.2.2 Instrumentation – Navigation Using Magnetic Field

The magnetic field at Jupiter is very strong and complex. To understand its nature better, the WB could carry a set of tri-axial magnetometers for attitude sensing and control. This is the same concept that is used for Low Earth Orbit satellites using Earth magnetic field

6.3 Automatic Detection of Thermals and Autonomous Soaring

Recent work proves automatic detection of thermals and autonomous soaring. Prototypes have been tested in flight on Earth with encouraging results [76]. The autonomous locators of thermals (ALOFT) project has shown a UAV could fly about 60 hours just finding the thermals and going over them gaining

altitude [6.4]. Relevant work has been also done in guidance and control for an autonomous soaring UAV [6.5], [6.6], and [6.7].

The U.S. Naval Research Laboratory (NRL) and the Air Vehicle Intelligence and Autonomy Lab at Pennsylvania State University (PSU) successfully have completed testing of cooperative autonomous soaring algorithms used to keep sail planes aloft for a sustained flight [6.4] and [6.7]. The team launched 23 flights, resulting in more than 30 hours of combined flight time. The tests concluded with two powered sailplanes sharing telemetry data and cooperatively and autonomously soaring at altitudes of more than one kilometer and for flight durations of more than five hours. The NRL's autonomous soaring algorithm called Autonomous Locator of Thermals (ALOFT) guided the laboratory's aircraft while the AutoSOAR autonomous soaring algorithm guided Pennsylvania State University aircraft, onboard. The NRL developed the ALOFT and AVIA (Air Vehicle Intelligence and Autonomy), drawing inspiration from NRL's ALOFT techniques [77]. *The atmospheric map then is integrated to guide both aircraft toward strong lift activity more quickly than if it was a single aircraft, which is a technique like that used by a flock of soaring birds, Edwards explained. The U.S. NRL and PSU's aircraft showed a robust autonomous soaring capability during the two weeks of testing. PSU's, aircraft, for example, flew many two-and a-half-mile flights, despite carrying a battery with only enough capacity for four minutes of motor time. Meanwhile, NRL's longest soaring flight lasted 5.3 hours while only running a motor-driven propeller for 27 minutes. Future testing will look at reducing the separation distance so that both aircraft can soar in the same thermal at the same altitude.*

6.4 Autonomy Challenges

Autonomy is a great challenge including, but not limited to, guidance, modeling, control and estimation. Other important aspects to be considered are the payload energy requirements and the various risk factors the payload instruments [78].

An example of a Guidance and Control flow is depicted in Figure 6-3.

1. Successful generation of a target cloud selection (using automated reasoning and state estimates);
2. Using the latest wind and density estimates (produced by the Environmental Estimators);
3. Generate the predicted trajectory to reach the target that accommodates wind uncertainty;
4. Compare actual position and attitude to the predicted trajectory;
5. Apply corrective control inputs to this "realistic" dynamic system to follow the trajectory as close as possible.

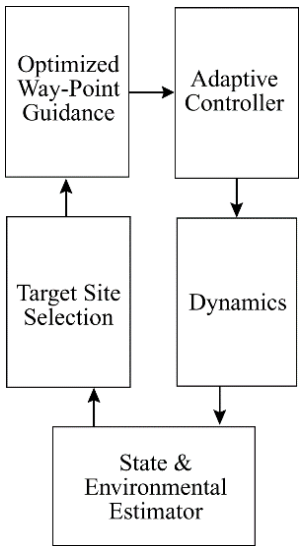

Figure 6-3: Block diagram showing the key Guidance and Control WB elements.

Figure 6-4 shows a functional block diagram of an autonomy architecture developed for a Titan Aerobot [78], which can be used as a starting point for the WB. This approach integrates accurate and robust vehicle and flight trajectory control, perception-based state estimation, hazard detection and avoidance, vehicle health monitoring and reflexive safe actions, vision-based localization and mapping, and long-range mission planning and monitoring. Some of these take new meaning in the context of Jupiter, in absence of land features – hazard detection would not refer to land obstacles but possible regions of downdrafts; etc. Autonomous ''go-to'' flight capability is needed to reach specific targets of interest but also for possible 'energy springs' e.g. updrafts. In addition to an IMU and cameras, other key sensors include atmospheric temperature, pressure and wind speed (atmospheric and gravitational environment knowledge), altimeter (altitude) and onboard temperature, pressure and electrical power (health monitoring).

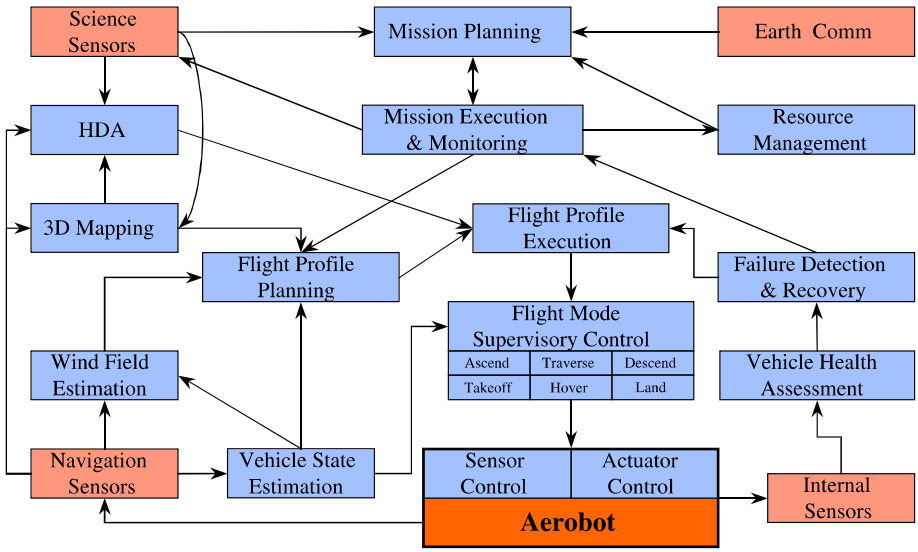

Figure 6-4: Aerobot Autonomy Architecture [79].

Star tracker and gyro measurements are processed to give the spacecraft attitude relative to an inertial frame. The trajectory commander plans the location of the waypoints used to navigate the pre-planned trajectory, by fixing the nominal inertial position of the vehicle at those waypoints. The attitude is also planned, consistently with the need to carry out turns at certain waypoints. Once the nominal trajectory has been planned and commanded, the trajectory guidance function implements it by assigning those commands to each controller. The controller implements a tracking control law, and translates the control forces in actuator deflections. This functionality is shown in Figure 6-5.

Important challenges in autonomy are:

- Guidance: path-planning in uncertain and turbulent atmosphere;
- Modeling: Complex aerodynamics, flight train dynamics, maneuvers during flight, negotiate wind gusts;
- Control: manage unpredicted disturbances, do science when disturbances are not too severe;
- Estimation: need to estimate environmental parameters (density, wind magnitude, and direction, etc.).

In general, the vehicle must know the maximum control authority, i.e., maximum allowed bank angle (varying with WB size). It must know control authority in wind, i.e., maximum allowed wind intensity to execute maneuvers. It must know where and how strong the wind is, thus a wind estimator running in near real-time. A possible aero-maneuvering control logic is as follows: if wind has z-windshear component, may adopt guidance law for flight in downburst (i.e., modulate a to avoid altitude loss, while simultaneously containing the velocity loss). Conversely, if wind is too severe, may require thrusting capability.

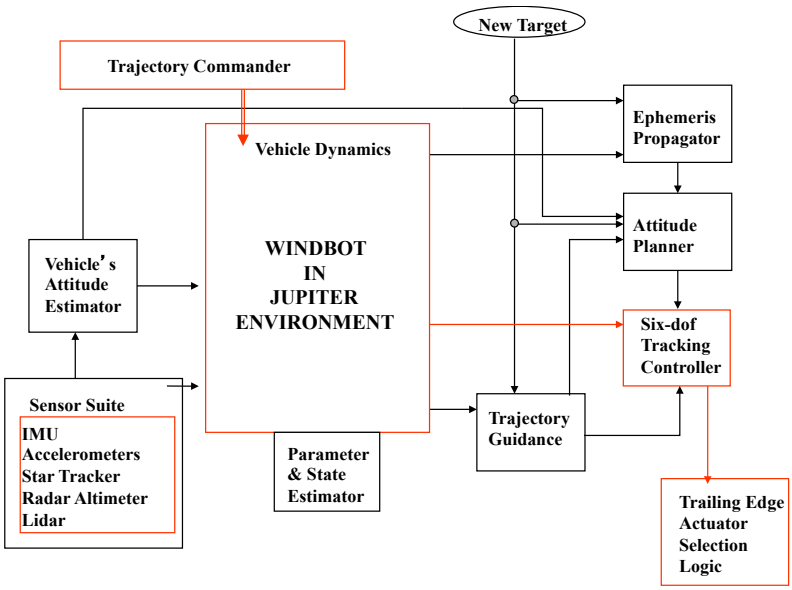

Figure 6-5: Illustration of a possible WindBot Autonomy Functional Diagram.

7 Summary and Conclusion

The need for in-situ exploration of Gas Giants using long-duration, multi-point autonomous vehicles, such as the proposed WB is real and apparent. Detailed information regarding the atmospheric structure and composition below the layer of visible clouds does not exist and is not readily achievable from an orbiting spacecraft. Within a mission context to explore this environment, we summarized what we know from previous missions, mostly Galileo, and identified sites of possible exploration and science instruments that the WB will need to carry for useful data collection. A mission scenario to the Great Red Spot focusing on measuring atmospheric conditions and composition was proposed as a Network of WindBots (NOW) to maximize spatial information harvesting.

We examined Jupiter atmospheric characteristics and options of WB mobility in the Jupiter environment, including various types of buoyancy control. The optimal region both for science and operations was determined to lie between 0.3 bar and 10 bar, within which all areas of known clouds is included. The Great Red Spot and the region located northwest of it, in the South Equatorial Belt, would be the most attractive point for launching WindBot missions.

We examined various types of buoyancy control and energy use through static and dynamic soaring. The lowest risk for mobility in covering long distances in South Equatorial Belt was found to be the buoyant hydrogen-based inflatable designs, with diameters exceeding 70 m, and with control mechanisms for enhanced mobility; gliders with L/D factors over 70 were found feasible, yet several challenges in automatically detecting and navigating to obtain lit from updrafts need to be overcome. For exploration in the Great Red Spot, riding in the eyewall, gliders would only need an L/D of 24, while also needing to solve the localization and moving towards to updrafts; a higher level of intelligent autonomy is needed in the GRS. A hybrid, inflatable design with control surfaces appears to be the solution with high risk high payoff.

We considered various options to harvest energy for operations. We analyzed vertical updrafts/thermals and horizontal components of the wind, and ways to convert mechanical into electrical energy. Both conversion of mechanical energy from rotors pushed by air flow such as in autorotation and use of energy from vibration were found effective. Harvesting hydrogen for fuel cells may be valuable for shorter duration missions.

As a recommendation, we propose as the next step to refine a mission concept to Great Red Spot, continuing the study of two alternate designs: an adaptive wing glider and a hydrogen-based buoyant design with controllable surfaces. An Addendum to this report, with an increased confidence in the recommendation is planned once new atmospheric data from Juno mission is provided.

8 References

[1] T. Greicius, "Juno Overview: Unlocking Jupiter's Secrets," NASA, 2016. [Online]. Available: http://www.nasa.gov/mission_pages/juno/overview/index.html.

[2] A. P. Ingersoll and et al., "Dynamics of Jupiter's atmosphere," in *Jupiter: The Planet, Satellites and Magnetosphere*, Cambridge University Press, 2004, pp. 105-128.

[3] A. A. Simon, M. H. Wong and G. S. Orton, "First results from the Hubble Opal Program: Jupiter in 2015," *The Astrophysical Journal,* vol. 812, no. 55, 2015.

[4] O. Mousis and et al., "Scientific rationale for Saturn's in situ exploration," *Planetary and Space Science,* vol. 104, pp. 29-47, 2014.

[5] R. E. Young, "The Galileo probe mission to Jupiter: Science overview," *Journal of Geophysical Research,* vol. 103, no. E10, 1998.

[6] Committee on Planetary and Lunar Exploration, Commission on Phys. Scis., Math., and Applications, Space Studies Board and Div. on Eng. and Phys. Scis., A Scientific Rationale for Mobility in Planetary Environments, National Research Council, 1998.

[7] D. L. Gallagher, L. Johnson, J. Moore and F. Bagenal, "Electrodynamic Tether Propulsion and Power Generation at Jupiter," National Aeronautics and Space Administration, 1998.

[8] G. P. Williams, "Jovian and comparative atmospheric modeling," *Adv. Geophys.,* vol. 28, pp. 381-429, 1985.

[9] T. E. Dowling, "Dynamics of Jovian atmospheres," *Annual Rev. of Fluid Mech.,* vol. 27, pp. 293-334, 1995.

[10] M. M. MacLow and A. P. Ingersoll, "Merging of vortices in the atmosphere of Jupiter: an analysis of Voyager images," *Icarus,* vol. 65, pp. 353-69, 1986.

[11] S. S. Limaye, "Jupiter: New estimates of the mean zonal flow at the cloud level," *Icarus,* vol. 65, p. 335, 1986.

[12] C. C. Poro and et al., "Cassini imaging of Jupiter's atmosphere, satellites, and rings," *Science,* vol. 299, pp. 1541-1547, 2003.

[13] A. B. Smith and et al., "The Jupiter System Through the Eyes of Voyager 1," *Science,* vol. 204, pp. 951-972, 1979.

[14] A. P. Ingersoll, "Atmospheric dynamics of the outer planets," *Science,* vol. 248, pp. 308-315, 1990.

[15] Seiff and et al, "Thermal structure of Jupiter's atmosphere near the edge of a 5-um hot spot in the north equatorial belt," *J. Geoph. Res.,* vol. 103, no. E10, pp. 22857-22889, 1998.

[16] C. J. Hansen, M. A. Caplinger, A. P. Ingersoll, M. A. Ravine, E. Jensen, S. Bolton and G. Orton, "Junocam: Juno's Outreach Camera," *Space Sci. Rev.,* 2014.

[17] R. E. Young, "The Galileo probe: how it has changed our understanding of Jupiter," *New Astronomy Rev.,* vol. 47, pp. 1-51, 2003.

[18] J. S. Lewis, "The clouds of Jupiter and NH3 - H2S systems," *Icarus,* vol. 10, pp. 365-378, 1969.

[19] A. Sánchez-Lavega, R. Hueso, S. Pérez-Hoyos, J. F. Rojas and R. G. French, "Saturn's cloud morphology and zonal winds before the Cassini encounter," *Icarus,* vol. 170, pp. 519-523, 2004.

[20] P. J. Gierasch and G. J. Conrath, "Dynamics of the atmospheres of the outer planets - Post-Voyager measurement objectives," *Journal of Geophysical Research,* vol. 98, no. E3, pp. 5459-5469, 1993.

[21] G. Maise, "Exploration of Jovian Atmosphere Using Nuclear Ramjet Flyer, Phase II - Final Report," 2003.

[22] O. Métais and M. Lesieur, "Spectral large-eddy simulation of isotropic and stably stratified turbulence," *Journal of Fluid Mechanics,* vol. 239, pp. 157-194, 1992.

[23] B. Galperin, J. Hoemann, S. Espa and G. Nitto, "Anisotropic turbulence and Rossby waves in an easterly jet: An experimental study," *Geophysical Reseach Letters,* vol. 41, no. 17, pp. 6237-6243, 2014.

[24] F. Davoodi, A. Hajimiri, N. Murphy, M. Mischna, I. Nesnas and S. Nikzad, "Gone with the Wind on Mars (GOWON): A Wind-Driven Networked System of Mobile Sensors on Mars," 2012.

[25] J. A. Jones and M. Heun, "Montgolfière Balloon Aerobots for Planetary Atmospheres," 1997.

[26] P. Malatere, "Long-Duration Balloon Flights in the Middle Stratosphere," *Adv. Space Rest,* vol. 13, no. 2, pp. (2)107 - (2)114, 1993.

[27] M. Cipolato and A. Stoica, "Windbots for Extreme Environments," 2016.

[28] D. Noel, "Lighter than aircraft using vacuum," *Speculations in Science and Technology,* vol. 6, no. 3, 1983.

[29] "Layered Shell Vacuum Balloons". US Patent US20060038062, 2006.

[30] T. T. Metlen, "Design of a lighter than air vehicle that achieves positive buyoancy in air using a vacuum," *M.S. Thesis, Air Force Institute of Technology,* 2012.

[31] R. Adorno-Rodriguez, "Nonlinear structural analysis of an icosahedron and its application to lighter than air vehicles under a vacuum," *M.S. Thesis, Air Force Institute of Technology,* 2014.

[32] W. J. Lucas, "Dynamic response analysis of an icosahdreon shaped lighter than air vehicle," *M.S. Thesis, Air Force Institute of Technology,* 2015.

[33] K. M. Aaron, N. C. Barnes, N. Nguyen, K. T. Nock, A. A. Pankine and R. S. Schlaifer, "Sailing the Planets: Science from Directed Aerial Robot Explorers (DARE)," *Phase II Final Report - NIAC, Global Aerospace Corporation,* 2006.

[34] J. Sherman, R. E. Davis, W. B. Owens and J. Valdes, "The Autonomous Underwater Glider Spray," *IEEE Journal of Oceanic Engineering,* vol. 26, no. 4, 2001.

[35] E. Lust and J. Stevens, "Autonomous Vehicle for Gathering Oceanographic Data in Littoral Regions," *Preliminary Design I,* 2016.

[36] H. Ludewig and et al., "Design of Particle Bed Reactor for the Space Nuclear Thermal Propulsion Program," *Progress in Nuclear Energy,* vol. 30, no. 1, pp. 1-66, 1996.

[37] N. Hall, "Gliders," 2015. [Online]. Available: https://www.grc.nasa.gov/www/k-12/airplane/glider.html.

[38] C. K. Poh and C. H. Poh, "Can the vertial motions in the eyewall of tropical cyclones support persistent UAV flight?".

[39] N. Hall, "What is drag?," 2015. [Online]. Available: https://www.grc.nasa.gov/www/k-12/airplane/drag1.html.

[40] S. Rimkus, "A Lab-Scale Experimental Framework for Studying the Phenomenon of Autorotation," *Diss. University of Central Florida,* 2014.

[41] S. Bilal, "An introductory study of the dynamis of autorotation for wind energy harvesting," *Univeristy of Central Florida,* 2014.

[42] J. Jacob, A. Simpson and S. Smith, "Design and Flight Testing of Inflatable Wings with Wing Warping," *Society of Automotive Engineers,* 2005.

[43] Pinero, 1962.

[44] C. Hoberman, "Radial expansion/retraction truss structures". US Patent 4942700, 1990.

[45] D. Rosenberg, "Novel Transformations of Foldable Structures".

[46] D. Brehm, "Buckle In," MIT, 2012. [Online]. Available: http://news.mit.edu/2012/buckliball-collapsible-structure-0326.

[47] K. Kuhlman and et al., "Tumbleweed: Wind-Propelled Measurements for Mars," *Concepts and Approaches for Mars Exploration,* 2012.

[48] "Tumbleweed Rover Goes on a Roll at South Pole," Jet Propulsion Laboratory, 2004. [Online]. Available: http://www.jpl.nasa.gov/news/news.php?feature=343.

[49] M. Sadraey, Aircraft Design: A Systems Engineering Approach, Wiley, 2012.

[50] S. Kota, R. Osborn, G. Ervin and D. Maric, "Mission Adaptive Compliant Wing - Design, Fabrication, and Flight Test," *Morphing Vehicles,* 2009.

[51] "Adaptive Compliant Trailing Edge Flight Experiment," NASA, 2014. [Online]. Available: http://www.nasa.gov/centers/armstrong/research/ACTE/index.html.

[52] J. Henrickson, R. Skelton and J. Valasek, "Shape Control of Tensegrity Airfoils," *AIAA,* 2016.

[53] "AD-1 Oblique Wing," NASA, 2009. [Online]. Available: http://www.nasa.gov/centers/dryden/history/pastprojects/AD1/index.html.

[54] H. Weimerskirch, C. Bishop, T. J. Jeanniard-du-Dot, A. Prudo and G. Sachs, "Frigate birds track atmospheric conditions over months-long transoceanic flights," vol. 353, no. 6294, 2016.

[55] Glider Flying Handbook, US Department of Transportation, Federal Aviation Administration, 2013, p. Chapter 10.

[56] T. Kiceniuk, "Technical Soaring," *An International Journal of Dynamic Soaring and Sailplane Energetics,* vol. 25, no. 4, 2001.

[57] N. e. a. Lawrance, "Wind Energy Based Path Planning for a Samll Gliding Unmanned Aerial Vehicle," *AIAA Guidance, Navigation, and Control Conference,* 10-13 August 2009.

[58] G. Sachs, "Minimum shear wind strength required for dynamic soaring of albatrosses," 2005.

[59] J. W. Merck, *The biomechanics of flight,* University of Maryland, 2007.

[60] A. L. Treaster and A. M. Yocum, "The Calibration and Application of Five-Hole Probes," *Technical Report,* 1978.

[61] G. Bracco, E. Giorcelli, G. Mattiazoo and M. Pastorelli, "Design of a Gyroscopic Wave Energy System," 2011.

[62] M. Kumagai and R. L. Hollis, "Development and Control of a Three DOF Spherical Induction Motor," *IEEE International Conference on Robotics and Automation,* 2013.

[63] L. Zhou, *Magnetically Suspended Reaction Sphere with One-axis Hysteresis Drive,* Department of Mechanical Engineering, Massachusetts Institute of Technology, 2014.

[64] E. M. Yeatman, "Energy harvesting from motion using rotating and gyroscopic proof masses," *Journal of Mechanical Engineering Science,* 2007.

[65] F. Cottone, G. Suresh and J. Punch.United States of America Patent 8350394B2.

[66] "Watch Movements," Tourneau, Inc., 2016. [Online]. Available: http://www.tourneau.com/watch-education/watch-movements.html. [Accessed 23 June 2016].

[67] S. e. a. Li, "Ambient wind energy harvesting using cross-flow fluttering," *Journal of Applied Physics,* vol. 109, 2011.

[68] M. e. a. Ferrari, "Piezoelectric multifrequency energy converter for power harvesting in autonomous microsystems," 2008.

[69] T. e. al., "Multimodal Energy Harvesting System: Piezoelectric and Electromagnetic," 2009.

[70] RWE npower, "Wind Turbine Power Calculations".

[71] E. Davies, "Where is the windiest place on Earth?," 9 October 2015.

[72] J. Barnes, *Survey of Astronomy,* 2006.

[73] T. Gastine, J. Wicht, L. D. V. Duarte, M. Heimpel and A. Becker, "Explaining Jupiter's magnetic field and equatorial jet dynamics," *Geophysical Research Letters,* 2014.

[74] "Low Density Supersonic Decelerators," NASA, 2015. [Online]. Available: http://www.nasa.gov/mission_pages/tdm/ldsd/overview.html.

[75] "DBR," 2014.

[76] A. Bailey, "NRL UAS projects mimic soaring birds, make UAVs undetectable," *USA TOday,* 2016.

[77] D. Parry, "NRL Tests Cooperative Soaring Concept for Sustained Flight of UAV Sailplanes," US Navy, 2016. [Online]. Available: http://www.navy.mil/submit/display.asp?story_id=92614.

[78] M. Pomerleau, "NRL tests low-power, long-endurance sail drone," Defense Systems, 2016. [Online]. Available: https://defensesystems.com/articles/2016/01/08/onr-penn-state-sailplanes-thermals.aspx .

[79] J. Hall and et al, "An Aerobot for Global In-Situ Exploration of Titan," *Adv. in Space Res.,* vol. 37, pp. 2108-2119, 2006.

[80] W. e. a. Al-Sabban, "Wind-Energy based Path Planning For Unmanned Aerial Vehicles Using Markov Decision Processes," 2013.

[81] D. Barton and S. Burrow, 2011.

[82] P. Pillatsch and e. al., 2012.

[83] O'Donoghue, Declan and et al., 2014.

[84] E. A. Haering, "Airdata Calibration of a High Performance Aircraft for Measuring Atmospheric Wind Profiles," *Technical Memorandum,* 1990.

[85] A. Behar, F. Carsey, J. Matthews and J. Jones, "An Antarctic Deployment of the NAS/JPL Tumbleweed Polar Rover," *IEEE,* 2004.

[86] K. Ang, J. Cui, T. Pang, K. Li, K. Wang, Y. Ke and B. Chen, "Development of an Unmanned Tail-sitter with Reconfigurable Wings: U-Lion," *IEEE,* 2014.

[87] A. Pankine, "Direct Aerial Robot Explorers (DARE) for Planetary Exploration," 2002.

[88] Seiff and et al, "Structure of the atmosphere of Jupiter: Galileo Probe measurements," *Science,* vol. 272, pp. 844-845, 1998.

[89] E. A. Haering, "Airdata Calibration of a High-Performance Aircraft for Measuring Atmospheric Wind Profiles," *Technical Memorandum NASA TM-101714,* 1990.

[90] D. J. Edwards, "Autonomous Locator of Thermals (ALOFT) Autonomous Soaring Algorithm".

[91] S. C. Daugherty and J. W. Langelaan, "Improving Autonomous Soaring via Energy State Estimation and Extremum Seeking Control," *AIAA Guidance, Navigation, and Control Conference,* 2014.

[92] M. J. Allen, "Guidance and control for an autonomous soaring UAV". USA Patent 7431243 B1, 2008.

[93] Faranak Davoodi, "Moball Network: A Self-Powered Intelligent Network of Controllable Spherical Mobile Sensors to Explore Solar Planets and Moons" http://arc.aiaa.org/doi/abs/10.2514/6.2014-4261

[94] F. Davoodi et al, "Autonomous and controllable systems of sensors and methods of using such systems", US 20130222115 A, https://www.google.com/patents/US20130222115

[95] Design for the Structure and the Mechanics of Moballs," NASA Technical Briefs 36 (10), 66–68, Oct 2012, http://ntrs.nasa.gov/archive/nasa/casi.ntrs.nasa.gov/20120016261.pdf

[96] F. Davoodi "Gone with the Wind on Mars (GOWON): A Wind-Driven Networked System of Mobile Sensors on Mars Concepts and Approaches for Mars Exploration, 2012, http://www.lpi.usra.edu/meetings/marsconcepts2012/pdf/4238.pdf

[97] Simple Motion Planning Strategies for Spherobot: A Spherical Mobile Robot IEEE Int'l Conference on Decision and Control, 3, 2132–2137, 1999, http://pirun.ku.ac.th/~fengjwp/publication/IEEE_DC1999.pdf

[98] Dynamic modeling and stability analysis of a power-generating tumbleweed rover, Multibody Syst Dyn, 24, 413–439, 2010, http://arrow.utias.utoronto.ca/~damaren/papers/ multitumble2010.pdf

[99] Exploring Mars Using a Group of Tumbleweed Rovers, Robotics and Automation, IEEE International Conference on. IEEE, 775–780, 2007

[100] De Pater et al "Peering through Jupiter's clouds with radio spectral imaging", Science, 03 Jun 2016, Vol 352. Issue 6290. Pp 1198-1201

[101] Woolsey, et al "A Self-sustaining, boundary-layer-adapted system for terrain exploration and environmental sampling' NIAC Phase I report, 2005

[102] http://www.astronomynotes.com/solarsys/s5.htm

[103] Overview of Wind-Driven Rovers for Planetary Exploration, 43rd AIAA Aerospace Meeting 2005 http://ntrs.nasa.gov/search.jsp?R=20050041752

[104] https://www.geol.umd.edu/~jmerck/geol212/lectures/21.html

[105] http://lasp.colorado.edu/~bagenal/3720/CLASS19/19GiantPlanets3.html

[106] https://www.geol.umd.edu/~jmerck/geol212/lectures/21.html.

[107] www.geol.umd.edu/~jmerck/geol212/lectures/21.html

[108] http://history.nasa.gov/SP-349/p11.htm